Molecular to Microscale Technologies for Immunoaffinity Based Tumor Cell Capture in Microchannels

BY

CARI LAUNIERE
B.S.E., Tulane University of Louisiana, 2008

THESIS

Submitted as partial fulfillment of the requirements
for the degree of Doctor of Philosophy in Bioengineering
in the Graduate College of the
University of Illinois at Chicago, 2012

Chicago, IL

Defense Committee:

David Eddington, Chair and Advisor
Christos Takoudis
Jun Cheng
Richard Gemeinhart, Biopharmaceutical Sciences
Seungpyo Hong, Biopharmaceutical Sciences

ACKNOWLEDGMENTS

This work was supported by supported by NSF Grant No. CBET-0931472, NIH-NCI (No. U54 CA151880), and the Chicago Biomedical Consortium with support from the Searle Funds at The Chicago Community Trust.

TABLE OF CONTENTS

TABLE OF CONTENTS (Continued)

TABLE OF CONTENTS (Continued)

TABLE OF CONTENTS (Continued)

LIST OF TABLES

LIST OF FIGURES

LIST OF FIGURES (Continued)

LIST OF ABREVIATIONS

aE-ES	anti-EpCAM plus E-selectin Protein Mixture
ANCOVA	Analysis of Covariance
ANOVA	Analysis of Variance
Anti-EpCAM	Anti-Epithelial Cell Adhesion Molecule
APC-anti-EpCAM	anti-human EpCAM/TROP1-Allophycocyanin
BSA	Bovine Serum Albumin
CTC	Circulating Tumor Cell
DMSO	Dimethyl sulfoxide
EDC	1-ethyl-3-(3-dimethylaminopropyl) carbodiimide
EGP-2	Epithelial Glycoprotein 2
EGTA	Ethylene glycol-bis (2-aminoethylether)-N, N, N', N'- tetra acetic acid
EpCAM	Recombinant Human EpCAM/TROP-1 Fc Chimera
ESA	Epithelial Surface Antigen
E-Selectin	Endothelial Selectin
FBS	Fetal Bovine Serum
FITC	Fluorescein Isothiocyanate
GMBS	γ-maleimidobutyryloxy succinimide
MCID	Microfluidic CTC Isolation Device

LIST OF ABREVIATIONS (Continued)

μCP	Microcontact Printing
MPTMS	3-mercaptopropyl trimethoxysilane
NHS	N-Hydroxysuccinimide
PAA	Polyacrylic Acid
PAMAM	Poly(amidoamine)
PBS	Phosphate Buffered Saline
PCR	Polymerase Chain Reaction
PDMS	Polydimethylsiloxane
PEG	Polyethylene Glycol
P-Selectin	Platelet Selectin
SAM	Self-assembled Monolayer
SHM	Staggered Herringbone Mixer
SPR	Surface Plasmon Resonance

Summary

When carcinoma cells are shed into the blood stream, they become circulating tumor cells (CTCs). CTCs are the vehicles by which carcinoma is spread throughout the body during tumor metastasis. CTCs are difficult to isolate and study because they are present at extremely low concentrations in the blood. Hence, little is known about CTCs and the complex process by which they differentiate, mutate, and colonize new tissues. For this reason, the metastatic spread of tumors continues to be the cause of 90% of all solid tumor cancer deaths. In order to develop new life-saving cancer treatments, clinicians and researchers need to learn more about CTCs and the deadly metastatic processes.

To meet this need, a variety of methods for isolating and analyzing CTCs have been developed recently. One of these methods involves the microfluidic processing of blood to isolate CTCs via immunoaffinity to antibodies immobilized on microchannel surfaces. This thesis describes a variety of techniques that have been investigated for improving the efficiency and purity of microfluidic immunoaffinity based tumor cell isolation.

A biomimetic combination of cell capture proteins was found to increase tumor cell capture efficiency in microfluidic channels. Also, patterning of the biomimetic proteins using a novel method was combined with a special elution buffer to reduce capture of leukocyte impurities. In addition, the use of mixers and hydrophoresis in microfluidic CTC isolation was investigated using computational modeling and physical flow studies. Furthermore, a blood analog was developed for use in the initial validation of microfluidic CTC isolation devices. Feasibility testing showed that the alginate based analog reduced problematic cell settling and did not alter specific or nonspecific cell capture in these devices. Finally, dendrimer facilitated multivalent binding was found to increase tumor cell capture at low flow rates in microfluidic CTC isolation devices.

CHAPTER I. INTRODUCTION

1.1 Tumor Formation and Tumor Metastasis

The surfaces and cavities of the human body are lined with epithelial tissue. Because epithelial tissue is exposed to the environment, epithelial cells are highly susceptible to genetic mutation by environmental mutagens such as chemicals and radiation. For this reason, epithelial cancers (carcinomas) are the most prevalent form of cancer in humans. Carcinomas begin when a single cell acquires enough gene mutations (usually 4 to 6) to override the many checks and balances that would normally prevent excessive and uncontrolled proliferation. The progeny of this cell, which is now considered cancerous, undergo uncontrolled and abnormal mitosis. This often results in the accumulation of additional mutations. As cell proliferation continues, a tumor is formed (figure 1a). These primary localized tumors, known as stage 0 in-situ carcinomas, are nearly 100% curable through excision of the tissue. However, as the disease progresses, a tumor grows until it breaks through the basal lamina - the membrane which separates the epithelium from the rest of the body (figure 1b). Once basal lamina penetration occurs, patient survival rates begin to drop. This is demonstrated in figure 2, which shows the 5 year survival rates for breast cancer patients by disease stage at diagnosis. Furthermore, once tumor cells have invaded non-epithelial tissues, they gain access to the capillaries. Carcinoma cells often enter the blood or lymph circulation via capillaries to become circulating tumor cells (CTCs) (figure 1c).

Although most CTCs die upon entering the harsh and unfamiliar environment of the blood stream, a small fraction of these cells do survive. Survival in the blood stream often requires that cells accumulate additional mutations or undergo differentiation. An even smaller fraction of CTCs not only survive the bloodstream, but also develop the ability exit the blood stream through the process of extravasation (figure 1d and 1e). During extravasation, CTCs

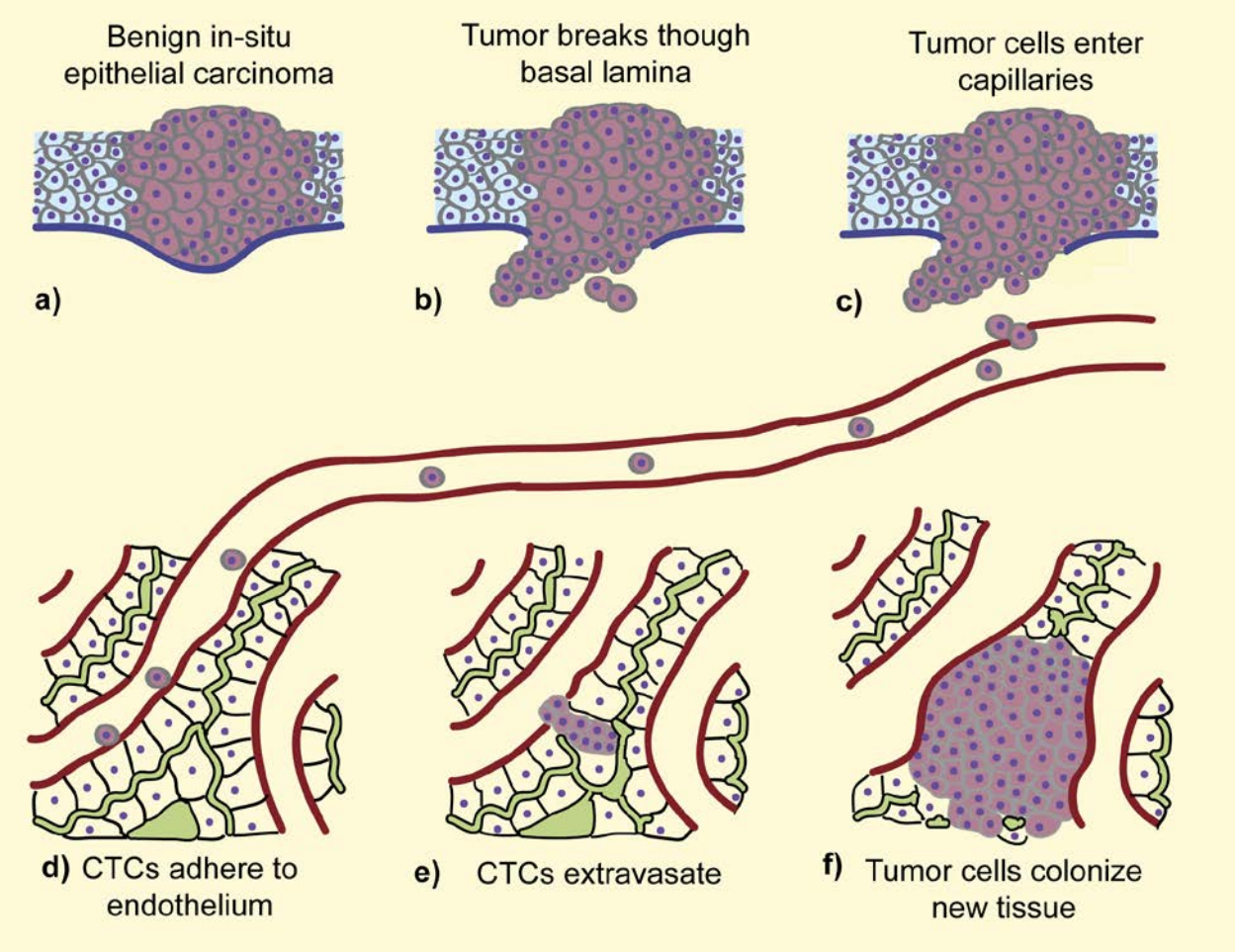

Figure 1. The Metastatic Process. Tumor cells often spread to secondary sites via the blood stream.

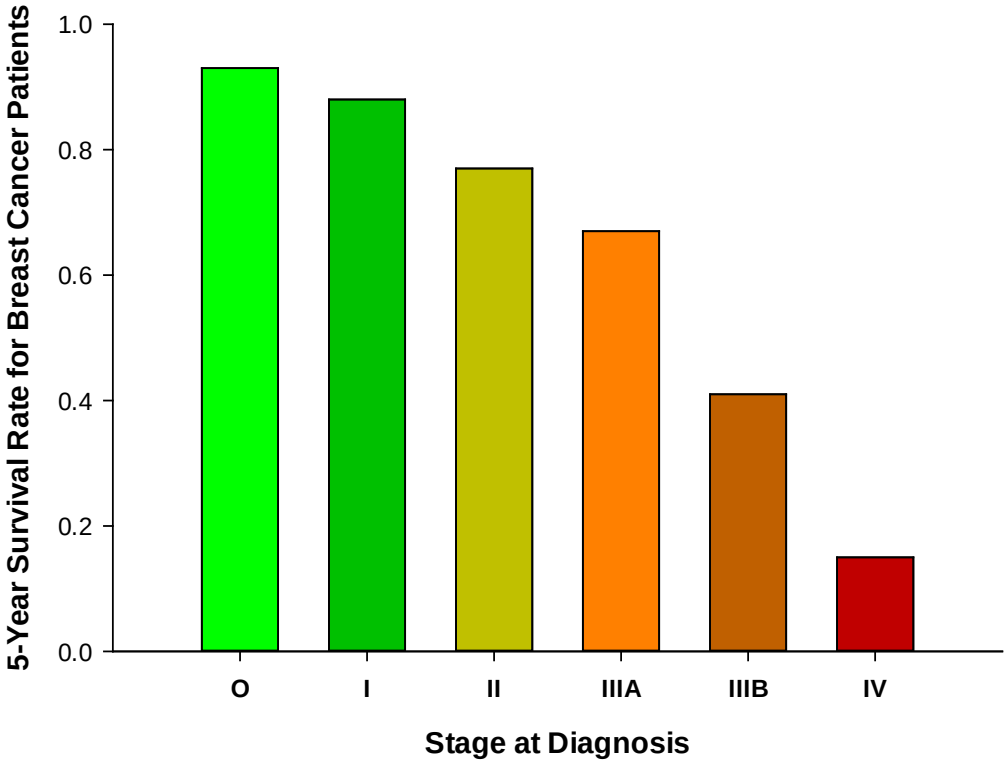

Figure 2. Five Year Breast Cancer Survival Rates. In the United States by stage at diagnosis. American Cancer Society, Cancer.org.

attach to the endothelium of a capillary (figure 1d) and push through the endothelial cells (figure 1e). If the extravasated tumor cells colonize this site, the new tumor is known as a secondary or metastatic tumor (figure 1f). Once a tumor has spread to a distant site through this metastatic process, a patient is considered to have stage IV disease. Patients with advanced stage IV metastatic cancer have the lowest survival rates (figure 2). This is because, unlike primary tumors which usually form in non-vital epithelial tissues - such as the skin or mammary glands - the metastatic spread of tumors often results in tumor formation in vital tissues - such as the liver or brain. As metastasis progresses, the total tumor mass in a body can grow to multiple kilograms. This much tumor tissue uses up significant resources and releases toxic substances into healthy tissue. Death can then result from the failure of an affected vital organ or, as in other wasting diseases, from a weakened body's inability to fight an infection. For these reasons, the metastatic spread of cancer is the cause of most cancer deaths.(Gupta 2006)

Although researchers and clinicians are very familiar with the devastating effects of tumor metastasis, the metastatic process is still poorly understood. In order to develop new life-saving cancer treatments, researchers and clinicians need to understand the processes of mutation and differentiation that allow tumor cells to intravasate, survive the circulation, extravasate, and colonize secondary tumor sites. To meet this challenge, researchers are developing methods to isolate CTCs from patient blood. The goal is to efficiently isolate CTCs and use the information extracted from these cells to improve our understanding of the metastatic process.

1.2 The Utility of CTC Isolation

Isolated CTCs can yield valuable information by many means. Captured CTCs can be collected after isolation or analyzed in-situ. In-situ analysis often involves fixation and staining

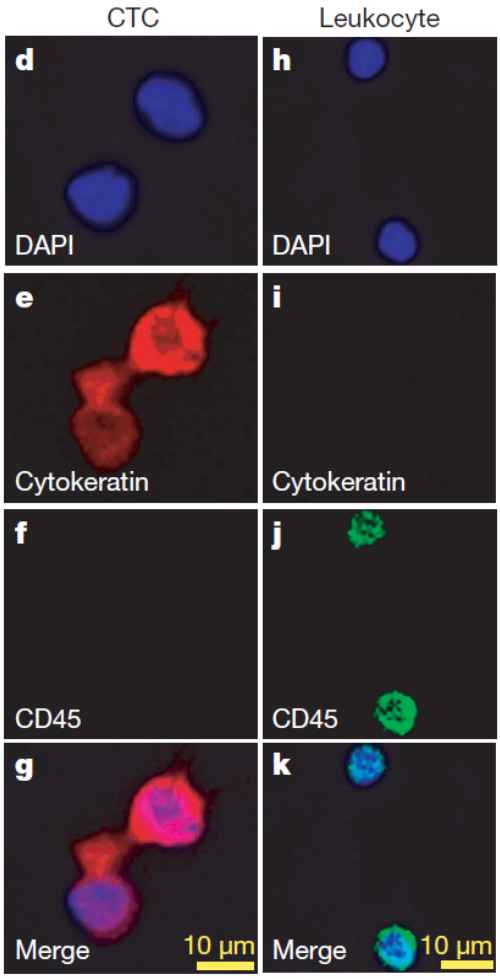

Figure 3. Cell Staining Scheme for Isolated Cells. Used to identify CTCs and distinguish them from leukocyte impurities. DAPI nuclear stain is used to identify cells, while cytokeratin and CD45 staining are used to identify CTCs and leukocytes, respectively. Reprinted from Nature Journal (Nagrath 2007) with permission from Nature Publishing Group. Copyright 2007.

(figure 3) to distinguish tumor cells from captured impurities. The stained CTCs are often enumerated to estimate the concentration of CTCs in the blood. In a clinical setting, the periodic enumeration of isolated CTCs can be used as a means of monitoring disease progression and treatment efficacy. Staining schemes can also be used to check for specific biomarkers, which can aid clinicians in cancer typing and provide researchers with important information about CTCs and the metastatic process.

In place of in-situ analysis, CTCs can be removed from the isolation apparatus for in-vitro culturing. In-vitro culturing is often necessary to generate enough biomass for analysis. In-vitro analysis often includes extensive molecular profiling (Sequist 2009), since current technology makes biomarker recognition and genetic analysis highly accessible. The information gained from these analyses can be used to monitor the efficacy of applied treatments, identify potential therapeutic targets, or develop personalized treatments.

Biopsied cells and surgical specimens from a primary tumor are sometimes molecularly profiled in order to develop personalized treatments for patients based on the specific molecular biology of their cancer. However, due to mutation and differentiation, the molecular profiles of these specimens may not match those of the CTCs spreading cancer through the patient's body.(Gerlinger 2012) This could explain the ineffectiveness of some current personalized therapies. For this reason, new technologies for the isolation and analysis of CTCs should have important impacts on individualized cancer therapy.

In addition to afore mentioned applications for CTC isolation, there is an aspiration to use CTC screening as a means of early cancer detection. Recent research with new and more sensitive isolation systems shows that CTCs can be detected in the blood of patients with early stage (non-metastatic) cancer and even in the blood of healthy control volunteers.(Hiraiwa 2008, Van der Auwera 2009, Stott 2010, Devriese 2012) This indicates that CTC screening could be used for early cancer detection. However, before CTC detection can become a

clinically useful tool for early cancer detection, a framework needs to be established about how to score isolated CTCs and CTC fragments, and also how to define what constitutes an unhealthy CTC profile that will require treatment. Furthermore, because the profiles of isolated CTCs are strongly influenced by the specific separation techniques and their limitations, more sensitive and reliable methods for CTC isolation will need to be developed before the goal of CTC based early detection of cancer can be realized.

1.3 CTC Isolation Methodology

Because CTCs originate from a variety of tissues and are constantly undergoing abnormal mitosis, they exhibit wide variability in properties such as: size, morphology, genotype, and biomarker expression. This, combined with the fact that the concentration of CTCs in blood can be less than one CTC per billion hematological cells, makes the isolation of CTCs a great and ongoing challenge.

The end application for CTC isolation is a key design consideration for CTC isolation systems. There are tradeoffs between capture efficiency, capture purity, cost of fabrication, and cost and ease of operation. Applications such as early cancer detection will require extremely high capture efficiencies due to the low numbers of CTCs present in early stage cancer. For applications that involve downstream processing(i.e. in-vitro culture), capture purity is the most important. The variability of CTCs and the diversity of end applications suggest that there will not be a single solution to CTC isolation. Instead it is likely that there will soon be a variety of isolation systems to suit the needs of each patient, clinician, and researcher.

Several early and current methods for CTC isolation are based on the overall physical properties of CTCs such as size, density, flexibility or charge. These methods are discussed in

section 2.2. Unfortunately, the physical properties of CTCs often overlap with those of hematological cells, resulting in low capture purities for CTCs isolation by physical means. For this reason, many have shifted their focus to affinity based separation, where one can take advantage of the unique biomarkers on CTCs. According to a recent review by Yu et al., antibody-based affinity capture has become the most common method of CTC isolation.(Yu 2011)

1.3.1 Affinity Separation

Traditionally, affinity separation has been applied for the highly effective separation of biomolecules in packed bed chromatography columns. However, due to clogging, whole cells and complex mixtures, such as blood, cannot be processed through delicate chromatography columns. CellSearch by Veridex was the first CTC isolation system to gain approval from the American Food and Drug Administration. This system is an extension of traditional packed bed affinity isolation, utilizing antibody coated particles to bind biomolecules on CTC surfaces (figure 4). However, this system avoids clogging by using magnetic particles that are free in suspension rather than immobilized in a column. The Veridex system pulls nanoparticle labeled target cells out of the complex mixture by applying a magnetic field (figure 4).

A downfall of the CellSearch system is that isolated CTCs are rendered non-viable during the complex isolation procedure, which requires cell fixation and places large amounts of shear stress on cells. Because of these inherent limitations of the Veridex method, many are turning to microfluidics for process simplification and increased control in microscale CTC isolation.

1.3.2 Microfluidics

Microfluidics can be defined as the precise control and manipulation of minute volumes of fluids that are geometrically constrained on a sub-millimeter scale. At this scale, inertial forces are small and dominating viscous forces result in parallel layers of fluid flow with little

momentum convection. This type of flow scheme, known as laminar flow, is what allows the precise control of fluids, including control of shear stress, within a microchannel (figure 5). The shear control available in microfluidics is advantageous in cell processing applications because it minimizes cell damage. Minimizing the effects of shear stress on cells is crucial if downstream cell culture and analysis are desired. High levels of shear can cause cell death, but even low levels of shear can cause unwanted changes in gene expression that will alter the results of molecular profiling experiments. The precise control of fluid flow and shear make microchannels an excellent alternative to microparticles for immunoaffinity isolation.

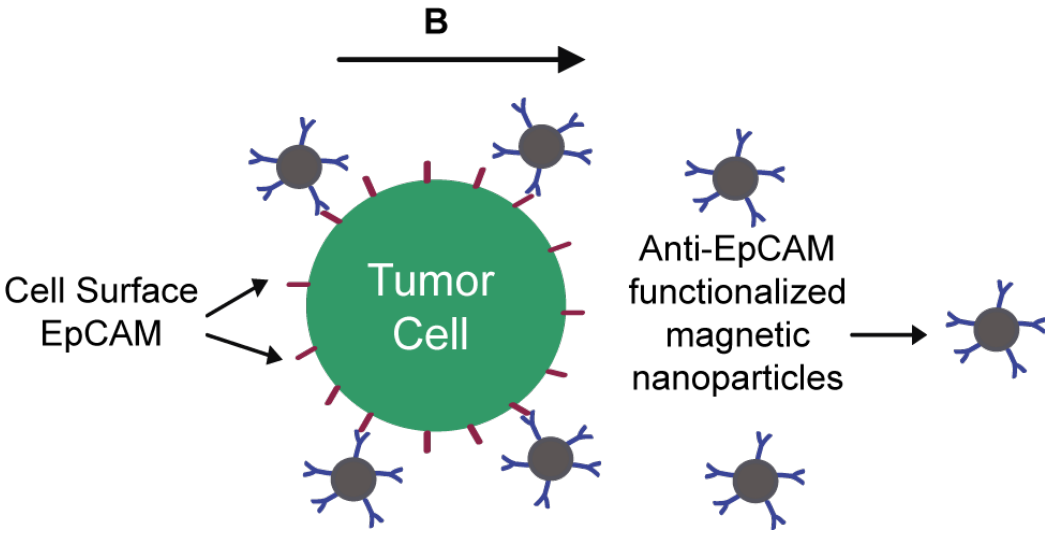

Figure 4. CellSearch CTC Isolation System, Basis of Operation. Antibody functionalized magnetic nanoparticles bind tumor cell surface antigens. A magnetic field (B) exerts a force on the nanoparticles which is transmitted to a tumor cell through the antibody-antigen bond. This allows tumor cells to be pulled out of the blood sample.

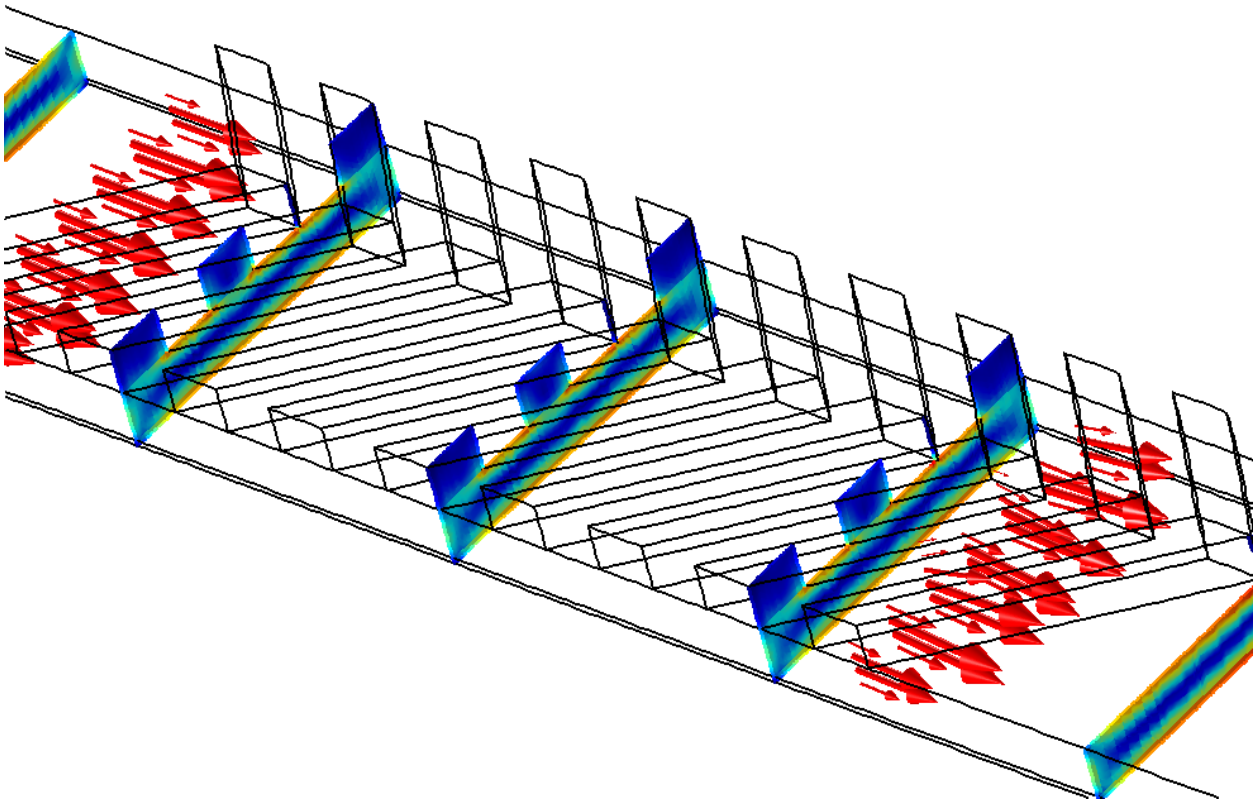

Figure 5. COMSOL Model of Fluid Flow in a Microfluidic Mixer. The red arrows represent fluid velocity and the cross sections indicate shear rate. These properties are very predictable and tunable in microchannels due to the laminar flow phenomenon.

Beyond shear control, microchannels boast a high surface area to volume ratio, which is important to maximize cell contact with capture surface immobilized antibodies. A final benefit of microchannels for affinity based CTC isolation is the simplicity compared to microparticle based approaches. Cells can be isolated from whole blood without any preprocessing with a single capture step followed by a single rinsing step.(Nagrath 2007, Stott 2010)

1.4 Outlook

CTC isolation is a rich field that spans many disciplines. The insights gained from CTC isolation research are valuable for the end clinical applications, but also foster advancement in many related fields. Fields such as - fluid dynamics, affinity isolation, rare cell detection, microfluidic processing of cell suspensions, and biological data analysis and processing - are the most likely to benefit from CTC isolation research.

This thesis describes new techniques for, protein patterning, microfluidic device validation, and maximizing the efficiency and purity of tumor cell isolation. While this work is intended to benefit applications in circulating tumor cell isolation, the work also has broader implications in the fields of surface functionalization, physical biochemistry, and microfluidics.

CHAPTER II. LITERATURE REVIEW

In 1869 Thomas Ashworth discovered CTCs during the autopsy of a patient with metastatic cancer. A century and a half later there are still too many mysteries shrouding CTCs and the metastatic process for clinicians to understand and effectively combat the deadly metastatic spread of tumors. The information deficiency is partially due to a lack of sufficiently sensitive CTC isolation methods. Only recently have CTC technologies begun to meet the needs of clinicians and researchers and give them the tools they need to uncover the mysteries of tumor metastasis. Below is a discussion of these technologies.

2.1 CTC Detection

Isolation of CTCs is not necessary if the goal is to merely indicate the presence of CTCs or CTC biomarkers. Towards this end many detection methods have been developed, which include high throughput microscopic scanning (Paterlini-Brechot 2000, Vona 2000, Xu 2009), nucleic acid detection (Papadopoulou 2006, Papadopoulou 2006, Gormally 2007, Zanetti-Dallenbach 2008, Yoon 2009), and detection of secreted CTC products (Alix-Panabieres 2007, Alix-Panabieres 2009).

2.2 CTC Isolation by Physical Means

Researchers have developed a diverse set of techniques to achieve isolation of CTCs from blood samples. Many of these operate based on the physical differences between hematological cells and CTCs. Despite some overlap, the physical properties of CTCs - density, size, charge and flexibility - can be used with some fidelity to distinguish and separate CTCs from hematological cells.

2.2.1 Density Based Separation

The earliest methods of CTC isolation relied on differences in buoyant density and were extensions of traditional methods for blood separation by gradient centrifugation. Early on, standard Ficoll gradient centrifugation was used to separate mononucleated cells, including CTCs and leukocytes, from red blood cells (figure 6).(Ko 1998) Later, systems designed specifically for CTC isolation (i.e. the OncoQuick system) were developed to decrease the number of white blood cell impurities in the final preparation. More recently, density based separation has been relegated to a preprocessing step used in conjunction with newer methods.(Wulfing 2006, Paris 2009, Lu 2010)

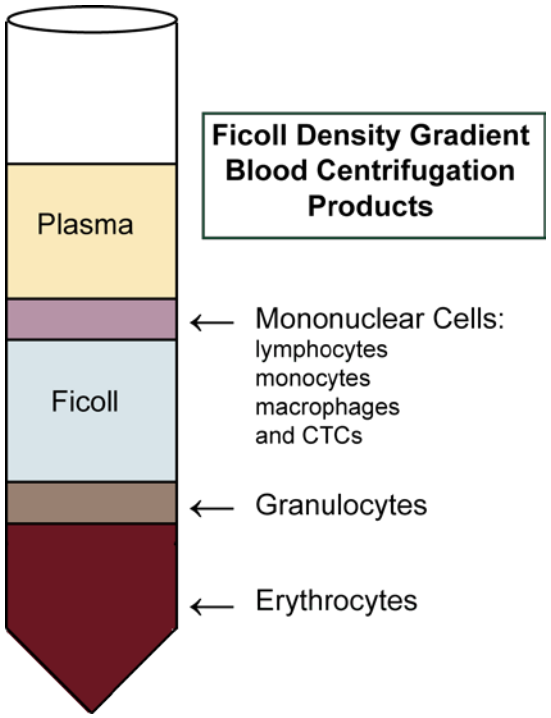

Figure 6. Ficoll Density Gradient Separation. Blood is loaded on top of Ficoll polysaccharide solution in a tube and processed by centrifugation. The separation products are depicted here.

2.2.2 Size Based Separation

The most popular method of physical separation, size based separation, operates based on the fact that most CTCs are larger than blood cells. The first attempts at size based separation relied on simple polycarbonate membranes filters with 8 μm pores.(Vona 2000, De Giorgi 2010) This method, however, required complex staining and detection procedures to identify CTCs among impurities. To improve on this system, Zheng et al. designed a micro-electro-mechanical system using a parylene-C membrane filter. This system provided in-situ electrolysis and PCR to simplify the detection procedure for the end user.(Zheng 2007)

Other groups have created more complex filters using photolithography and elastomer micromolding (soft lithography) techniques. Tan et al. reported a polydimethylsiloxane (PDMS) microdevice that included on-chip pre-filtering and an array of crescent shaped isolation wells (figure 7).(Tan 2009) This system also took advantage of blood cell flexibility, leaving 5 μm holes in the crescent wells for hematological cells to squeeze through. An array configuration, relative to a membrane filter, reduces the cells' exposure to shear stress, decreases instances of clogging and improves release of captured cells by flow reversal (figure 7c). Another system by Mohamed et al. reduced clogging with an array of filtering pores arranged by decreasing size (figure 8).(Mohamed 2009)

Devices which separate CTCs by size do not require costly biomolecules, translating to reduced costs and longer shelf lives compared to affinity separation devices. Also, isolation is not limited to CTCs with a specific biomarker profile. Unfortunately, these systems are all limited by the size range of CTCs that they can capture. Most CTCs are larger than leukocytes; however CTCs have a wide morphological variability (Marrinucci 2007). CTC diameters can overlap with leukocyte diameters (Stott 2010) leading to either low capture purity, or low capture efficiency depending on the chosen pore size.

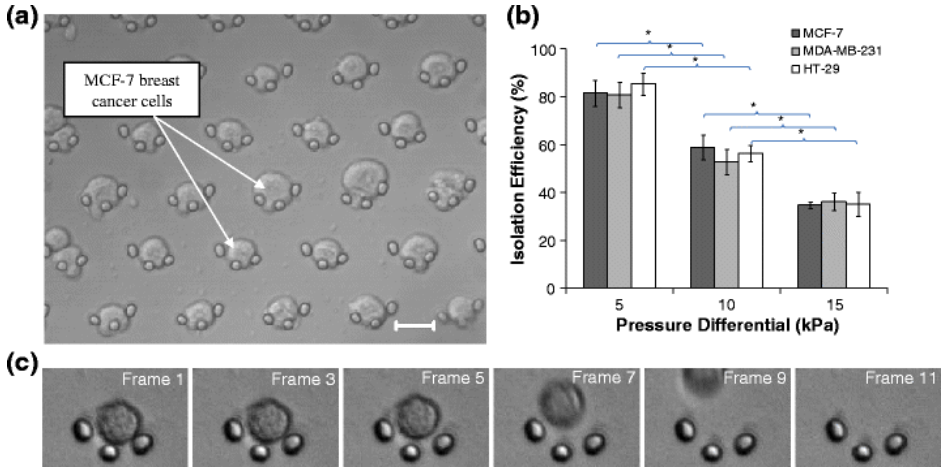

Figure 7. Size-Based CTC Isolation Device 1. (a) Carcinoma cells captured under flow conditions. (b) Isolation efficiency under different pressure conditions with 3 CTC models. (c) Captured cells released by flow reversal. This figure was reprinted from (Tan 2009) with kind permission from Springer Science and Business Media. Copyright 2009.

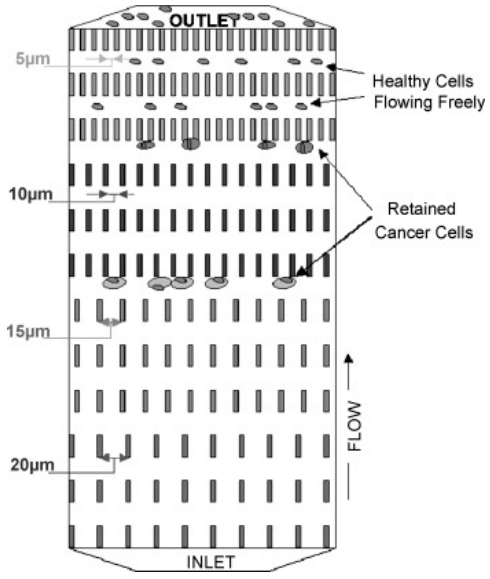

Figure 8. Size-Based CTC Isolation Device 2. The filter array depicted here exhibits decreasing channel-gap widths to reduce clogging and separate cells based on size and deformability. Reprinted from (Mohamed 2009) with permission from Elsevier Ltd. Copyright 2009.

2.3 Other Non-Immunoaffinity Methods of Isolation

While immunoaffinity separation is the most common method of CTC isolation, researchers have developed a wide range of creative solutions. One method relies on the invasive properties of CTCs. In this technique, mono-nucleated cells isolated by Ficoll density gradient centrifugation are seeded on a collagen adhesion matrix. The cells then separate themselves from the mixture by invading the matrix.(Paris 2009, Lu 2010) Another method relies on differential plasma membrane areas to achieve separation using dielectrophoretic field-flow fractionation.(Gascoyne 2009) Hur et al. reported a microfluidic method to separate tumor cells from diluted suspensions based on a cell's deformability-dependent lateral dynamic equilibrium position.(Hur 2011) Finally, a method similar to immunoaffinity separation has been developed that uses aptamers instead of antibodies to bond tumor cell surface markers.(Dharmasiri 2009, Phillips 2009, Xu 2009, Wan 2011)

2.4 CTC Isolation by Immunoaffinity

Other methods of CTC isolation are still under active investigation, but the most widely employed isolation techniques are those based on immunoaffinity to cell surface biomarkers. Anti-EpCAM is an antibody directed against human epithelial cell adhesion molecule (EpCAM). EpCAM is also known as epithelial surface antigen (ESA) and epithelial glycoprotein 2 (EGP-2). It is expressed in non-squamous epithelial cells and tumors derived from these epithelia. Anti-EpCAM can be used for the enrichment of tumor cells from bone marrow or peripheral blood because EpCAM is expressed at some level in nearly all CTCs but is not expressed in normal hematologic cells.(Latza 1990, Hardingham 1993, Naume 1997)

2.4.1 CellSearch and Related Systems

As mentioned previously, an early immunoaffinity based isolation device is the CellSearch system by Veridex (Riethdorf 2007), which uses anti-EpCAM functionalized magnetic nanoparticles to pull cells out of blood in the presence of a magnetic field (figure 4). It has been used clinically to monitor CTC counts in patients with metastatic breast, colon and prostate cancer.(Riethdorf 2007) CellSearch and related immunomagnetic bead based isolation systems are currently the most popular for use in clinical studies.(Wang 2000, Moreno 2001, Moreno 2005, Danila 2007, Fizazi 2007, Fehm 2008) Talasaz et al. reported a device called the MagSweeper which used a magnetic stir bar functionalized with anti-EpCAM in place of the nanoparticles used in the CellSearch system.(Talasaz 2009) Galanzha et al. proposed to overcome the limitation of CTC rarity in blood samples by going in-vivo, and injecting magnetic nanoparticles functionalized to target breast cancer cells directly into the blood stream of murine models.(Galanzha 2009) This was combined with photoacoustic imaging for in-vivo detection of carcinoma cells. Besides non-viable cell products, the other main downfall of the CellSearch system is low CTC capture efficiency. Using CellSearch, researchers report an average recovery of just 1 CTC per mL of blood from patients with metastatic disease.(Riethdorf 2007) Meanwhile, the newer microfluidic isolation devices report values greater than 50 CTCs per mL.(Stott 2010)

Another method of surface marker based CTC isolation uses fluorescence-activated cell sorting flow cytometry. (Simpson 1995, Krivacic 2004, Allan 2005, Cruz 2005) Also under investigation is the isolation of CTCs via the removal of non-target cells (i.e. blood cells). This strategy, termed negative selection, has the advantage of isolation independent of CTC surface markers. However, this technique will require further development before it will have clinical utility, since existing systems have low yields.(Tong 2007, Tkaczuk 2008, Balasubramanian 2009, Yang 2009)

2.4.2 CTC-chip Isolation System

Nagrath et al. developed the first microfluidic device for anti-EpCAM immunoaffinity isolation of CTCs from whole blood.(Nagrath 2007, Maheswaran 2008) This silicon channel, termed the “CTC-chip”, had 78,000 microposts to improve cell contact with an immunoaffinity capture surface. In microchannels, cell transport from bulk flow to surfaces is limited by the laminar nature of the fluid flow. In a laminar flow, viscous forces dominate and there is little momentum convection. The lack of convective mixing combined with the inherent low diffusivity of CTCs limits cell transport to the capture surface. Nagrath et al. took steps to overcome this limitation using microposts to bring the capture surfaces into the flow path and increase the capture surface area (figure 9).

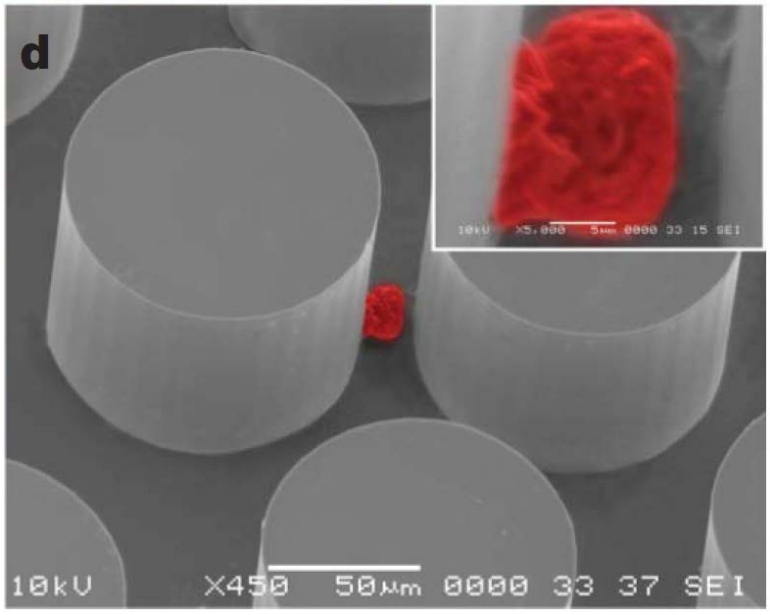

Figure 9. CTC-chip. An electron micrograph of the CTC-chip with a tumor cell captured on a micropost. Reprinted from Nature Journal (Nagrath 2007) with permission from Nature Publishing Group. Copyright 2007.

The CTC-chip had significantly higher CTC capture efficiency than existing systems. It also boasted simple operation and the ability to process whole blood without preprocessing. Additionally, the process did not require cell fixation and retained viable cells for in-vitro culture and analysis. For these reasons, the CTC-chip became the benchmark device to which new CTC isolation systems were compared. The limitations of the CTC-chip are primarily a result of its silicon fabrication, which is costly and complicated compared to fabrication in plastic or elastomer. Also, options for optical analysis are limited because silicon is not transparent.

2.4.3 Herringbone Chip Isolation System

Stott et al. (Stott 2010) reported a microfluidic device, the herringbone chip, that overcame some of the limitations of the CTC-chip. The device was fabricated in the transparent elastomer PDMS instead of silicon. This improved imaging and simplified fabrication significantly. The herringbone chip incorporated a passive microfluidic mixer (figures 5, 11 and 12) in place of microposts to help overcome the transport limitations in microchannels. This method achieved higher capture efficiency than the CTC-chip. Passive microfluidic mixers were created to overcome the lack of convective mixing in laminar flow devices, and are discussed more thoroughly in the next section (section 2.5.1).

Cells captured by the herringbone chip were fixed and stained with antibodies to epithelial markers, and CD45. CD45 staining was intended to identify captured leukocyte impurities. Interestingly however, many captured cells stained positive for both CD45 and epithelial markers (figure 10). These cells were not scored as CTCs during cell enumeration, since the nature of these cells is still poorly understood. The presence of these dual-positive cells emphasizes the need to develop standards for the characterization and analysis of isolated cells. Result validation studies are being conducted in parallel with the development CTC isolation systems in order to meet this need.(Danila 2011)

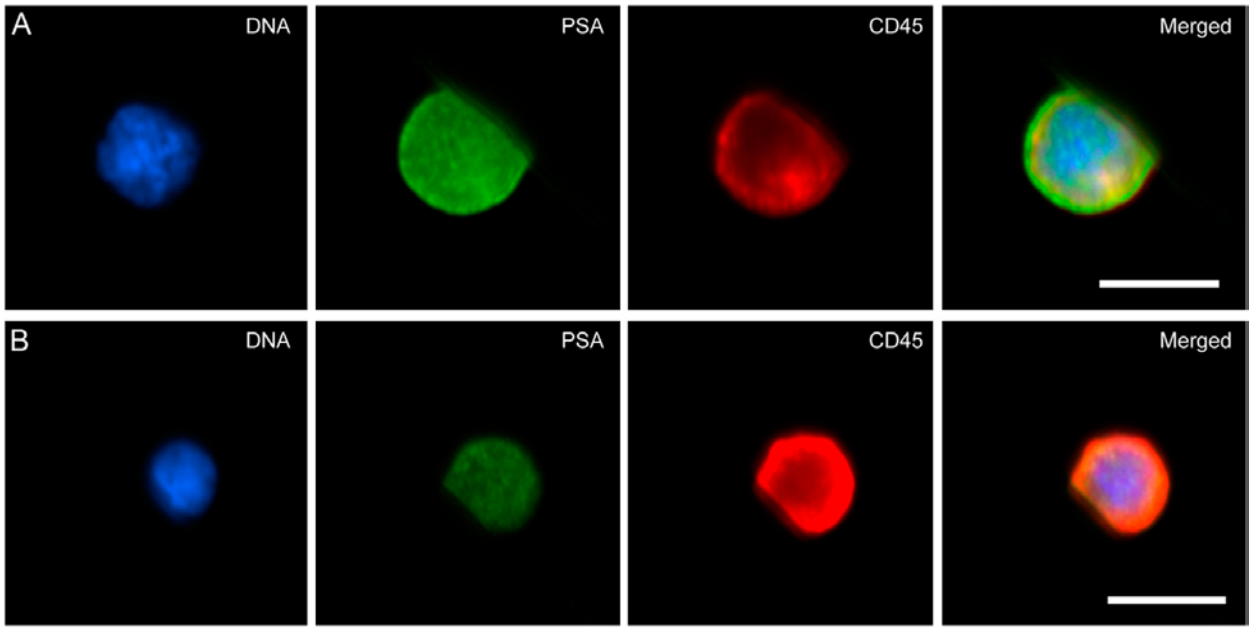

Figure 10. Herringbone Chip Dual Positive Cells. Micrographs of cells isolated with the herringbone chip from the blood of a metastatic prostate cancer patient. These cells were not classified as CTCs due to their dual positivity for both prostate specific antigen (PSA, epithelial marker, green) and CD45 (leukocyte marker, red). Reprinted from (Stott 2010) with permission from the National Academy of Sciences of the United States of America. Copyright 2010.

2.5 Microfluidic Mixing and Hydrophoresis

While the high surface-area-to-volume ratio in microfluidic devices is beneficial for surface cell capture, another feature of microscale flow is not. As discussed in section 2.4.2, viscous forces dominate on the microscale resulting laminar flow profiles with almost no convective mixing. Laminar flow, combined with the inherent low diffusivity of CTCs, limits cell transport to capture surfaces in a microfluidic device.

Microfluidic technologies that rely on cell binding to a capture surface sometimes employ methods to counteract microscale transport limitations and increase cell contact with functionalized surfaces. One strategy to increase cell-surface contact is to place capture surface structures in the path of fluid flow. Examples of this include the CTC-chip pillars (Nagrath 2007) (figure 9) and the MagSweeper stir bar (Talasaz 2009). Another strategy is to take advantage of centrifugal force in a curved channel.(Adams 2008) Finally, some groups have taken advantage of microfluidic passive mixing technology to improve cell transport toward capture surfaces.(Stott 2010)

2.5.1 Chaotic Advection Micromixers

Microfluidic passive mixers were originally devised to overcome the lack of convective mixing that prevents two fluids from mixing in a microchannel. The term passive mixing refers to the fact that these mixers don't have moving parts or a power source. These types of mixers are preferred over the more expensive and complex active mixers, particularly in chemical and biological microfluidic applications.(Capretto 2011) One type of passive mixing is based on chaotic advection. In microchannels, advection tends to occur in the direction of bulk fluid flow. Advection in other directions, called chaotic advection (Ottino 1989), can be induced in channels that are bent (Mengeaud 2002), curved (Jiang 2004) or convoluted (Liu 2000, Chen 2004) or by grooved structures on one or more channel walls (Johnson 2001, Stroock 2002, Stroock 2002)

(figures 5, 11 and 12). This chaotic advection creates a transverse component to axial pressure gradients generated by gravity or a pump. The resulting transverse flows greatly improve fluid mixing by folding the flow streams and increasing the interfacial area between the components being mixed (figure 12).(Stroock 2002)

One of the most effective advection mixers is the staggered herringbone mixer (SHM).(Stroock 2002) The SHM consists of asymmetric chevron grooves or “herringbones” in the channel floor (figures 5, 11, and 12). The direction of asymmetry of the herringbones switches with respect to the centerline of the channel after every 10 grooves (figure 11).

The SHM has been adapted for use in circulating tumor cell isolation. As mentioned in section 2.4.3., Stott et al. reported an anti-EpCAM based immunoaffinity CTC capture device that took advantage of SHM features to mix blood in the channel and improve the sensitivity of CTC capture.(Stott 2010) Another group has also used the herringbone mixer in combination with antibody-coated silicon nanopillars (figure 11).(Wang 2011) Both of these systems relied on parameter optimizations intended for the mixing of two continuous fluids (figure 12). However, the goal in this application is not to mix two continuous fluids but to optimize transport for bringing discrete particles (cells) into contact with the channel surface. This goal requires a different set of computational and physical optimization experiments based on hydrophoresis and not fluid mixing.

2.5.2 Hydrophoresis

Hydrophoresis can be defined as “the movement of suspended particles under the influence of a micro-structure induced pressure field”.(Choi 2007) This process is occurring in the herringbone chip and this process (not fluid mixing) should be optimized for maximum CTC capture (figure 18). With increasing numbers of microfluidic applications involving particle suspensions, there is a growing interest in particle manipulation by hydrophoresis. Most of the

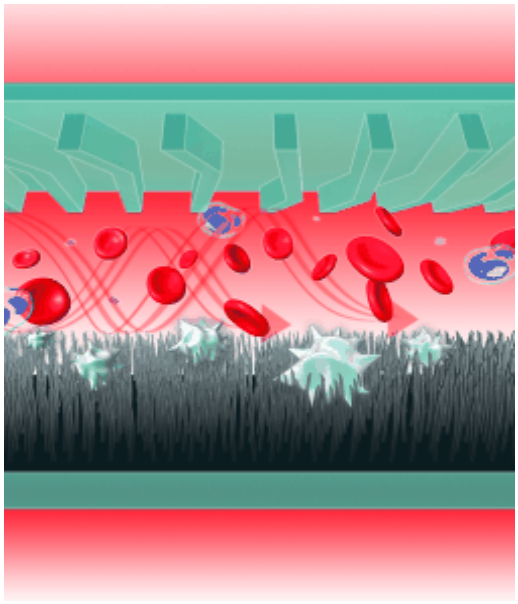

Figure 11. Anti-EpCAM Functionalized Silicon Nanopillars. Used in conjunction with a staggered herringbone mixer to isolate CTCs from other blood components. Reprinted from Angewandte Chemie International Edition (Wang 2011) with permission from John Wiley and Sons. Copyright 2011.

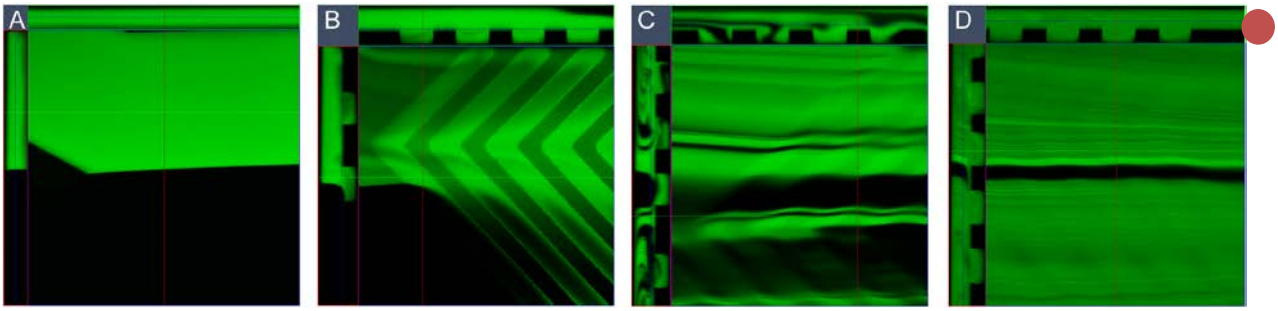

Figure 12. Fluid Mixing in Herringbone Chip. Orthogonal projections of the fluid flow profiles in a herringbone mixer at intervals along the z-axis. Reprinted from Stott et al. (Stott 2010) with permission from the National Academy of Sciences of the United States of America. Copyright 2010.

physical and computational work in this field uses dilute suspensions of particles to achieve simplification and maximum control.

Choi and Park accomplished hydrophoretic size-based separation of microparticles in a microchannel with slanted obstacles.(Choi 2007) Chen et al. used microchannels with slanted or V-shaped grooves to achieve alignment and enrichment of cells and particles in flow.(Chen 2009) Hsu et al expanded this idea by using arrays of V-shaped grooves to guide and sort particles.(Hsu 2008) Finally, Choi et al. combined hydrophoresis with filtering to achieve microfluidic separation of red and white blood cells.(Choi 2007) While these studies helped develop a framework for passive particle manipulation in microchannels, there is still a lot to be learned about cell and particle migration within dense suspensions.

There is little computational work on microfluidic hydrophoresis in dense cell suspensions. However, simple seminal studies are being conducted on hydrophoretic cell transport towards capture surfaces in microfluidic devices. Forbes and Kralj studied particle surface interactions in herringbone mixers using the computational fluid dynamics software package ESI-CFD-ACE.(Forbes 2012) Herein we report modeling studies on particle transport in micromixers using the multi-physics modeling software COMSOL.

2.6 Protein Immobilization

Several methods for immobilizing and patterning proteins onto solid substrates have been developed recently in order to meet demands in fields including: biointerface science, biosensing, proteomics, cell culture, tissue engineering, and smart materials. While nucleic acids have been used in arrays for decades, proteins are not as robust and are highly susceptible to damage and denaturation during immobilization (Predki 2004, Jonkheijm 2008).

For this reason, protein immobilization continues to be a challenge both in industry and in research.

2.6.1 Substrates for Protein Immobilization

The different substrates for protein immobilization are gold, glass, silicon and polymers. These surfaces are functionalized to facilitate protein binding using a variety of techniques.

Gold surfaces are popular for the study of protein immobilization and biosensing because of their excellent electrical conductivity and compatibility with electrochemical sensing and surface plasmon resonance (SPR) applications.(Lee 2005) Gold surfaces can be functionalization by self-assembled monolayer (SAM) formation using thiol and sulfide compounds. SAMs have been extensively studied (Love 2005), are easily tunable, and are commercially available with a variety of functional head groups for protein binding.

Glass is a popular substrate for DNA microarrays and many techniques developed for DNA or small molecule immobilization on glass have translated well to protein immobilization. Glass is generally functionalized by silanization of surface silanol groups.(Sagiv 1980) Silanol groups are created by treatment of the surface with oxygen plasma or with a mixture of sulfuric acid and hydrogen peroxide. Silanization can be carried out via vapor or chemical vapor deposition, or by immersion in aqueous or organic solution.(del Campo 2005) Silanization reagents are commercially available with amine, carboxy, epoxide, mercapto, sulfido, thiol and several other functional head groups (Dow Corning).

Silicon protein immobilization substrates have advantages which include: high electrical conductivity, mechanical stability, flatness, resistance to solvents, low intrinsic fluorescence and low cost (due to its bulk fabrication for the semiconductor industry). To prepare silane surfaces for functionalization with proteins, they are first treated with hydrogen fluoride (del Campo 2005)

or oxygen plasma to generate hydrogen terminated silanes or oxygen terminated silanes, respectively. The hydrogen terminated silanes can be reacted with ω-unsaturated alkyl esters using UV irradiation.(Strother 2000) The ester group can then be used for further modification. Oxygen terminated silanes can be functionalized with the same silanes used to fuctionalize glass.

Polymers are becoming increasingly popular as substrates for protein immobilization and for biochips in general. This is due to their low cost and tunable properties. Frequently utilized polymer substrates are polycarbonate, PDMS, poly(methyl methacrylate) and polystyrene. PDMS can be activated by oxygen plasma to generate oxygen terminated silanes which can be functionalized by silanization reagents in a manner analogous to silicon and glass.

In addition to the two dimensional substrates described above, proteins can also be immobilized on three dimensional matrixes such as nitrocellulose, nylon, agarose, acrylamide and other hydrogels, polysaccharides such as chitosan or dextran, biodegradable polyesters and various copolymers.(Jonkheijm 2008)

2.6.2 Protein Immobilization Schemes: Adsorption

Proteins can be immobilized onto the substrates delineated in the previous section by one of three immobilization schemes: non-specific physical adsorption (called physisorption), covalent binding (chemisorption), or bioaffinity interactions.

Adsorption of proteins occurs through any combination of: electrostatic, van der Waals, or Lewis acid-base interactions.(Hlady 1996) Immobilization can also occur via entropically based effects such as the hydrophobic effect. This is what facilitates physisorption onto the popular hydrophobic substrate - polystyrene. Protein adsorption is less expensive than covalent immobilization and tends to be very efficient (figure 13). Because of this, physisorption is a

common method of protein immobilization in microtiter-plate assays such as ELISA.(Niemeyer 2007) However, because protein adsorption a reversible process, proteins immobilized by adsorption do not perform well when subjected to fluid shear.

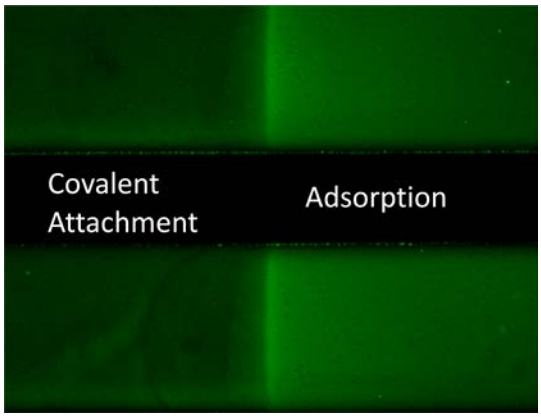

Figure 13. Adsorption and Silane-Based Covalent Immobilization of Fluorescent BSA on PDMS.

Unfortunately, surfaces that are amenable to protein adsorption are also susceptible to the unwanted adsorption of proteins and other analytes from biological samples. This can result in poor signal to noise ratios (Niemeyer 2007), which is why methods to control and prevent non-specific adsorption are under active investigation. Materials scientists have developed different types of non-fouling surfaces to reduce unwanted protein adsorption. Since physisorption is facilitated by a variety of interactions, the ideal non-fouling surface will depend on the application and the composition of the sample. Surfaces and surface treatments that block non-specific adsorption include: bovine serum albumin (BSA), milk powder, elastin,

sarcosine, agarose, cellulose, polysaccharides, phospholipids, fluorocarbon polymers, mannitol alkanethiolates, poly(ethylene glycol)(PEG), poly(vinyl alcohol), poly(glycerol), poly(carboxybetaine), polyelectrolytes, and peptide-based molecules.(Jonkheijm 2008, Ganesan 2010)

2.6.3 Protein Immobilization Schemes: Covalent

Covalent immobilization of proteins onto a substrate can be achieved by direct reaction with activated surfaces (i.e. surfaces coated with SAMs, silanes, or other functional groups) or by indirect binding via a linker or spacer molecule. Spacers, such as PEG, can function to reduce denaturation upon immobilization and prevent steric constraint of protein functionality.(Jonkheijm 2008) The surface reactive groups for direct covalent attachment and covalent attachment via spacers are generally the same. These include: aldehyde, amide, amine, aminoalcohol, carboxylic acid, epoxy, imine, isothiocyanate, maleimide, and thiourea groups.(Jonkheijm 2008) These functional groups are reacted with functional groups on proteins including: terminal and lysine side chain amines, terminal and aspartic/glutamic acid carboxyl groups, and thiol groups on cysteine residues.(Lee 2003)

The most common of these schemes is the immobilization of proteins by amide bond formations between N-Hydroxysuccinimide (NHS) activated surface carboxyl groups and amine groups on lysine side chains (figure 22d in the methods chapter).(Johnsson 1991) Alternately, proteins can be modified to present a variety of functional groups, many of which are used for bioaffinity immobilization as discussed in the next section.

2.6.4 Protein Immobilization Schemes: Bioaffinity

Two disadvantages of protein immobilization by covalent bonding are the potentially damaging chemicals and the protein deformation that occurs upon protein binding. A gentler alternative to covalent immobilization is immobilization by bioaffinity interactions. Many of the

techniques for bioaffinity immobilization were adopted from chromatography techniques used to isolated engineered proteins. In these techniques, the strong and specific interactions between biotin and avidin, His_6 tag and nickel, or DNA and proteins are used to immobilize proteins in a specific orientation.(Rusmini 2007)

2.7 Protein Patterning

Protein patterning techniques can be categorized based on their requirement for direct contact with the substrate. With the exception of robotic spotters and dip pen nanolithography (which will not be discussed here), contact methods tend to be simpler and less expensive. Conversely, non-contact methods tend to be more complicated and costly but have greater versatility than contact methods.

2.7.1 Contact Based Methods: Microcontact Printing (μCP)

Some of the simplest methods for protein patterning are based on microcontact printing (μCP).(Bernard 2000) This process uses a patterned stamp created by soft lithography to transfer molecules to a surface. μCP was first described by Kumar et al. (Kumar 1993) as a method for patterning SAMs on gold substrates. Due to the simplicity of this technique it was soon adapted for a variety of applications including protein patterning. The technique can be used with protein “ink” to directly pattern proteins by adsorption.(Bernard 1998, Bernard 2001, Schmalenberg 2004) It can also be used to pattern chemical platforms (such as those mentioned in sections 2.6.3 and 2.6.4) to which proteins can be attached. Popular chemical platforms in μCP include avidin-biotin affinity (Bieri 1999, Patel 2000), alkylsilanes, and alkylthiols (Quist 2005). Alternately, μCP can be used to pattern non-fouling blocking regents such as alkanethiols or PEG to prevent protein immobilization in those regions.(Lee 2011) In this case, the proteins are immobilized by backfilling the remaining spaces (figure 14).

.

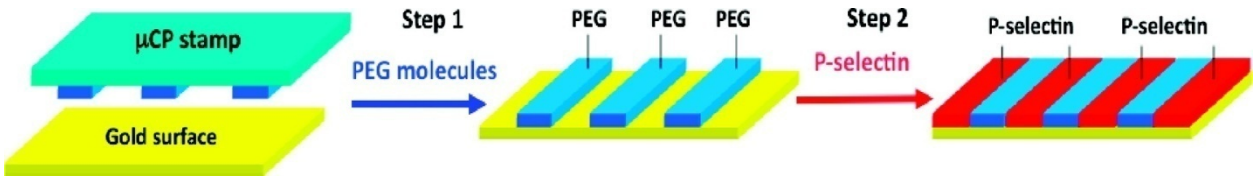

Figure 14. Micro-contact Printing. μCP of PEG molecules used to pattern P-selectin proteins via backfilling. Reprinted from (Lee 2011) with permission from the American Chemical Society. Copyright 2011.

2.7.2 Contact Based Methods: Fluidic Patterning

Another simple method for protein patterning is to place a microfluidic channel (Delamarche 1997) on the substrate and flow a protein solution through the channel. Similar to μCP, this technique can be used to immobilize proteins via covalent conjugation reactions, bioaffinity, or adsorption. In fluidic patterning, one can take advantage of existing microfluidic technologies to process protein solutions. As an example, a microfluidic gradient generator can be used to pattern gradients of proteins.(Fiddes 2010) Another iteration of microfluidic patterning uses a simple gasket in place of a microchannel.(Karnik 2008, Myung 2010) A major constraint of microcontact printing and microfluidic patterning is that they both require direct contact with the substrate. This can make these techniques impractical for applications where the patterned surface is to be enclosed in a channel. Most microfluidic devices require plasma or chemical bonding for assembly. Bonding devices after protein immobilization (a requirement for contact based printing) can result in the deactivation or ablating away of proteins and surface treatments. This can be avoided by enclosing the patterned surface in a commercially available

pressure sealed flow chamber.(Karnik 2008) However, there will be a loss of functionality and rapid prototyping capabilities that are available with custom made and soft lithography devices. Also, because pressure sealed flow chambers require a vacuum pump; they can be impractical for commercialization.

A final consideration of contact printing is that, because contact patterning is often done by hand, it can be difficult to achieve precise alignment for patterning that requires more than one step. To overcome these limitations researches have devised methods for protein patterning that do not require direct contact with the surface. These include photolithographic and photochemical methods.

2.7.3 Non Contact Patterning: Photolithographic Methods

Photolithography relies upon chemicals (photoresists) which become insoluble or soluble in a solvent when exposed to light of a specific wavelength. Photolithography is a very mature technology that was initially developed for use in the microelectronics industry. This technology also benefits from an existing framework for scale-up and bulk fabrication. Photolithography can be used in two ways to generate patterns on substrate surfaces. The first method is to use patterned photoresists to block regions on a substrate, so proteins may be immobilized on the remaining regions.(Falconnet 2004, Jackson 2006, Kwon 2011) The second method is to immobilize proteins onto the patterned photoresist itself.(Ganesan 2008) A common application of this method involves adsorption of serum proteins (He 2004, Kim 2006) or covalent immobilization of biomolecules (Li 2008) to facilitate cell patterning. A related method involves plasma-(Sorribas 2002), electron beam-(Christman 2008) or ion beam-(Brizzolara 2000) ablating of proteins that have been pre-adsorbed onto substrates. Early photolithography protein patterning techniques had limitations due to the solvent based developers and heat treatments that are required for photoresist processing. To avoid damage to the sensitive biomolecules,

novel photoresists were developed that can be processed under mild aqueous conditions.(Douvas 2002, Doh 2004, Katz 2006)

2.7.4 Non Contact Patterning: Photochemical Methods

Protein patterns can be generated using agents that are activated upon exposure to electromagnetic radiation or electron-beams.(Dillmore 2004, Chan 2008) For example SAMs with nitro functional groups can be reduced to amines in specified regions using electron-beam lithography.(Turchanin 2008) The amine groups are then available for modification with cross linkers or proteins. Another common reaction for photochemical based immobilization is the conversion of arylazides to reactive nitrenes, which can be inserted in carbon-hydrogen bonds.(Köhn 2009) Alternately, proteins can be patterned by free radical generation upon the photobleaching of fluorescent tags.(Holden 2003, Holden 2004)

A second photochemical method uses photo-labile protecting groups to block or “cage” functional groups. Photo-irradiation through a photomask can selectively cleave off (photolyse) the protective groups to expose functional groups for immobilization. For example SAM amine functional head groups can be blocked with an o-nitrobenzyl protecting groups that cleave upon exposure to UV light, so that regions subjected to photolysis are available for reaction.(Ryan 2004, Chen 2009) The protecting group technique is generally used for covalent attachment, (Waichman 2010) but is also frequently used with bioaffinity based immobilization such as the His-tag (Jonkheijm 2008, Reynolds 2009) and biotin (Blawas 1998, Holden 2004, Ganesan 2009) systems and even adsorption based immobilization (Belisle 2008, Belisle 2009). In other versions of this technique, electrochemical perturbation (Kim 2004) or heat (Chang 2007) are used to release the protecting groups.

2.8 Multivalent Binding and Dendrimers

2.8.1 Multivalent Binding

Multivalent binding is characterized by the simultaneous binding of multiple ligands on one entity (such as a surface or molecule) to multiple receptors on another entity. These polyvalent interactions can be orders of magnitude stronger than equivalent monovalent interactions, making them a powerful component in many biological systems.(Kiessling 1996) The most studied multivalent binding platforms are those for viral and bacterial pathogen-host attachment. However, multivalent binding is also found in neutrophil-endothelial binding, macrophage-antigen binding, and transcription factor-DNA binding. (Mammen 1998, Lee 2000)

Researchers have begun to harness the power of multivalent biological activity through the creation of synthetic multi-ligand constructs. These constructs can be used to improve the biological activity of weakly binding ligands, such as an anthrax toxin inhibitor.(Mourez 2001) Synthetic multi-ligand constructs have also been indicated in the targeting of specific cell types, such as tumor cells.(Quintana 2002, Weissleder 2005) The afore mentioned constructs are intended for use in-vivo, but in-vitro applications are also becoming increasingly popular.(Gestwicki 2002) For example, these platforms can be used to study biological recognition events, such as protein-carbohydrate interactions, that are otherwise difficult to study because of low monovalent affinity.(Kiessling 1996)

2.8.2 Dendrimers

Dendrimers are repetitively branched synthetic molecules.(Astruc 2010) They are spherical and monodisperse with tunable surface functional groups. A commonly used dendrimer is Poly(amidoamine), or PAMAM. PAMAM has a diamine core (most often ethylenediamine), which is reacted with methyl acrylate followed by ethylenediamine.(Tomalia 1985) This core is considered a generation-0 (G0) PAMAM dendrimer. Higher generation

dendrimers can be produced via subsequent reactions with ethylenediamine. Computational models of PAMAM G1 through G7 dendrimers are depicted in figure 15. Dendrimer stiffness and the density of surface functional groups increase with generation number. G7 and larger dendrimer are generally considered to be rigid particles.(Hermanson 2008) PAMAM's structure and easily tunable surface functional groups make it a good platform for organizing and orienting ligands in order to facilitate multivalent binding.(Woller 2003, Wolfenden 2006, Hong 2007)

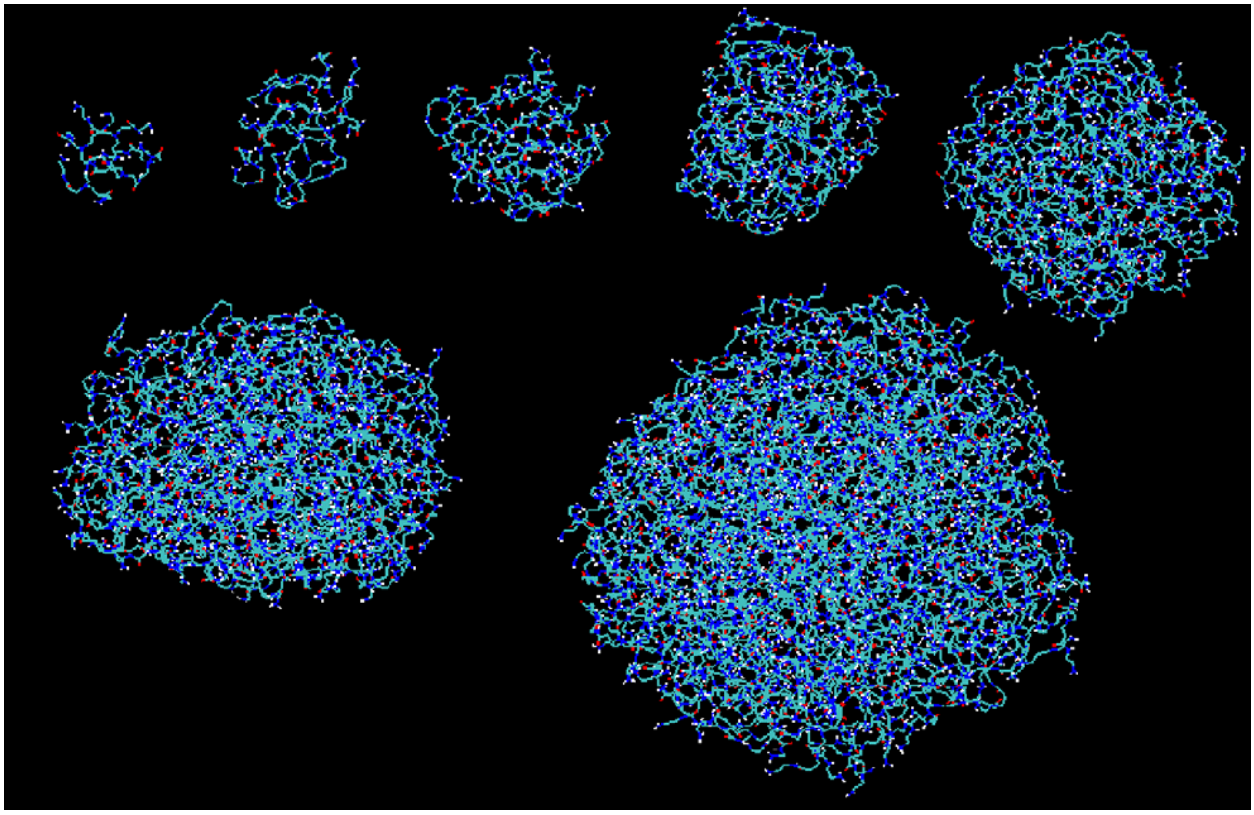

Figure 15. Material Studio Models of G1 through G7 PAMAM Dendrimers. Reprinted from (Han 2005) with permission from Elsevier Ltd. Copyright 2005.

CHAPTER III.THEORY

3.1 Biomimetic Protein Combinations for Increased Tumor Cell Capture Efficiency

As affinity-based cell capture in microfluidic devices becomes increases in popularity, scientists are beginning to look more closely at the physics of cell-surface binding reactions that occur under shear.(Gaver 1998, Lu 2004, Lopez 2008, Zheng 2011) These computational and physical studies agree with the intuitive assumption that capture frequency generally decreases with increasing shear rates. Current isolation devices are limited to the low flow rates that are required for efficient CTC capture.(Nagrath 2007, Stott 2010) This limitation translates to low throughput or additional costs to scale up devices via parallelization. In the work reported herein we propose to surpass these limitations by increasing immunoaffinity capture under shear with a second capture protein: E-selectin.

3.1.1 Cell Rolling on Selectins

The migration of cells along the vascular endothelium, under the shear of blood flow, is called cell rolling. Cell rolling is mediated by transient interactions between transmembrane cell adhesion glycoproteins (E-selectin and P-selectin) on endothelial cells and specific sugar moieties on hematologic and carcinoma cells.(Tedder 1995) Cell rolling is best known as part of the inflammation immune response when leukocytes are recruited to a site of injury by binding to and rolling along activated endothelia that is expressing E-selectin (also called endothelial-leukocyte adhesion molecule-1). Cell rolling on E-selectin is the first step in white blood cell extravasation, but is also an important step in carcinoma metastasis. It appears that carcinoma cells have high-jacked the rolling mechanism to facilitate extravasation for themselves.(Barthel 2007) Selectins bind their ligands with rapid bond kinetics, which make them ideal for binding to quickly moving cells and pulling these cells out of bulk flow.(Long 2001) However, selectin bond lifetimes are relatively short under physiological flow conditions, hence the repeated bond formation and breaking that results in cell rolling. To become arrested on the endothelium after

initial selectin-based tethering, in-vivo leukocytes form strong bonds with activated integrins on the endothelial surface. This combination of tethering, followed by strong bond formation can be mimicked in-vitro in a microfluidic device by combining E-selectin with a second capture molecule, such as anti-EpCAM.

3.1.2 In-vitro Applications for Selectins

The E-selectin glycoprotein has evolved specifically to bind cells in blood flow by forming catch bonds, with rapid binding kinetics, with its ligands on leukocytes.(Tedder 1995, Long 2001) Because CTCs share these same surface ligands, they are also able to bind E-selectin in the high shear environment of the blood stream.(Barthel 2007)

Researchers have recognized the utility of selectins and have begun to incorporate them into in-vitro systems involving the binding of cells under shear. The P-selectin receptor has been indicated for lateral displacement-based cell separation and analysis under flow.(Hong 2007, Lee 2011) Also, E-selectin has been combined with TNF-related apoptosis inducing ligand in an application to induce apoptosis of CTCs under flow conditions.(King 2009, Rana 2009) Our group has co-immobilized E-selectin and anti-EpCAM on the capture surface of a flow device and demonstrated that the addition E-selectin increases the capture rate of tumor cells up to 3 fold.(Myung 2010) Later, Hughes et al. further supported the addition of E-selectin to CTC immunoaffinity based isolation devices by demonstrating tumor cell capture in microtubes at higher shear rates than is possible with anti-EpCAM alone.(Hughes 2012)

3.1.3 Mechanism of Increased Cell Capture under Shear

During the immune response, leukocytes experience initial tethering and rolling on endothelial selectins followed by firm adhesion to integrins. In the work described herein, we mimic this natural process in a microfluidic device by combining E-selectin for initial cell tethering with anti-EpCAM for firm adhesion. In this microfluidic device, E-selectin pulls cells out of flow and increases the interaction between the cells and anti-EpCAM. Once target cells form

initial bonds with E-selectin, the change in Gibbs free energy for anti-EpCAM binding to cell surface EpCAM is decreased (it becomes more negative). This is the result of enthalpic contributions from the decrease in cell velocity and entropic contributions from the cells' partial immobilization on E-selectin. The loss of rotational and translation entropy upon E-selectin binding prepays some of the entropy penalty for anti-EpCAM binding and immobilization. This decrease in the change in free energy of binding leads to a higher percentage of binding events per contact with the binding surface. The end result is improved tumor cell capture efficiency over a capture surface functionalized with anti-EpCAM alone.(Myung 2010, Launiere 2012)

3.2 Protein Patterning and Rinse Buffers for Increased Tumor Cell Capture Purity

3.2.1 Patterning of Biomimetic Protein Combinations for Increased Capture Purity

Hematological cells that interact with E-selectin include eosinophils, lymphocytes, monocytes, neutrophils, and platelets, which comprise about 10% of blood cells. These cells will roll across E-selectin functionalized surfaces and (depending on the surface density of E-selectin) usually do not bind strongly enough to become arrested under flow conditions. In the work described here, we take advantage of this rolling phenomenon to isolate CTCs from hematologic cells in a microfluidic flow device. This separation of CTCs from other E-selectin binding cells is achieved by creating a capture surface with regions of anti-EpCAM/E-selectin mixture interspaced with regions of anti-EpCAM. Regions with only anti-EpCAM provide a space where the other cell types, mainly white blood cells, can be released from their rolling on E-selectin (figure 16). This patterning improves the capture purity of E-selectin augmented tumor cell capture in immunoaffinity based devices (Launiere 2012). It also may improve capture efficiency by preventing a build-up of white blood cells on the capture surface, which could otherwise interfere with the surface interaction of CTCs.

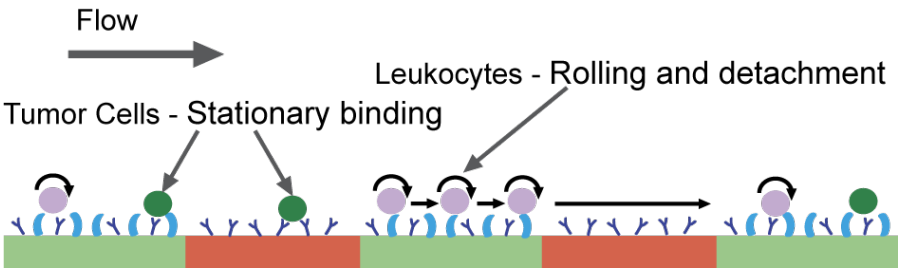

Figure 16. Cell Capture on Patterned Protein Functionalized Surface. Leukocytes and tumor cells interacting with capture surface proteins under flow conditions. Tumor cells bind stationarily across the entire capture surface. Leukocytes roll on protein mixture functionalized regions and detach upon reaching an anti-EpCAM functionalized surface.

3.2.2 Novel Protein Patterning Method

The in-situ dual protein patterning procedure described in section 4.2.2 takes advantage of the light permeability of PDMS to covalently pattern alternating proteins inside a sealed microfluidic channel. Polyacrylic acid (PAA) photopolymerized on a channel surface (Fiddes 2010) is used, both as a chemistry for protein attachment, and as a protective layer for the spatial control of protein immobilization using a second attachment chemistry: a silane backfill. This novel patterning process allows the spatially controlled immobilization of two proteins inside a permanently bonded PDMS channel. This process was developed specifically to create microfluidic capture surfaces with contiguous alternating regions of anti-EpCAM protein and anti-EpCAM plus E-selectin protein mixture (aE-ES) with the goal of optimum tumor cell sequestration with minimum leukocyte capture.

3.2.3 Comparison with Existing Patterning Techniques

The new protein immobilization procedure for creating contiguous regions of alternating anti-EpCAM and aE-ES is outlined in figure 22 in the methods chapter. Similar photopolymerization procedures have been used to pattern hydrophilic regions (Schneider

2010) or protein gradients (Fiddes 2010) inside a sealed microfluidic channel. However, this new technique combines photopolymerization with silanization backfilling to achieve alternating and contiguous two component protein patterning.

Some multi-component protein pattering methods use identical conjugation chemistries to immobilize each of the proteins.(Pritchard 1995, Brizzolara 2000, Bhatnagar 2010) These methods require alignment equipment to define the regions for each component, which adds complexity and cost to a fabrication protocol. Other protein patterning methods use different conjugation chemistries for each component. These methods rely on biochemical differences between the different proteins to spatially control their immobilization. Biochemical differences are based on the presence of cysteine residues, non-natural amino acids, genetically engineered tags, or chemical modifications. These methods have the advantage that they do not require alignment; however, their utility is limited to proteins with naturally distinguishable characteristics or proteins that are not damaged by modification.

The patterning technique reported herein is a combination of these two approaches. Two different attachment chemistries are used in the procedure, but they are distinguished only by their requirement for soluble crosslinkers. Due to this distinction, proteins added without crosslinker are immobilized on one part of the pattern and proteins added with crosslinker are immobilized on the remaining regions. No alignment is required. However, the 2 attachment chemistries are alike in that both components are immobilized by amide bond formation between surface carboxyl groups and protein amine groups. Therefore this patterning method has the advantage of being able to immobilize any two proteins or protein mixtures regardless of their composition or tolerance for modification.

Photolithographic patterning is commonly used in protein patterning. This involves the selective removal or deposition of photoresist to expose or cover reactive chemistries or adsorption surfaces (section 2.7.3). In this technique, proteins can be immobilized on the

exposed surface, while the photoresist acts as a blocking reagent to prevent immobilization on the rest of the surface. Often the photoresist is removed to backfill the remaining surface. In another version of photolithographic patterning, proteins can be immobilized onto the patterned photoresist itself. The new multi-component patterning technique described herein, uses a combination of these two methods. A photopatterned polymer is used in a similar manner as a photoresist; it acts as a blocking reagent to prevent protein immobilization on the silane surface. However, it is used not only as a blocking reagent, but also as the basis for the second immobilization chemistry. This makes the new technique simpler than many existing photolithographic patterning procedures because there is only one photopatterning step, no photomask alignment, and no photoresist removal steps.

In the multi-component patterning technique described here, the patterning is carried out after a channel is sealed and before proteins are immobilized. This avoids complications such as surface-modification effects on device bonding, bonding effects on surface modifications and biomolecule damage from radiation or patterning reagents. Also, because the entire patterning process is carried out in a sealed channel, the technique can be incorporated into almost any PDMS device, regardless of its complexity or the processing required for assembling it. A final benefit of the technique is that the reagents are inexpensive, readily available, and commonly used in other CTC isolation devices.(Nagrath 2007, Stott 2010)

3.2.4 E-selectin Deactivation through Calcium Displacement and Removal

In addition to the protein patterning discussed in section 3.2.1, a second method of counteracting unwanted leukocyte capture was devised. This method prevents E-selectin binding to facilitate leukocyte release during the device rinsing step.

E-selectin has a glycosylated ligand binding site that is complexed with a bivalent calcium ion (figure 17). If the Ca^{2+} is removed, the binding site conformation is altered and E-selectin no longer has strong affinity for its ligands. Due to the calcium dependence of E-selectin

binding, calcium free buffer has been suggested for rinsing in E-selectin functionalized devices.(King 2009) In the work described herein we take this idea further with the molecular displacement of Ca^{2+} with Mg^{2+}, and the chelation of Ca^{2+}using a Ca^{2+} specific cheating agent. The Ca^{2+} specific cheating agent ethylene glycol-bis(2-aminoethylether)-N,N,N',N'- tetra acetic acid (EGTA), was previously used in combination with Mg^{2+}. These Mg^{2+}/EGTA buffers were shown to abolish ligand binding to L-selectin but not P-selectin molecules in affinity chromatography columns.(Koenig 1998) Herein we show that this elution buffer is effective for disrupting leukocyte binding to E-selectin in a microfluidic device (section 5.1).

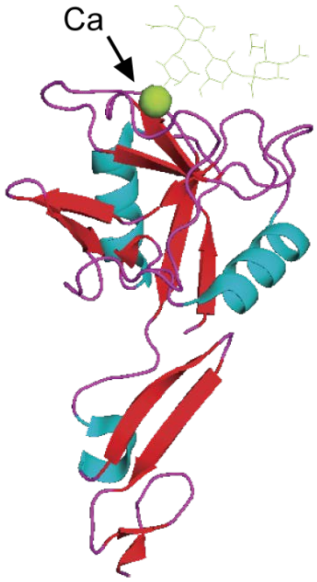

Figure 17. E-selectin. PyMOL rendering of glycosylated E-selectin molecule with bound Ca^{2+} (Protein Database 1g1t (Somers 2000)).

3.3 Hydrophoretic Cell Manipulation

As discussed in section 2.5.1, chaotic advection, which is generated from grooves in a channel wall, creates a transverse component to the axial pressure gradient generated by fluid pumping. The resulting transverse flows are forced downward at boundaries due to the incompressibility of fluids, resulting in circular flows. Cells within these flows are carried in spiral paths (figure 18) and towards channel surfaces in a process known as hydrophoresis.

In the work described herein, this process was investigated with computational modeling and flow studies with the goal of optimizing CTC contact with microchannel capture surfaces. These studies were carried out to replace traditional fluid mixing studies, which were optimized to finely fold 2 continuous fluids into each other to increase the interfacial area between components.

Continuous fluids observe very different paths than discrete particles (e.g. cells) in a micromixer. For example, the predicted paths of tumor cells through a channel are depicted in figure 18. The movement of these cells is much more confined than the movements of fluids in the similar micromixer in figure 12. Because of this disparity it seems prudent to explore the process of hydrophoresis and not fluid mixing for the optimization of CTC isolation micromixers.

In addition, the finely folded flows of the herringbone mixer may be excessive for the simple hydrophoretic focusing of large CTCs (depicted to scale as the red circle next to figure 12). For this reason, chevron mixers were investigated in addition to herringbone mixers to determine their effectiveness at hydrophoretically focusing CTCs towards immunoaffinity capture surfaces.

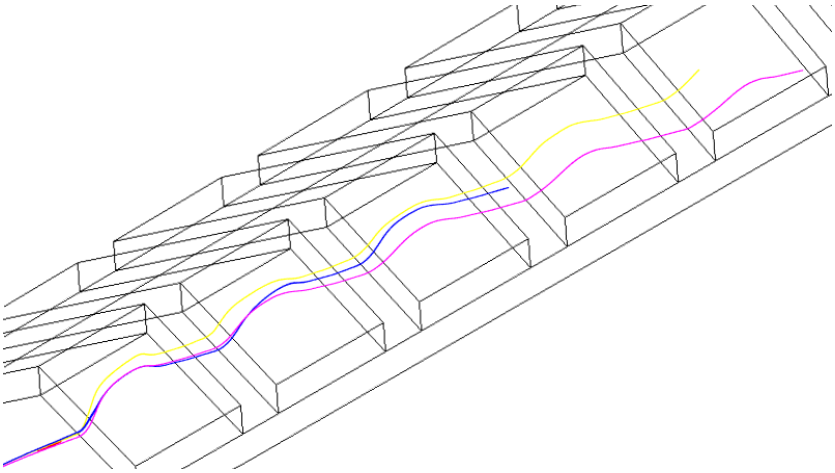

Figure 18. Modeled Cells in Microfluidic Mixer. Predicted cell paths in a chevron micromixer modeled in COMSOL Multiphysics modeling software version 3.5. The different models include the effects of gravitational settling or deceleration near channel walls.

3.4 Rheologically Biomimetic Cell Suspensions

Many microfluidic devices operate with cells suspended in buffer solutions. Researchers who work with large cell types in these devices must contend with problems of gravitational cell settling. A method for reducing this problematic settling is discussed here using microfluidic CTC isolation devices (MCIDs) as a model system.

3.4.1 Cell Settling in Tumor Cell Suspensions

Initial validation of MCIDs is carried out using buffer solutions spiked with in-vitro carcinoma cell lines. Researchers use these simplified systems for the optimization of parameters including: device configuration, device dimensions, capture surface composition, and functionalization chemistries.(Nagrath 2007, Zheng 2007, Dharmasiri 2009, Talasaz 2009, Tan 2009, Xu 2009, Gleghorn 2010) Initial experiments with carcinoma cells spiked in buffer

solution allow scientists to remove variables related to the complexity and variation of human blood. In this way, cells can be visualized and analyzed under controlled conditions.

One downfall of this method, however, is that buffer solutions have different rheological properties than whole blood, and so are of limited use in the optimization of new devices. Additionally, the low viscosities of buffer solutions result in cell settling out of suspension. This cell settling is an impediment to standardized device validation because it leads to variable cell concentrations in the test buffer. Here we describe the use of solutions containing alginate in phosphate buffered saline (PBS) to mimic blood rheology and reduce cell settling during preliminary device validation experiments.

3.4.2 Maintaining Cells in Suspension

Large cell types, such as carcinoma cells (up to 25 μm), chondrocytes (~ 20 μm), liver cells (~ 20 μm), macrophages (20–80 μm), hematopoietic stem cells (30–40 μm), and plant cells (10–100 μm) settle through buffer fluids more quickly than smaller cell types due to the larger gravitational volume force acting on these cells. PBS, a common suspension medium for cells, is a Newtonian fluid with a viscosity that is constant with respect to shear rate. Conversely, blood exhibits shear thinning with variable viscosity (figure 19 at the end of this section). PBS solutions have a viscosity close to that of water (~1 cP); while blood has a shear dependent viscosity that ranges from 3.4 cP at high shear rates to 56 cP as the shear approaches zero.(Cho 1991) The rheology of a carrier fluid affects behaviors of cells in suspension (e.g. settling velocity and aggregation).

Cells in buffer solution can be roughly approximated as rigid spheres with settling velocities described by the equation (Lamb 1994):

$$\frac{2r^2(\Delta\rho)g}{9\mu}$$

Where r is the cell radius, $\Delta\rho$ is the difference in density between the particle and the fluid, g is gravitational acceleration, and μ is the fluid viscosity. Based on this approximation, the settling velocity of a spherical cell in a dilute PBS solution is roughly 2.6 mm min^{-1}. A typical microfluidic setup may include 1.6 mm diameter feed-tubing in which cells quickly settle and adhere to the tubing walls, causing a time dependent decrease in the number of cells entering the microfluidic device (figure 37 in the results chapter). To maintain cells in suspension (in order to maintain experimental consistency), the cell suspension can be agitated or the settling velocity can be decreased in one of two ways. One way to decrease gravitational settling in fluidic applications is to use density matched buffer solutions. Unfortunately, additives for density matching are often not biocompatible. For example, sugar and other common additives increase osmolarity and otherwise perturb cells. This is not ideal for cells that will be cultured and analyzed after being microfluidically processed. Also, in complex biological fluids, the density of cells can be variable, making it difficult to match cell and fluid densities.

Since the settling velocity of a spherical particle is inversely proportional to the solution viscosity, another approach to decrease settling is to increase the viscosity of the carrier fluid. Adding a thickening agent to the buffer solutions allows one to maintain a simple experimental set-up and is a cost-effective alternative to an agitation or rocker apparatus. And unlike agitation, thickening agents have the additional benefit of reducing cell settling in the feed tubing.

Polymers provide large increases in viscosity per mole compared to other thickeners and so avoid unwanted osmolarity perturbations. Synthetic polymer solutions (such as polyacrylamide and polyvinylpyrrolidone) have been used in microfluidic devices for their rheological properties as particle carriers.(Leshansky 2007) Natural agents such as glycerine and the biopolymers xanthan gum (Brookshier 1993) and alginate have been used to mimic the

rheology of blood in flow studies. Based on precedence, these substances present themselves as potential candidates for a blood analog to be used in MCID testing.

Alginates are natural polysaccharides which are structural components of marine brown algae cell walls. They have rheological properties valuable for thickening and stabilizing, which make them popular in research and in the food, paper, textiles, cosmetics and pharmaceutical industries.(Vauchel 2008) Their rheological properties have been utilized in microfluidic devices involving ex-vivo mammalian cell preparations.(Wu 2008) Also, alginate solutions have been introduced directly into the blood circulation in animal studies.(Cabrales 2004, Cabrales 2005) Several biological and artificial polymers could be used to increase the viscosity of a cell suspension. However alginate was chosen here because of its previous application in-vivo in mammalian blood streams, which indicates that it is unlikely to interfere with the specific binding interactions in the MCID system. Cho and Kensey (Cho 1991) developed a constitutive model for the shear dependent viscosity of blood, and Brandenberger and Widmer (Brandenberger 1998) empirically determined the parameters of the power-law model for alginate solutions. These models of shear dependent viscosity are plotted in figure 19. Although the viscosities of blood and alginate solutions are variable, they are at least an order of magnitude greater than PBS solution viscosities for the typical shear range in a syringe. For the shear range within an MCID, the viscosities of alginate solutions are approximately equivalent to those of whole blood. These are at least 3 times the viscosity of PBS solutions in this range.

Besides causing a decrease in cell settling, the biomimetic rheology of alginate solutions allow for device operation at the same shear stresses and pressure drops as the final system, which will use whole blood. This is beneficial for the process of optimization, particularly if the system involves more complex fluid processing, such as passive mixing.

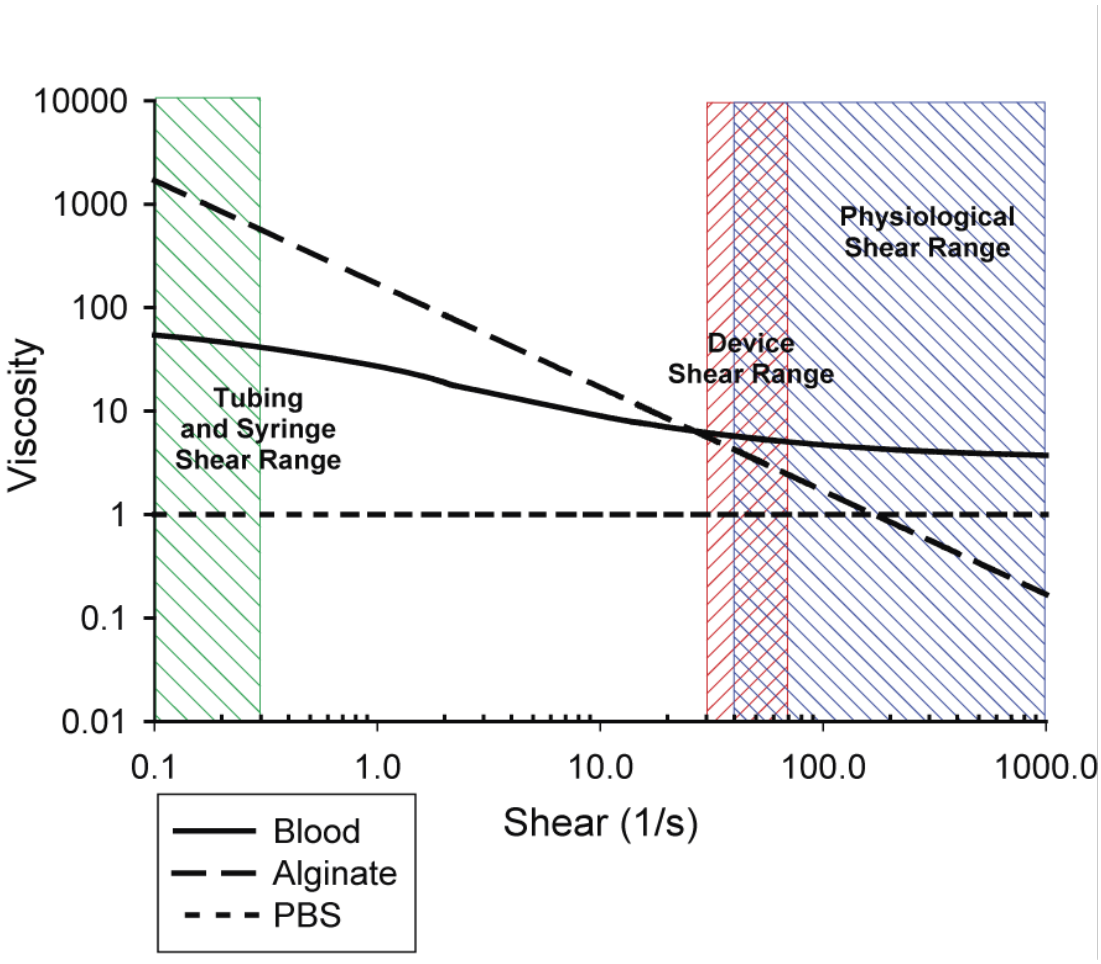

Figure 19. Plot of Viscosity in cP as a Function of Shear Rate. Plotted from constitutive models for blood (Cho 1991) and alginate (Brandenberger 1998). Blood and alginate solutions exhibit shear thinning. Note that the slope and intercept of the alginate plot will depend on the concentration and properties of the specific alginate preparation. The rheology of alginate solutions can be tailored to approximate that of blood for the shear range in any specific MCID.

3.5 Dendrimers in CTC Isolation

As discussed in section 2.8, multivalent binding that is facilitated by synthetic mult-ligand constructs is becoming popular for variety of in-vitro applications in which increased binding strength is desired. This concept has recently been applied to tumor cell isolation. Myung et al. (Myung 2011) recently reported on the use of surface immobilized seventh-generation (G7) PAMAM dendrimers that were functionalized with anti-EpCAM (figure 20). This construct enhanced tumor cell binding stability under static conditions compared to monovalent constructs, and captured up to 4 times the tumor cells from buffer suspension in a parallel plate flow chamber. Herein we report an extension of the dendrimer-mediated multivalent binding technique by its use in micromixer channels.

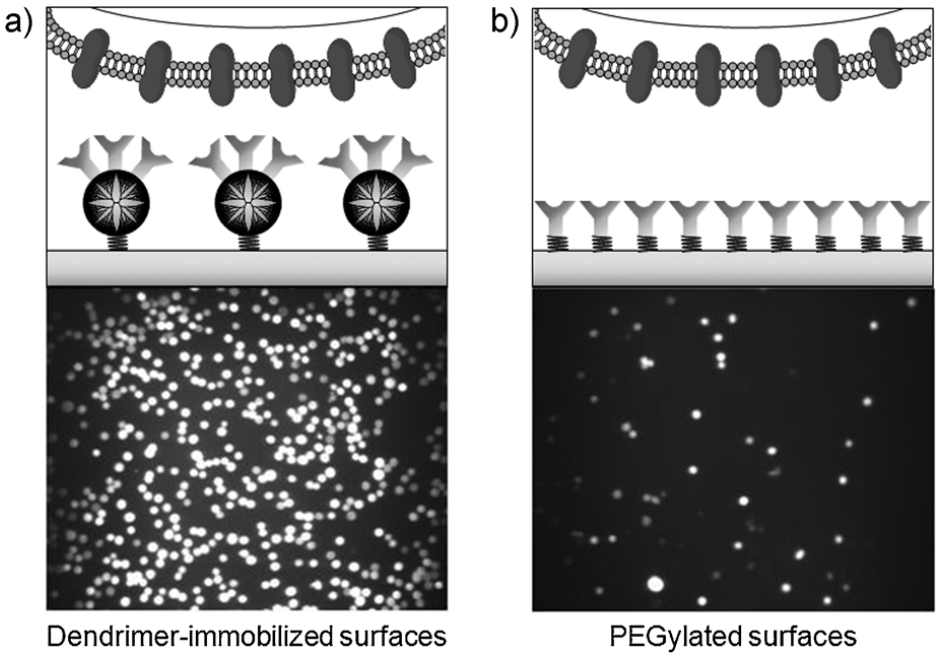

Figure 20. Tumor Cell Capture on Multivalent and Monovalent Surfaces. This image was reproduced from Myung et al.(Myung 2011) with permission from John Wiley and Sons. Copyright 2011.

CHAPTER IV. METHODS

4.1 Cell Culture and Preparation for Flow Experiments

4.1.1 Cell Culture Conditions

Flow experiments were carried out with HL-60, MCF-7, and MDA-MB-468 cell lines. HL-60 cells are derived from a human leukemia specimen and were used as a white blood cell model. MCF-7 and MDA-MB-468 are mammary gland adenocarcinomas and were used as CTC models. Cells were purchased from the American Type Culture Collection (Manassas, VA). HL-60 cells were cultured in Iscove's Modified Dulbecco's Medium supplemented with 20% (v/v) fetal bovine serum (FBS) and 1% (v/v) penicillin/streptomycin (pen/strep) in a humidified incubator at 37°C in 5% CO_2. MCF-7 cells were cultured in Eagle's Minimum Essential Medium supplemented with 10% (v/v) FBS and 1% (v/v) pen/strep in a humidified incubator at 37°C in 5% CO_2. MDA-MB-468 cells were cultured in Leibovitz L-15 media supplemented with 10% (v/v) FBS and 1% (v/v) pen/strep in a humidified incubator at 37°C in 100% air.

4.1.2 Cell Staining for Patterned-Surface Flow Experiments

Before use in flow experiments, cells were grown to 60–70% confluence in T-25 culture flasks. For clear visualization and straightforward image processing, cells were stained with Calcein AM (Sigma).(Abbitt 2000, King 2009) Carcinoma cells were washed with 3 mL PBS with cations (PBS^+), followed by incubation in 2 mL of 4 or 12 μM Calcein AM in PBS^+ at 37°C in the dark for 30 minutes. HL-60 cells were incubated with 1 or 4 μM Calcein AM in complete media at 37°C in the dark for 30 minutes. Next, carcinoma cells were washed with 3 mL PBS^+ and then 3 mL PBS without cations (PBS) to remove extracellular stain and calcium. The carcinoma cells were treated with 1 mL trypsin to detach them from the surface. Next both cell types were centrifuged, carcinoma cells at 400 rcf for 4 minutes and HL-60 cells at 500 rcf for 5 minutes. After centrifugation the cells were resuspended in 5 mL PBS^+ and then centrifuged and

resuspended again. Finally, the cell suspension concentrations were estimated using a hemocytometer and the cells were suspended in PBS^{+} at the concentrations listed below.

Homogeneous (single cell line) cell suspensions were stained with 4 µM Calcein AM. For the cell mixtures, HL-60 cells and MCF-7 cells were stained with 1 µM, and 12 µM Calcein AM, respectively. This staining scheme causes the slightly larger MCF-7 cells to appear much larger through a FITC filter set on a fluorescent microscope (figure 21). This allows the two cell types to be distinguished, so that both MCF-7 and HL-60 cell capture efficiencies can be determined for each trial. Cell suspensions of 10^4 HL-60 or 10^4 MCF-7 cells mL^{-1} in PBS^{+} were used as homogeneous cell suspensions. A combination of 10^6 HL-60 and 10^3 MCF-7 cells mL^{-1} comprised the heterogeneous cell suspensions.

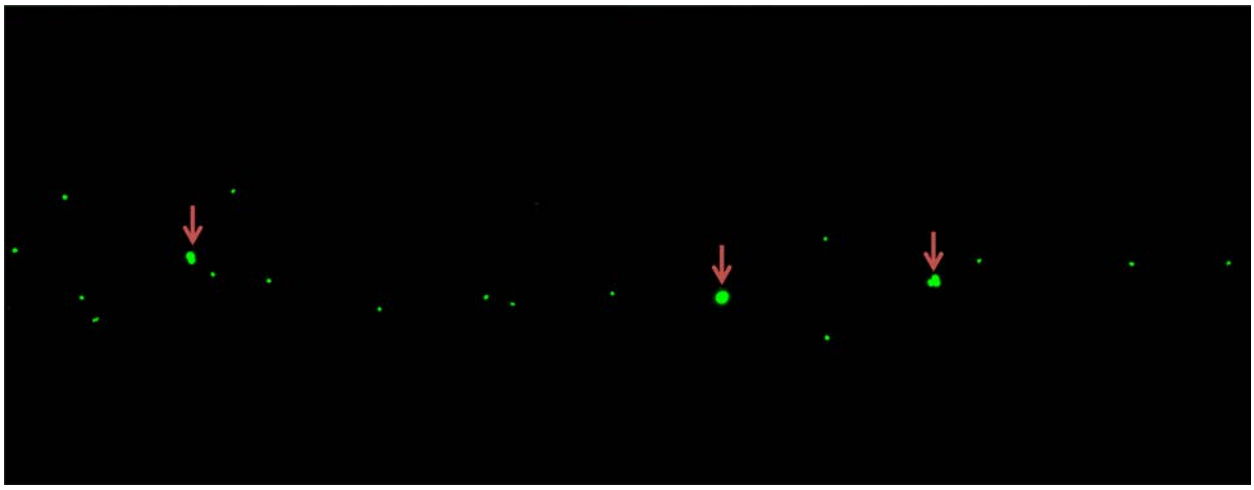

Figure 21. Image of Calcein AM Stained Cells in Microchannel. MCF-7 cells (red arrows) were stained with 12 µM Calcein AM and HL-60 cells were stained with 1 µM Calcein AM. Size and fluorescent intensity were used to score cells as HL-60 or MCF-7.

4.1.3 Cell Preparation for Blood Analog Flow Experiments

Alginate solutions were made with alginic acid sodium salt from brown algae (Sigma) dissolved in PBS. Apparent viscosity measurements of these solutions were taken with a Cannon-Ubbelohde Semi-Micro calibrated viscometer (Cannon Instrument Company, State College, PA). HL-60 and MDA-MB-468 cells were stained with 4 μM Calcein AM in PBS^{+} as described in section 4.1.2. Following centrifugation, the cells were resuspended at 10^4 cells mL^{-1} in PBS or 0.04 mg mL^{-1} alginate solution.

4.2 Micropatterning Alternating Proteins

Since blood comprises about 1% leukocytes and sometimes less than 1 CTC per billion hematological cells, it is necessary to minimize leukocyte build up on an MCID capture surface to prevent interference with CTC capture and achieve desired purity. This can be accomplished by patterning the proteins on the capture surface. In the technique described in this section, the entire capture surface of the microfluidic device is functionalized with anti-EpCAM, while regions of E-selectin are interspersed between regions without E-selectin (figure 16). As a result of this configuration, leukocytes can roll to the edge of E-selectin regions, where binding destabilization and detachment occur due to a lack of specific interactions to maintain adherence (figure 16).

4.2.1 Device Fabrication

Devices were fabricated in PDMS (Dow-Corning Corporation) with a 10:1 elastomer to curing agent ratio, using standard soft lithography techniques described by Duffy et al. (Duffy 1998) Glass slides were spin coated with PDMS at 1000 rpm for 1 minute. Devices consisted of 10 parallel channels (each with dimensions 90 μm x 660 μm x 40 mm) with a single inlet and outlet. The devices were plasma bonded to the coated slides with a hand-held corona discharge wand (Model BD-20, Electro-technic Products Inc., Chicago, IL) immediately before micropatterning.

4.2.2 Protein Patterning

Recombinant human E-selectin/Fc chimera (E-selectin), anti-human EpCAM/TROP1 polyclonal antibody (anti-EpCAM), recombinant human EpCAM/TROP-1 Fc Chimera (EpCAM), fluorescein-conjugated mouse monoclonal antihuman E-selectin (fluorescein-anti-E-selectin), and anti-human EpCAM/TROP1-Allophycocyanin (APC-anti-EpCAM) were all purchased from R&D systems (Minneapolis, MN). Unconjugated goat anti-human IgG (H + L) was acquired from Pierce Biotechnology, Inc. (Rockford, IL). All other chemicals were purchased from Sigma Aldrich (St. Louis, MO).

Surface photopolymerization of acrylic acid was used to define regions for protein immobilization. First benzophenone (BP, ≥ 99%) photo initiator was absorbed into the PDMS channel surfaces by injecting 10% BP in acetone though the channel for 10 minutes (swelling due to acetone allows BP to enter the PDMS) (figure 22a). The device was flushed with nitrogen and dried under vacuum for 15 minutes to remove the residual acetone and oxygen as oxygen quenches the polymerization reaction. A vacuum pressure below 0.01 Torr was found to produce consistent results. The devices were transferred to a nitrogen environment for 15 minutes. A solution of 20% acrylic acid monomer (≥ 99.0%) in water was degassed for 1.5 hours to remove dissolved oxygen. Degassed monomer solution was injected into the channels under the nitrogen environment to reduce oxygen diffusion into the PDMS device (figure 22a). The bottom of the device was promptly exposed to 0.5 mW cm^{-1}, 375 nm ultraviolet (UV) radiation for 210 s through a photomask (figure 22a). The UV activated the photoinitiator allowing polymerization to occur at the PDMS surface in the regions defined by the photomask. The device was flushed with water to remove the monomer solution and then flushed with ethanol to remove the BP.

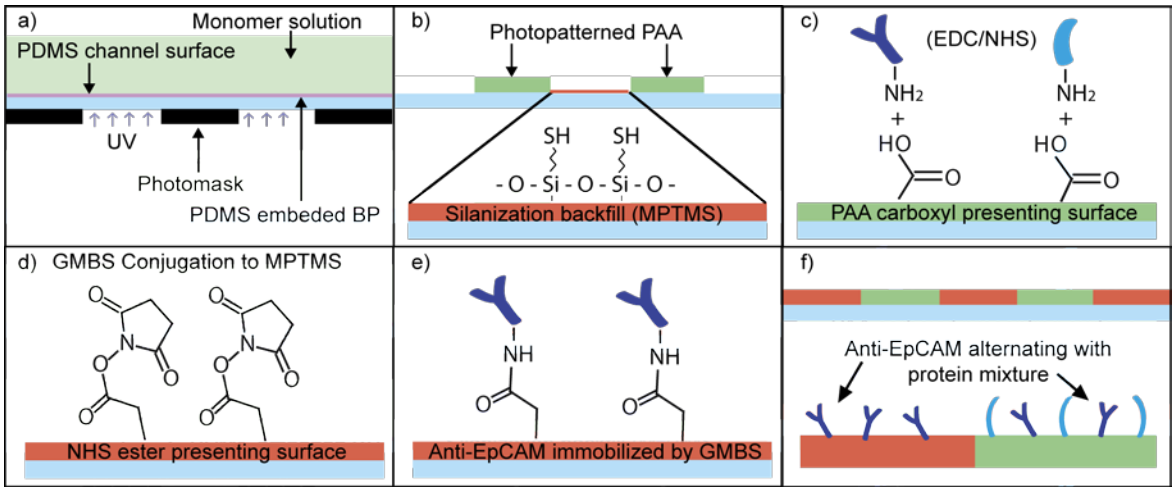

Figure 22. Surface Functionalization Process. (a) Photoinitiator (benzophenone) absorbed in the PDMS channel walls is activated by UV radiation through a photomask, initiating graft photopolymerization of the acrylic acid monomers in the channel. (b) PAA is patterned on the PDMS channel surface, blocking those regions from silanization with MPTMS. (c) PAA also provides a carboxyl presenting surface to which the protein mixture is attached using an EDC/NHS bioconjugation system. (d) Crosslinking reagent GMBS is immobilized to the sulfhydryl groups of MPTMS. (e) Anti-EpCAM is reacted with the NHS ester of the GMBS crosslinker. (f) Resultant pattern of alternating anti-EpCAM and protein mixture. Notice that both attachment chemistries involve amide bond formation between surface carboxyl groups and protein amine groups. The two surfaces are distinguished in that the PAA carboxyl presenting surface requires a soluble crosslinking agent (EDC/NHS) for amide bond formation, while the NHS ester presenting surface has a built-in cross linking agent.

This polymerization reaction was used to create channel surfaces with 1 mm, 600 µm, and 300 µm wide alternating regions of PDMS and PAA as shown in figures 23a and 22b. An asymmetric pattern with 1 mm PAA widths and 300 µm PDMS widths was also created. PAA film heights were .5 to 2 µm thick as determined using a custom built interferometer.(Yen 2011) The PAA regions created by this photopatterning presented carboxyl groups for use in the attachment of the aE-ES (figure 22c) and also blocked those regions from PDMS modification by silanization (figure 22b). After placing the devices in a vacuum chamber for 30 minutes to remove oxygen and traces of water, silanization of the remaining exposed PDMS surfaces was carried out in a nitrogen filled glove bag with the sulfhydryl-functionalized silanization reagent 3-mercaptopropyl trimethoxysilane (MPTMS (95%), 4% v/v in absolute ethanol) (figure 22b).

Next the PAA surfaces were functionalized by incubation for 2 hours in a mixture of anti-EpCAM (10 µg/mL) and E-selectin (3.9 µg/mL) in phosphate buffered saline without cations (PBS) with soluble crosslinker (0.8 mM 1-ethyl-3-(3-dimethylaminopropyl) carbodiimide, EDC and 0.8 mM N-Hydroxysuccinimide, NHS, ≥ 98.5%) (figure 20c). Subsequently 0.01 mM of the amine-to-sulfhydryl crosslinker γ-maleimidobutyryloxy succinimide in ethanol (GMBS, ≥ 98.0%) was attached to the MPTMS (figure 22d). 10 µg/mL anti-EpCAM in PBS was reacted with the GMBS for 2 hours (figure 22e). Finally, the channel was treated with 1% bovine serum albumin to cover any remaining surfaces and block nonspecific interactions between cells and the capture surface. Figure 23b shows fluorescently stained E-selectin and anti-EpCAM patterned on a channel surface using this method.

4.2.3 Protein Immobilization on Non-patterned Surfaces

Non-patterned devices were also fabricated using silane or PAA based immobilization methods. Silane devices were made using MPTMS silanization reagent and GMBS, as described above, to immobilize anti-EpCAM only (10 µg/mL), aE-ES protein mixture (10 µg/mL each) or (as a negative control) 10,000 MW methyl polyethylene glycol amine (mPEG, 50 µg/mL). Non-patterned PAA devices were made by photopolymerization of acrylic acid followed by immobilization of proteins using EDC/NHS soluble cross linker, as described above. Non-patterned PAA devices included anti-EpCAM only (10 µg/mL), aE-ES (10 µg/mL anti-EpCAM and 3.9 µg/mL E-selectin) and mPEG.

4.2.4 Fluorescent Surface Characterization

Microchannel surfaces with immobilized anti-EpCAM and E-selectin were characterized by immunostaining with APC-anti-EpCAM and fluorescein-anti-E-selectin, respectively. For the detection of E-selectin, microfluidic channels with the different PAA and silane based surface treatments were incubated with 20 µg/mL fluorescein-anti-E-selectin in PBS at 4 °C in the dark for 30 minutes, followed rinsing with PBS.

Neither a fluorophore-tagged EpCAM nor a fluorescent secondary antibody specific to anti-EpCAM is commercially available, so anti-EpCAM functionalized surfaces were fluorescently labeled in a two step procedure (Figure 24a). First, channel surfaces were incubated with 10 µg/mL EpCAM in PBS for 30 minutes at room temperature. Next channel surfaces were incubated with 20 µg/mL APC-anti-EpCAM in PBS at 4 °C in the dark for 30 minutes. Devices were then rinsed with PBS at a low shear rate.

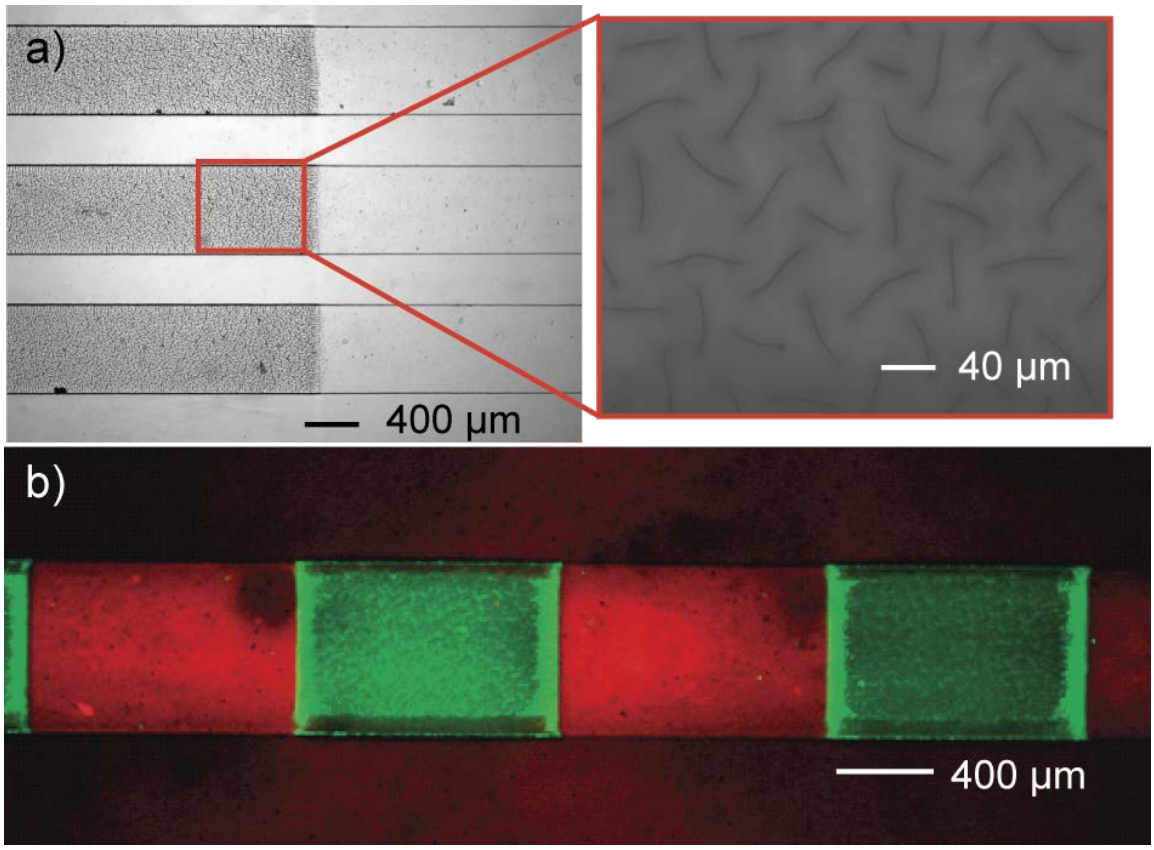

Figure 23. Patterned Microchannel Surfaces. (a) Photopatterned PAA on PDMS channel surface. (b) Patterned alternating regions of E-selectin and anti-EpCAM immunostained with APC-anti-EpCAM (red) and fluorescein-E-selectin (green).

Fluorescence images were taken using Metamorph software version 7.7.1 (Molecular Devices, Downingtown, PA) and an Olympus IX70 inverted microscope (Olympus IX70, Olympus America, Inc., Center Valley, VA) equipped with an Olympus fluorescence illuminator (AH2-RX-T), and automated stage (Prior ProScan II, Prior Scientific, Cambridge, UK). Images were captured with a CCD camera (Hamamatsu C8484) using a 10X objective and filters for FITC (488 nm excitation and 520 nm emission) and APC (650 nm excitation and 660 nm emission). Independent triplicates of each channel surface treatment were fabricated. Each channel was imaged at 10, 20 and 30 mm downstream in the 40 mm long channel. For each image, average pixel intensity values were measured using Metamorph software.

A schematic of the different characterized surfaces is presented in figure 34 in the results chapter. Devices were made with protein concentrations of 1, 3.9, 10, or 20 μg mL^{-1}. Negative controls were made by immobilizing 10 μg mL^{-1} IgG in place of the proteins. The average intensity values of the negative control were subtracted from the intensities obtained from all functionalized slides. The intensity measurements resulting after background subtraction were normalized by the average intensity values of the negative control. For the fluorescein-anti-E-selectin treated negative controls, the difference in fluorescent intensity was negligible for the silane immobilized IgG and the PAA immobilized IgG ($p = .11$). In this case the intensity measurements for all negative controls were averaged and used for background subtraction and normalizing. For the APC-anti-EpCAM treated negative controls, the difference in fluorescent intensity for the silane immobilized IgG and the PAA immobilized IgG was significant ($p < .001$). In this case, separate PAA and silane negative controls were used for background subtraction and normalizing.

4.2.5 Patterned Surface Flow Experiments

Cell suspensions were hydrodynamically processed using a syringe pump and tubing that were positioned vertically to reduce the effects of cell settling (figure 26).(Launiere

2011) A flow rate of 8 μL min^{-1} was used for all experiments. For exact capture efficiency measurements, all incoming cells were imaged on an inverted microscope (section 4.2.4) with a FITC filter as they entered the device as described in the following section (4.2.6). The two cell types in the cell mixture suspension were distinguished by size and fluorescent intensity (figure 21). Incoming cells were automatically enumerated through image analysis. For visualization of cell capture, a 100 to 1 ratio of HL-60 to MCF-7 cells (10^6 and 10^4 cells per mL respectively) were processed in the device in the same manner as the cell capture experiments.

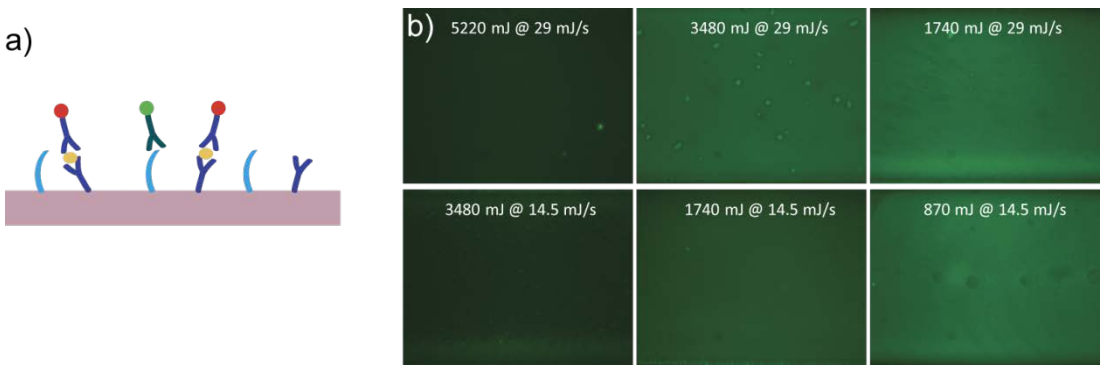

Figure 24. Immunostaining of Immobilized Proteins. (a) Immunostaining of surface immobilized anti-EpCAM (purple) and E-selectin (blue). During the two step staining of anti-EpCAM, the surface was first treated with EpCAM (yellow), followed by treatment with APC labeled anti-EpCAM (purple and red). E-selectin was directly labeled with fluorescein tagged antibody to E-selectin (green). (b) PAA surfaces, created with various UV exposure photopolymerization conditions, were functionalized with E-selectin and immunostained with fluorescein-anti-E-selectin. UV exposure intensities during photopolymerization showed a correlation with immobilization density of E-selectin.

The different surfaces tested in flow studies include: silane or PAA immobilized anti-EpCAM, silane or PAA immobilized aE-ES, a pattern of alternating anti-EpCAM and aE-ES with 1 mm, 600 µm, 300 µm or asymmetric spacing, or silane or PAA immobilized PEG as a negative control. For capture efficiency experiments, cell suspensions were injected into the device for 10 minutes followed by device rinsing for 10 minutes. A rinse buffer, containing the calcium specific chelating agent ethylene glycol-bis(2-aminoethylether)-N,N,N',N'- tetra acetic acid (EGTA, 5 mM, ≥ 97.0%), and 3 mM $MgCl_2$ in PBS at 295 mOsm total, was used to remove leukocytes without displacing captured tumor cells. After rinsing, the number of captured cells was enumerated and divided by the number of cells which had entered the device to calculate the capture efficiency. Rinsing studies were carried out in a similar fashion except cells captured on protein mixture functionalized surfaces were enumerated before and after rinsing with 295 mOsm total: PBS^{+}, PBS, PBS with 5 mM EGTA, or PBS with 5 mM EGTA plus 3 mM Mg^{2+}.

4.2.6 Data Processing and Statistical Analysis

As cell suspensions were injected into the device, the inlet imaging region (figure 25) was imaged at one frame per cell residence time in the field of view using the inverted microscope described in section 4.2.4. This was done to monitor the number of incoming cells.(Launiere 2011) Image analysis was executed using MetaMorph software and the integrated morphometry analysis feature was used to identify and enumerate the fluorescently labeled cells (figure 25). Cell dimensions were recorded and all data was exported to an excel file for further analysis. A custom visual basic for applications program was written to analyze the objects identified as cells. Objects with areas more than 1.5 standard deviations above or below the average object area were considered cell debris or imaging artifacts and were not included in the final cell count. For 10 trials, the cells were also counted by hand to estimate the fidelity of the automated counting system. There was an acceptable 4.3% average difference between the automated and hand cell counts.

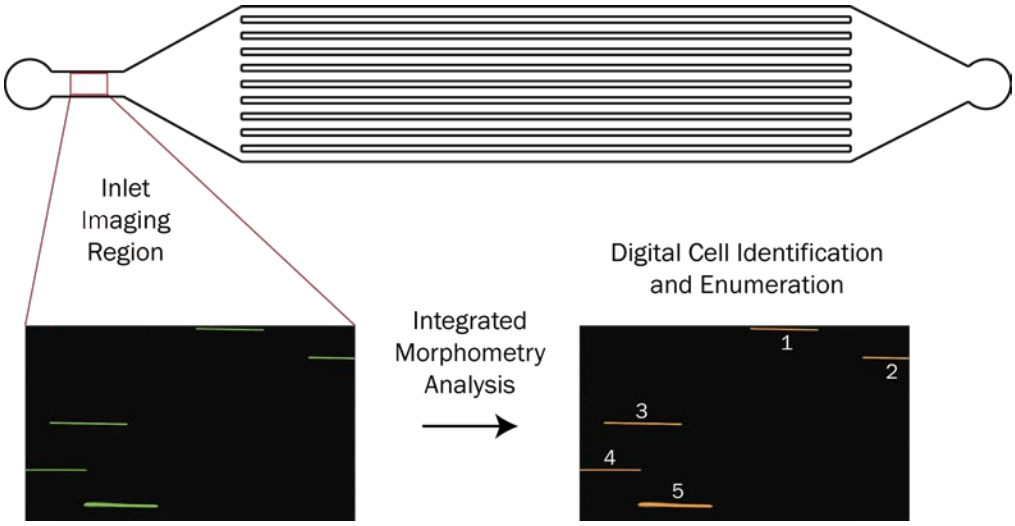

Figure 25. Inlet Imaging Region. Fluorescently labeled cells are imaged as they enter the device. Cells are identified with image processing software and enumerated for accurate capture efficiency measurements.

For cell capture experiments, captured cells were counted under flow to distinguish between bound cells and cells remaining in bulk flow. Only bound cells were counted. The number of captured cells was divided by the number of cells which entered the device to get the capture efficiency. One-way ANOVA, conducted with GraphPad InStat software version 3.10, was used to compare the mean capture efficiencies of the different surfaces.

4.3 Dendrimers

4.3.1 Dendrimer based anti-EpCAM immobilization

PDMS channels were bonded to glass slides using a handheld corona discharge wand. Bonded devices were baked at 65°C for 2 minutes following bonding. Devices were then placed in a vacuum chamber for 30 minutes followed by venting the vacuum to nitrogen and transferring the devices to a nitrogen filled glove bag. Devices were equilibrated for 15 minutesbefore being injected with a 4% solution of MPTMS in ethanol. Devices were monitored for solvent evaporation over 1 hour and refilled as necessary. Devices were then removed from the glove bag and flushed with ethanol. Next a solution of 1 µM GMBS was made by dissolving GMBS in 10% DMSO and adding 90% ethanol. This solution was injected into the channel immediately and incubated for 30 minutes. Afterward, the device was flushed with ethanol and treated with heterobifunctional PEG in water (NH2-PEG-COOH, MW 10,000, 0.5 mg/mL, 0.1 mM) for 2 hours. The unreacted PEG was rinsed out with water. A solution of 0.8 mM EDC and 0.8 mM NHS in water was prepared and incubated in the channels for 30 minutes. Without rinsing, the channels were then treated with partially carboxylated G7 PAMAM dendrimer (5.6 µM in pH 9.0 PBS buffer, kindly provided by Seungpyo Hong at the University of Illinois at Chicago) for 2 hours. Unreacted dendrimer was flushed out with water. A fresh solution of 0.8 mM EDC and NHS in water was prepared and incubated in the channels for 30 minutes at room

temperature. Next, the channels were treated with a solution of 10 µg/mL anti-EpCAM in PBS for 2 hours at room temperature. Unreacted anti-EpCAM was removed by rinsing with PBS. Finally, the devices were treated with a 1% solution of BSA in PBS. All devices were used within 2 days.

Other surfaces used in flow experiments were made by immobilizing of 10 µg/mL anti-EpCAM in PBS onto the EDC/NHS activated PEG surface (in place of dendrimer). Surfaces were also fabricated by immobilizing anti-EpCAM or aE-ES directly onto the GMBS surface (in place of PEG). A control surface was made by immobilizing mPEG in place of PEG on the capture surface as described in section 4.2.3.

4.3.2 Dendrimer flow studies

Cells were stained and prepared at a concentration of 10^4 cells mL^{-1} in PBS as described in section 4.1.2. Cell suspensions were hydrodynamically processed through devices at a shear rate of 15 s^{-1} for 10 minutes followed by 10 minutes of rinsing with PBS at the same flow rate. Capture efficiency was determined as described in section 4.2.6. In the capture and retention efficiency studies, either the capture step or the rinse step flow rate was held constant while the other step was performed at variable shear including: 15, 30, 60 and 120 s^{-1} (corresponding to flow rates of 8, 16, 32 and 64 µL min^{-1}). For retention efficiency measurements the number of cells bound on the capture surface after rinsing was divided by the number of cells bound on the capture surface before rinsing.

4.4 Blood Analog for Preliminary Device Validation

A blood analog was created by the addition of alginate biopolymer to cell suspension buffer. The feasibility of using this analog for the validation of immunoaffinity CTC isolation devices was examined.

4.4.1 Microfluidic Device Design and fabrication

Sample CTC isolation devices were used in the blood analog studies, which consisted of 10 parallel rectangular channels (660 μm width × 90 μm height × 40 mm length) with an extended imaging region near the inlet (figure 25). The ceilings and walls were fabricated in PDMS and were covalently bound to 35 mm × 75 mm glass slides by oxygen plasma treatment (Plasmatic Systems, Inc. Plasma-Preen II-862, North Brunswick, NJ).

4.4.2 Device Surface Modification

Incoming cell studies were carried out to analyze the cell suspension properties of the blood analog. For incoming cell enumeration studies, the microchannels were coated with albumin from bovine serum (BSA, Sigma-Aldrich, Inc., St. Louis, MO) to block cell interactions with the channel surfaces. Solutions of 1.0% w/v BSA in PBS were injected into the devices. Devices were incubated for 30 minutes at ambient temperature to allow for protein adsorption. They were then flushed with 2 mL PBS.

For cell capture experiments, microchannel surfaces were functionalized by adsorption of 10 μg/mL anti-EpCAM in PBS. Devices were incubated with the protein solution for 4 h at ambient temperature followed by flushing with 2 mL PBS. Lastly, the microchannels were treated with BSA solution to block non-specific interactions. The prepared devices were kept at 4°C in PBS to prevent damage to the immobilized proteins and were used within 2 days.

4.4.3 Cell Suspension Flow Experiments

Cell suspensions were hydrodynamically processed using a syringe pump (New Era Pump Systems Inc., Farmingdale, NY) positioned horizontally or vertically (figure 26a). Gauge 8 tubing (1.57 mm I.D. X 3.18 mm O.D., Dow corning, Midland, MI) was used to connect the syringes (5 mL, Becton Dickinson, Franklin Lakes, NJ) to the devices. For the horizontal condition, the pump, syringes, and tubing were all on the same horizontal plane as the device (section 4.5.1 figure 26a right). For the vertical condition, these components were orthogonal to

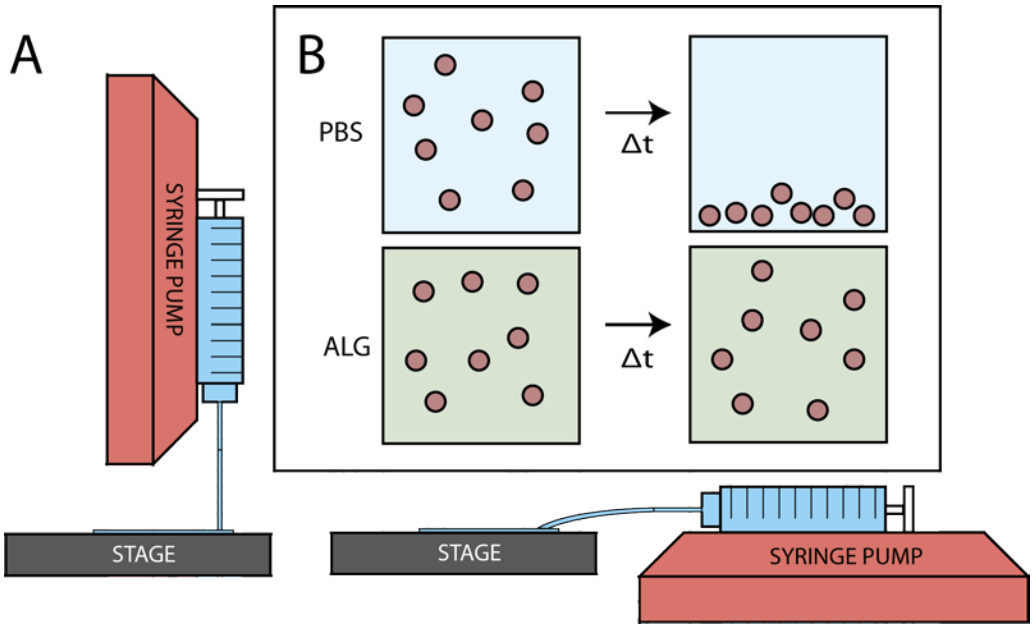

Figure 26. Feed Tubing Configurations and Cell Settling. (a) Syringe and inlet tubing configurations. (b) Cell settling in alginate and PBS suspensions.

the device (figure 26a left). A flow rate of 8 µl min^{-1} (shear rate of 15 s^{-1}) was used for all experiments.

For all flow studies, cell suspensions were agitated before each trial to re-suspend settled cells. For incoming cell enumeration studies, cell suspensions were injected into the device for 10 min. For cell capture experiments, cell suspensions were injected into the device for 5 minutes followed by flushing with PBS for 10 minutes to remove suspended or loosely bound cells.

4.4.4 Data Acquisition and Statistical Analysis

Images were taken using the inverted microscope system described in section 4.2.4, and incoming and captured cells were enumerated using the method described in section 4.2.6.

Statistical analysis was carried out using GraphPad Prism software version 2.1. Two-tailed ANCOVAs were conducted to compare regression curve slopes for the incoming cell enumeration data. For the capture efficiency experiments, results were compared using a two-tailed unpaired t-test.

4.5 Hydrophoresis Studies

4.5.1 Early Iteration Mixer Devices

Several mixer device designs were tested for their ability to improve tumor cell capture in devices functionalized with anti-EpCAM. PDMS devices with ceiling mixer features were oxygen-plasma bonded to glass slides using a corona discharge wand. The channel surfaces were functionalized by adsorption of anti-EpCAM (5 μg mL^{-1} in PBS, incubated for 4 hours at room temperature). Devices were treated with 1% BSA in PBS for 30 minutes to cover remaining surface to reduce non-specific binding of cells to the capture surface. The devices were stored at 4ºC and used within two days.

Mixer devices were compared to flat channel devices with the same average height in flow studies using MCF-7 and MDA-MB-468 cells suspended in PBS^{+}. Initially, wide single channel devices with multiple rows of ceiling mixer features were tested (figure 27), because this type of device has a high throughput relative to individual channels having a single row of mixer features.

However, this design type was not effective at increasing tumor cell capture. It was determined that walls are required for maximum conversion of ceiling feature generated transverse flows into flows that carry cells towards the capture surface. The flows in the multi-row device instead acted to focus the cells into streamlines (figure 27b).

a)

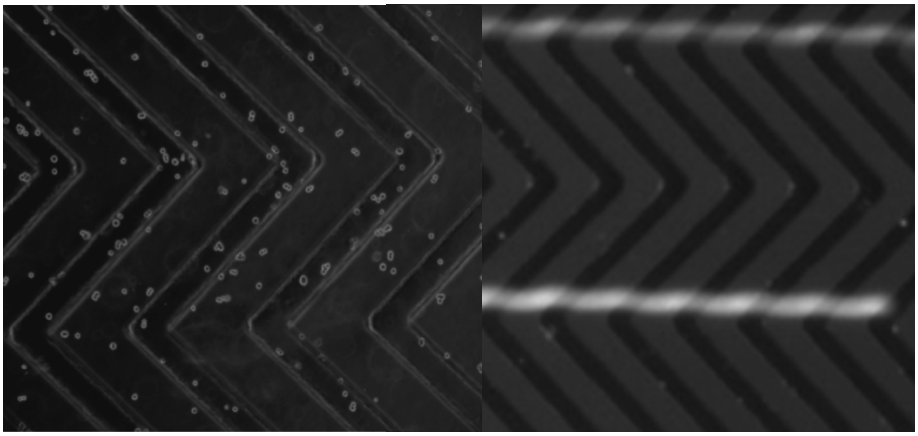

Figure 27. Cell Focusing in Multi-Chevron Mixers. Upstream in multiple row chevron mixers (left), cells are randomly distributed. Downstream (right) in multiple row chevron mixers, cells are focused into streamlines.

4.5.2 COMSOL Version 3.5 Modeling Studies

Several models were constructed in COMSOL multiphysics modeling software version 3.5 to analyze flow and cell migration in MCIDs. These models included a 10 channel flat walled device with a single inlet and outlet (figure 28), and single channel mixers of various heights (figure 30). The pressure and velocity fields were solved for in the 10 channel device model to investigate entrance effects for the design. It was determined that a larger 8 gauge inlet tube (figure 28b) is preferable to 11 gauge inlet tubing to reduce uneven flows in the capture channels. These models concurred with experimental findings (figure 28c and 28d).

Cell migration in single channel slanted groove mixers (figures 29a and 30) were analyzed using the particle tracing module in COMSOL 3.5 (figure 30b).

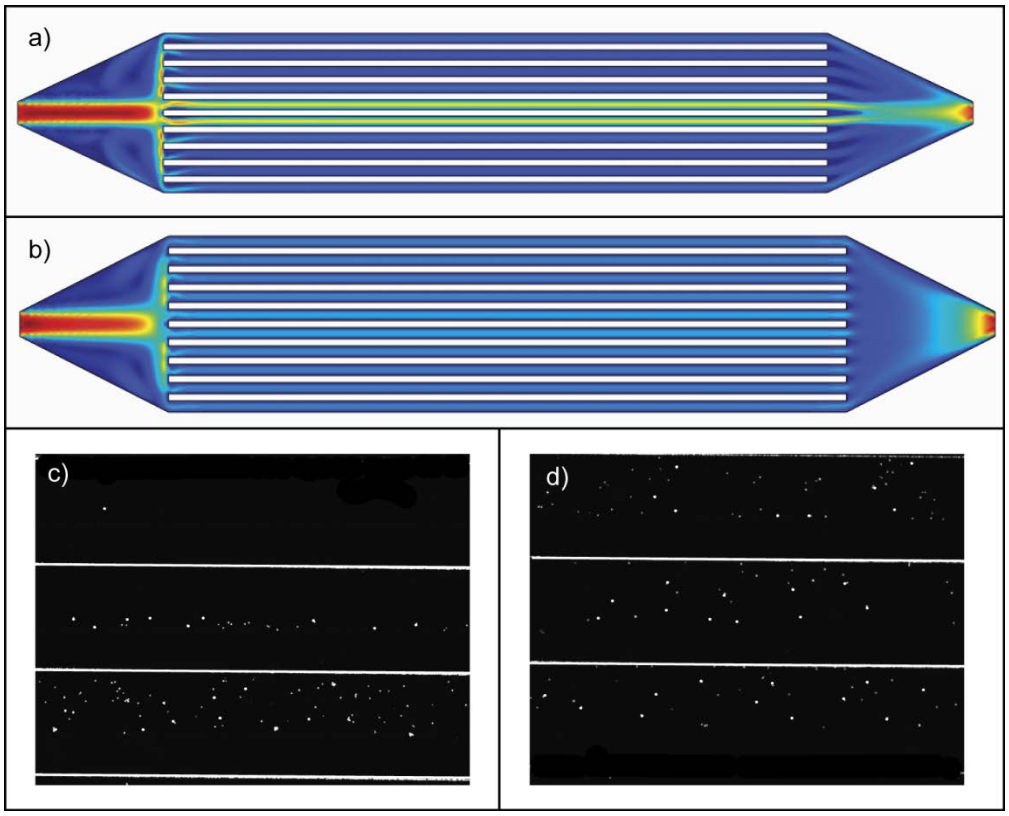

Figure 28. Channel Entrance Effects. COMSOL rendering of fluid velocity field in microfluidic device with 11 gauge (a) or 8 gauge (b) feed tubing. Bright field microscope images of cells fed into device with 11 gauge (c) or 8 gauge (d) tubing. Notice the uneven (c) and even (d) distribution of cells with the different feed tubing diameters.

Figure 29. Ceiling Groove Structures for Hydrophoresis.
(a) Slanted groove (b) Chevron and (c) Herringbone mixers.

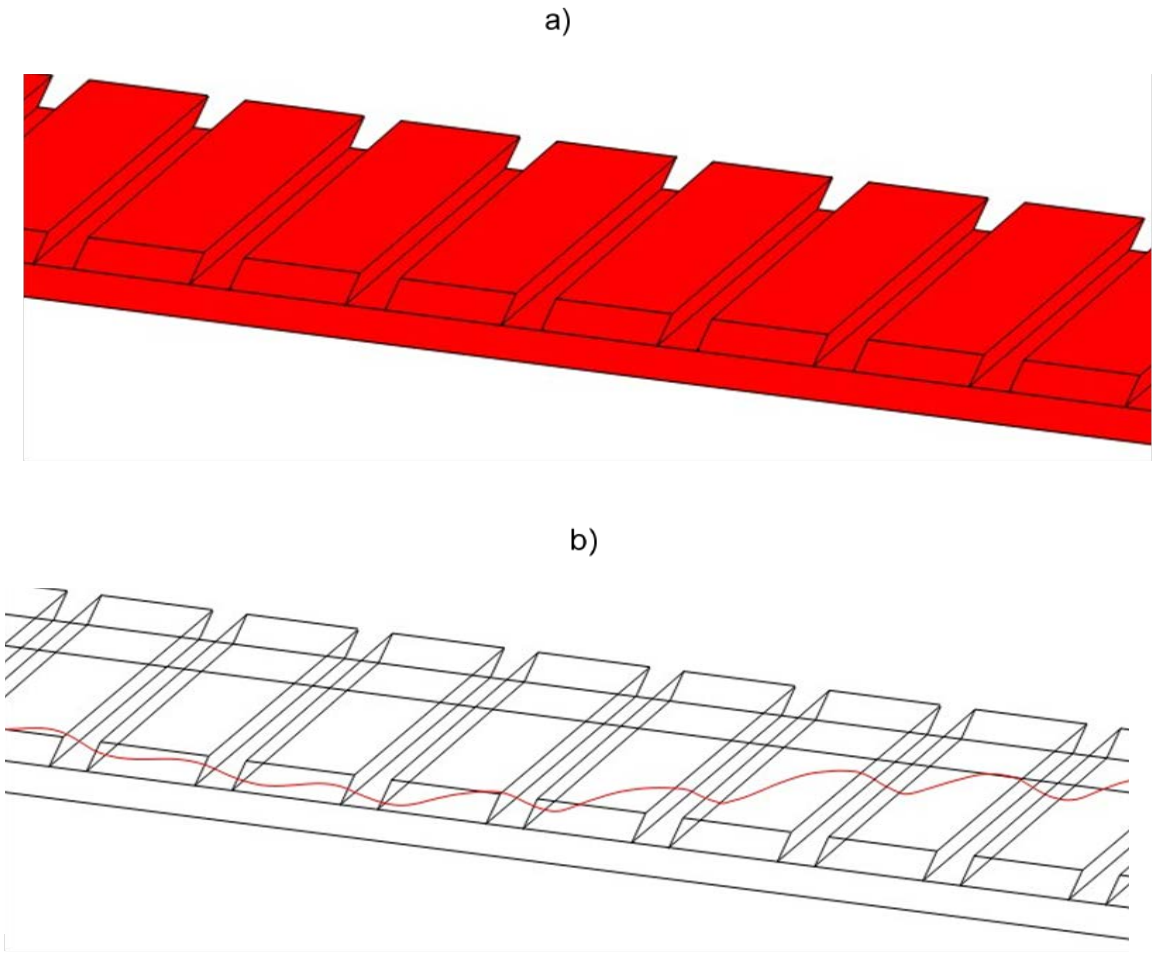

Figure 30. Slanted Groove Mixer Channel. (a) Solid view. (b) Wireframe view with trace of estimated cell path through the micromixer channel.

Pressure and velocity fields in the model device were solved for and used to predict the paths of cells under drag forces in mixer with heights and groove depths ranging from 50 µm to 100 µm. The models were solved for using both PBS and blood viscosities.

4.5.3 Second Iteration Mixer Devices

Second iteration mixer designs for this work had 10 parallel channels with a single inlet and outlet (figure 25). The channel height and groove depth of 50 µm was selected based on the COMSOL 3.5 modeling results reported in section 5.4.1. The other mixer parameters were optimized based on the 50 µm dimension using calculations from previously reported numerical studies for fluid mixing.(Lynn 2007) The final dimensions for the chevron micromixers (figure 29b) used in flow studies were: 50 µm channel height, 50 µm groove depth, 330 µm groove width, 100 µm ridge width and 660 µm channel width. Control flat walled channels were also fabricated that had the same average height as the mixer devices.

PDMS channels with grooved ceiling features were oxygen plasma bonded to glass slides using a corona discharge wand. Mixer efficacies were tested with anti-EpCAM covalently immobilized on the channel surfaces in one of two ways. One was by the dendrimer immobilization procedure described in section 4.3.1. The second immobilization scheme included the immobilization of anti-EpCAM directly onto PEG in place of the dendrimer (using the same EDC/NHS treatment).

4.5.4 COMSOL 4.2a Modeling Studies

A detailed description of the COMSOL 4.2a modeling studies is reported in the appendix. Two different hydrophoresis inducing mixers were investigated. These were the chevron mixer (figure 29b) and the herringbone mixer (figure 29c). 6 mm sections of mixer were modeled, and steady state velocity and pressure fields were solved for. After stationary solver computations, the time dependent particle tracing module in COMSOL was used to predict the

paths of 100 cells through each device. The transmission efficiency, the fraction of cells that did not contact a surface in the 6 mm mixer section, was determined for each model.

CHAPTER V. RESULTS

5.1 Leukocyte Elution Buffer for Increased Capture Purity

The MCF-7 and HL-60 cell retention rates after rinsing with the 3 different leukocyte elution buffers (plus PBS^{+} as a control) are presented in figure 31.These elution buffers include PBS, PBS plus EGTA, and PBS plus EGTA with Mg^{2+}.

Cell retention rates were calculated by dividing the number of surface bound cells remaining after rinsing by the original number of captured cells. There were no significant differences ($p > 0.05$) in carcinoma cell retention for any of the 4 buffers. These surfaces had 92-95% retention of MCF-7 carcinoma cells on the aE-ES surface after the 10 minute rinsing period. This is expected because the carcinoma cells are firmly adhered to the anti-EpCAM. Conversely, these same surfaces had a high, 56%, leukocyte retention rate with the PBS^{+} rinse, which dropped significantly to 31%, 19% and 13% for the PBS, EGTA, and EGTA plus Mg^{2+} buffers, respectively ($p < 0.001$). A visualization of captured cells before and after rinsing with elution buffer is presented in figure 32a and 32b, respectively.

Another measure of the effects of rinsing buffer on leukocytes is presented in figure 33. This graph shows the average migration/rolling speed of HL-60 cells in flow devices with E-selectin functionalized surfaces. HL-60 cells in PBS^{+} rinse buffer had the slowest rates of migration over the E-selectin surfaces. In the calcium free EGTA buffer, the cells migrated significantly faster ($p < 0.001$). Adding Mg^{2+} to the rinse buffer resulted in another significant increase in HL-60 cell migration over the E-selectin surface ($p < 0.05$).

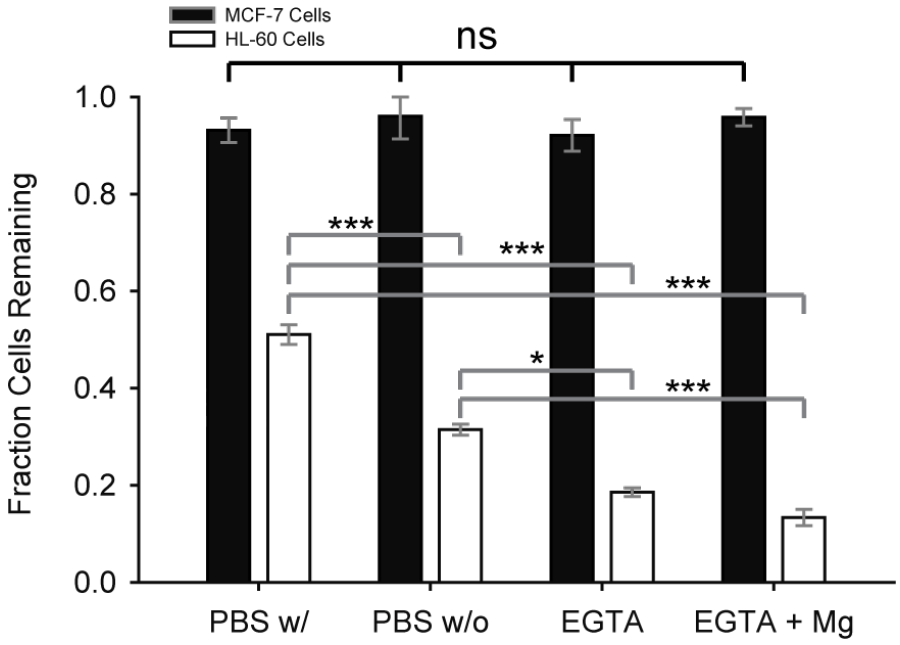

Figure 31. Rinsing Buffer Effects on Leukocyte Retention. Leukocyte or tumor cell retention on protein mixture functionalized surfaces after rinsing with various elution buffers (n = 4). Error bars denote standard error. One way ANOVA: ns = not significantly different from others of same cell type. *** p< 0.001. * p< 0.05.

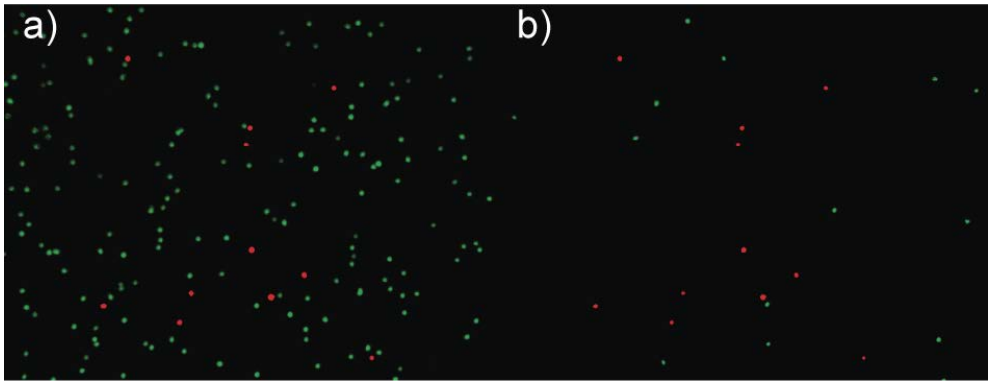

Figure 32. Cells Captured on aE-ES Surface. (a) Before and (b) After rinsing with leukocyte elution buffer.

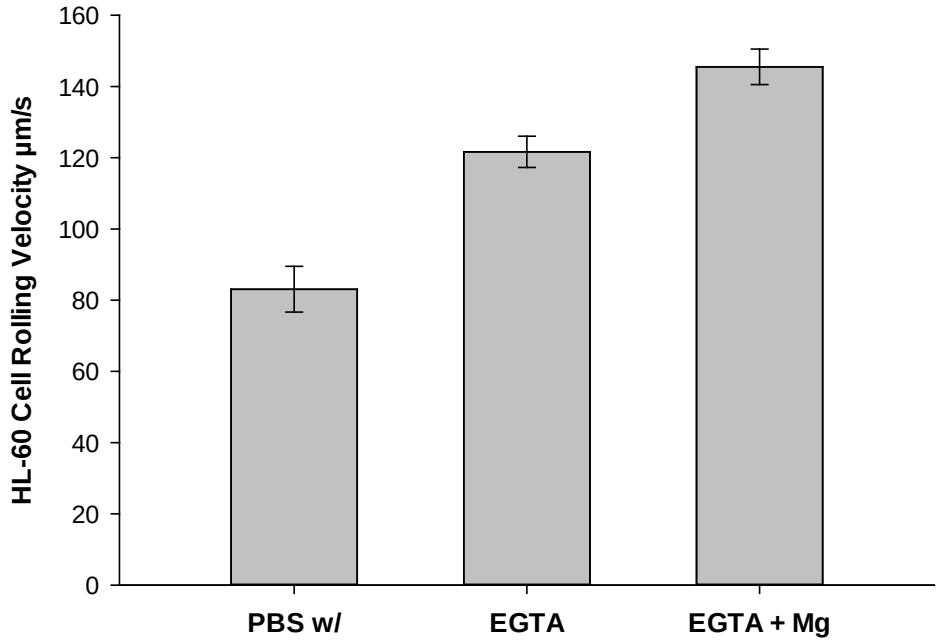

Figure 33. HL-60 Cell Rolling Velocity. On E-selectin functionalized surfaces under flow (shear rate of 15 s^{-1}) with various rinsing buffers.

5.2 Two Component Protein Micropatterning for Increased Tumor Cell Capture Efficiency and Capture Purity

Although the EGTA plus Mg^{2+} elution buffer is 60% more effective at removing captured leukocytes during the rinsing step than PBS^{+}, it only rinses away 87% of the leukocytes captured during sample processing step. For this reason, another method is employed to reduce the number of leukocytes originally captured on the protein mixture surface during the sample processing step. The second method for reducing leukocyte capture involves patterning alternating regions with and without E-selectin. On this surface, captured leukocytes may roll a short distance and detach (figure 16), thus decreasing the number of captured leukocyte impurities.

5.2.1 Surface Characterization

The first step in the validation of the novel protein patterning technique was the characterization of the protein functionalized surfaces. The different surfaces analyzed by fluorescent immunostaining are pictured in figure 34. The results from the E-selectin immunostaining study are presented in table I. A regression analysis of the results from the 1, 10, and 20 µg/mL E-selectin concentration surfaces indicated that an E-selectin concentration of 3.9 µg/mL immobilized on a PAA surface will produce the same surface density of E-selectin as the 10 µg/mL silane surface. This was confirmed by fluorescent characterization of the 3.9 µg/mL surface. The results from the anti-EpCAM immunostaining study are presented in table II.

The results of the fluorescent characterization studies show that there is not a significant difference in fluorescent intensity between the 10 µg/mL and 20 µg/mL groups ($p > 0.05$). This indicates that 10 µg/mL is sufficient to saturate the surfaces. This is further supported by the decrease in intensity between the silane-immobilized anti-EpCAM and the anti-EpCAM in the silane-immobilized protein mixture. It is important to note the significant ($P < 0.001$) increase in fluorescent intensity for the pattern PAA immobilized E-selectin over the non-patterned silane immobilized E-selectin for both the 10 µg/mL and 20 µg/mL groups. The intensity increase could be a result of a higher protein immobilization density, which could be due to the greater surface area of the textured PAA surface (figure 23a). To account for this discrepancy, an E-selectin concentration of 3.9 µg/mL was used with the PAA surfaces in the flow studies to create a surface with the same surface density as the silane surfaces. It is likely that the anti-EpCAM co-immobilized with E-selectin on the patterned PAA surface is also greater than the anti-EpCAM co-immobilized on the silane surface, although in this case a direct comparison is not possible due to the difference in fluorescent background intensities.

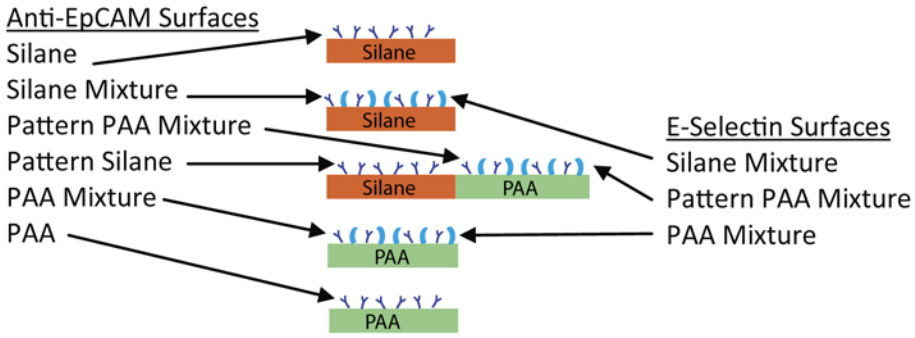

Figure 34. Surfaces Characterized by Immunostaining

Table I. Fluorescent Intensities of Surfaces Treated with Fluorescein-anti-E-selectin.

Surface Treatment	1 µg/mL	3.9 µg/mL	10 µg/mL	20 µg/mL
Silane Mixture	6.3 ± 2.5	24.2 ± 18.1	62.4 ± 16.9	67.4 ± 13.5
Pattern PAA Mixture	14.1 ± 13.0	67.1 ± 25.3	165 ± 18.5	156 ± 35.7
PAA Mixture	20.9 ± 6.9	75.8 ± 31.0	181 ± 25.8	192 ± 43.9

Table II. Fluorescent Intensities of Surfaces Treated with APC-anti-EpCAM.

Surface Treatment	1 µg/mL	10 µg/mL	20 µg/mL
Silane	2.2 ± 1.6	11.1 ± 6.7	14.2 ± 2.9
Silane Mixture	2.6 ± 3.5	5.6 ± 3.8	8.3 ± 4.5
Pattern Silane	2.5 ± 2.5	9.8 ± 5.1	11.8 ± 3.2
Pattern PAA Mixture	2.9 ± 2.3	12.6 ± 4.8	18.0 ± 4.3
PAA	3.4 ± 3.9	16.9 ± 4.7	19.7 ± 8.6
PAA Mixture	2.1 ± 1.5	15.4 ± 6.2	21.2 ± 7.1

5.2.2 Flow Studies

Flow studies were carried out to test the efficacy of the patterned surfaces compared to monolithic surfaces. Devices were functionalized with: silane or PAA immobilized anti-EpCAM, silane or PAA immobilized aE-ES, a pattern of alternating silane/anti-EpCAM and PAA/aE-ES with 1 mm, 600 µm, 300 µm or asymmetric spacing, and silane or PAA immobilized PEG (negative controls). These devices were tested with cell suspensions that were either homogeneous, 10^4 cells mL^{-1}, or cell mixtures with 10^6 HL-60 and 10^3 MCF-7 cells mL^{-1}. All devices were rinsed with the EGTA/Mg^{2+} solution for 10 minutes after cell suspensions were processed through the devices.

Table III shows the results from the flow studies. It is organized, first, by the basis of protein immobilization (silane, PAA, or the pattern of alternating silane and PAA), and then by the proteins immobilized by this method (anti-EpCAM or aE-ES) or by the spacing of the pattern sections. The capture efficiencies are reported as the mean ± the standard error. The statistical analysis of the flow study results is summarized in table IV.

Table III. MCF-7 and HL-60 Cell Capture on Patterned and Non-patterned Surfaces. Mean cell capture efficiency ± standard error. (n = 3 or 4)

Capture Surfaces		Mean Capture Efficiency (% ± std.err.)	
Immobilization Base	Immobilized Proteins or *Pattern Spacing	*Homogeneous Cell Suspensions* MCF-7 (10^4 mL^{-1})	HL-60 (10^4 mL^{-1})
Silane	anti-EpCAM	47.1 ± 3.8	7.0 ± 1.3
Silane	Mixture	79.4 ± 5.1	30.1 ± 1.2
Silane	PEG	8.0 ± 2.3	4.2 ± 1.7
PAA	anti-EpCAM	60.6 ± 5.3	5.5 ± 0.7
PAA	Mixture	86.7 ± 2.0	26.5 ± 3.2
PAA	PEG	4.9 ± 0.7	4.7 ± 1.0
Pattern	*Asymmetric	90.1 ± 4.4	16.1 ± 2.7
Pattern	*1000 µm	85.7 ± 4.6	8.4 ± 0.9
Pattern	*600 µm	86.9 ± 4.3	8.1 ± 1.0
Pattern	*300 µm	89.6 ± 2.5	5.4 ± 0.6
		Cell Mixture Suspensions MCF-7 (10^3 mL^{-1})	HL-60 (10^6 mL^{-1})
Silane	anti-EpCAM	42.2 ± 5.6	4.9 ± 0.8
PAA	anti-EpCAM	44.9 ± 4.9	5.0 ± 1.0
Pattern	*300 µm	84.1 ± 10.3	5.2 ± 0.6

Table IV. Index of Statistical Analysis for MCF-7 and HL-60 Cell Capture. This table summarizes the level of statistical significance for the differences in capture efficiencies for the different experimental groups discussed in the text. One way ANOVA was used to determine the statistical significance of differences in mean capture efficiency. Superscripts: ns not significantly different ($p > 0.05$), *** $p < 0.001$, ** $p < 0.01$, * $p < 0.05$

Capture Surfaces		Mean (%)	Statistical Analysis	Mean (%)	Statistical Analysis
Immobilization Base	Protein(s) or *Pattern Spacing	*Homogeneous Cell Suspensions*			
		MCF-7 (10^4 mL^{-1})		HL-60 (10^4 mL^{-1})	
Silane	anti-EpCAM	47.1	a^{ns}, c*, e^{x}	7.0	j^{ns}, k***
Silane	Mixture	79.4	b^{ns}, c*, f^{ns}	30.1	o^{ns}, k***, m^{x}
Silane	PEG	8.0	j^{ns}	4.2	j^{ns}
PAA	anti-EpCAM	60.6	a^{ns}, d*, g^{x}	5.5	j^{ns}, l**
PAA	Mixture	86.7	b^{ns}, d*, f^{ns}	26.5	o^{ns}, l**, n^{x}
PAA	PEG	4.9	j^{ns}	4.7	j^{ns}
Pattern	*Asymmetric	90.1	e***, f^{ns} g*	16.1	m***, n**
Pattern	*1000 µm	85.7	e**, f^{ns}	8.4	j^{ns}, m***, n***
Pattern	*600 µm	86.9	e***, f^{ns}, g*	8.1	j^{ns}, m***, n***
Pattern	*300 µm	89.6	e***, f^{ns}, g*	5.4	j^{ns}, m***, n***
		Cell Mixture Suspensions			
		MCF-7 (10^3 mL^{-1})		HL-60 (10^6 mL^{-1})	
Silane	anti-EpCAM	42.2	a^{ns}, h***	4.9	j^{ns}
PAA	anti-EpCAM	44.9	a^{ns}, i***	5.0	j^{ns}
Pattern	*300 µm	84.1	f^{ns}, h***, i***	5.2	j^{ns}

5.2.3 Carcinoma Cell Capture

The goal of microfluidic immunoaffinity based CTC isolation is to separate CTCs from other blood components through specific binding to a capture surface. Due to the rarity of CTCs in blood, it is important to achieve a high CTC capture efficiency to limit the amount of blood needed from a patient. Here we compared the capture efficiencies of the capture surfaces discussed above using MCF-7 cells as a CTC model.

As expected based on our previous results (Myung 2010) and the known ability of E-selectin to pull cells out of flow, there was a significant increase in MCF-7 cell capture between the anti-EpCAM and aE-ES functionalized surfaces (table IV c and d). Adding E-selectin to the capture surface increased MCF-7 capture 1.6 fold for the silane surface and 1.7 fold for the PAA surface.

Alternately, there was not a significant difference in MCF-7 capture efficiencies between the aE-ES functionalized capture surfaces and any of the pattern functionalized surfaces (table IV f). This demonstrates that the patterned capture surfaces were able to increase anti-EpCAM based capture as effectively as the aE-ES surface, (100% E-selectin coverage) despite having only 50% or 77% of their surface areas functionalized with E-selectin.

The MCF-7 cell capture efficiencies increased up to 1.9 fold between the anti-EpCAM and patterned surfaces (table IV e and g). There was a similar result in the cell mixture flow studies. The 300 μm patterned surface had a significant 1.5 fold increase in MCF-7 cell capture efficiency over the anti-EpCAM surfaces (table IV h and i). The pattern geometry did not appear to have an effect on MCF-7 capture as there was not a significant difference in MCF-7 capture between any of the patterned surfaces (table IV f).

There was a small decrease in anti-EpCAM based MCF-7 capture efficiency between the homogeneous cell suspensions and the cell mixture suspensions, indicating that a

physiological concentration of HL-60 cells may interfere with MCF-7 capture. However, the difference was not statistically significant (table IV a), which supports the use of this technique with real biological samples.

5.2.4 Leukocyte Capture

Because leukocytes are the most similar to CTCs in terms of the physical properties, expression of biomarkers, and functional characteristics that are the basis of CTC separations (Yu), they are the most common hematologic impurity captured in CTC isolation. Therefore, it is important to study the effects of capture surface functionalizations on leukocyte impurity capture. We have done so here using HL-60 cells as a leukocyte model.

Fluorescent characterization studies showed that a 3.9 μg mL^{-1} E-selectin treatment of the PAA surface results in approximately the same surface density of E-selectin as a 10 μg mL^{-1} E-selectin treatment of the silane surface. This is further supported by the flow studies, where the silane/aE-ES and PAA/aE-ES surfaces did not have statistically different HL-60 cell capture efficiencies (table IV o).

An important feature of E-selectin is its affinity for ligands on leukocytes. The effect of this affinity can be seen in the increase in HL-60 cell capture efficiency that occurs between the anti-EpCAM and aE-ES surfaces. The addition of E-selectin to the capture surface resulted in a 4.3 and 4.8 fold increase in HL-60 cell capture efficiency for the silane and PAA surfaces, respectively (table IV k and l). This unwanted increase in HL-60 cell capture can be negated by patterning the two capture proteins on the capture surface.

The pattern surfaces were effective at reducing HL-60 cell capture. This is demonstrated by a comparison between the pattern surfaces' HL-60 cell capture efficiencies and the capture efficiencies of the negative control surfaces (table IV j). Negative controls include MCF-7 cell capture on PEG surfaces and HL-60 cell capture on anti-EpCAM and PEG surfaces. There was

no significant difference between HL-60 cell capture on the pattern surfaces and the negative control surfaces (table IV j). This means that the HL-60 cell capture on patterned surfaces was not higher than the HL-60 cell capture that results from non-specific electrostatic interactions on the negative control surfaces.

Different pattern section widths were tested to study the effect of pattern geometry on cell capture. All patterned surfaces had significantly less HL-60 capture than the aE-ES surfaces (table IV m and n). The most effective was the 300 μm pattern, which had 5.6 fold lower HL-60 cell capture than the aE-ES surface.

Unlike MCF-7 cell capture, HL-60 cell capture was variable for the different pattern geometries. As expected, the asymmetric pattern - which has about 77% of its surface functionalized with E-selectin - had the highest HL-60 cell capture efficiency of all the patterned surfaces. The symmetric patterns (with 50% surface E-selectin coverage) had lower HL-60 cell capture efficiencies, which decreased with decreasing pattern width. Figure 35 illustrates the effects of E-selectin coverage and pattern dimensions on HL-60 cell capture. In the plot, capture efficiencies are normalized to the capture efficiency of the PAA aE-ES surface (100% E-selectin coverage). The plot shows a decrease in HL-60 cell capture with percent E-selectin coverage. It also shows a decrease in HL-60 cell capture with decreasing pattern width (independent of percent E-selectin coverage).

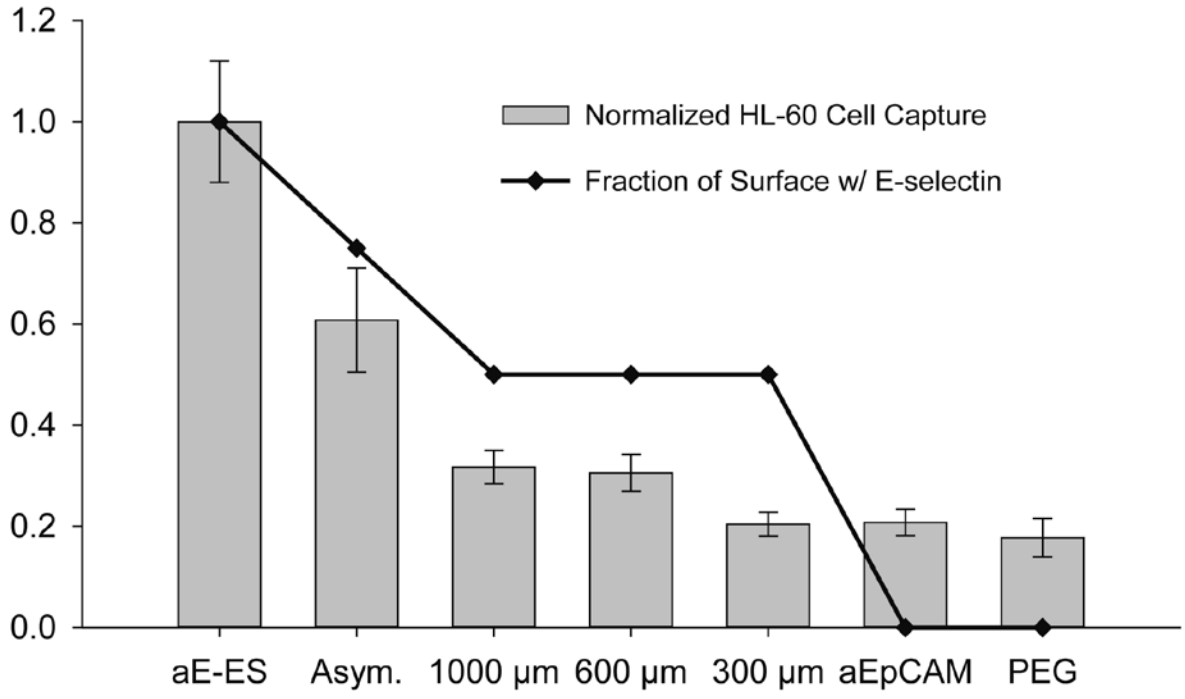

Figure 35. HL-60 Cell Capture on Patterned Surfaces. HL-60 cell capture efficiencies (grey bars, normalized to capture efficiency of the PAA aE-ES surface). Fraction of capture surfaces functionalized with E-selectin (black diamonds).

5.3 Rheologically Biomimetic Cell Suspensions

Described here is a blood analog created by the addition of alginate biopolymer to cell suspension buffer. The feasibility of using this analog for the validation of immunoaffinity CTC isolation devices (MCIDs) was examined in two ways. First examined was the ability of alginate solutions to maintain cells in suspension for a constant flux of cells into the device (section 5.3.1). Second, the effects of alginate on specific and non-specific cell to surface binding were analyzed by comparing leukocyte and carcinoma cell capture in PBS and alginate solutions (section 5.3.2).

A plot of apparent viscosity of PBS-alginate solutions versus alginate concentration is shown in figure 36. A concentration of 4 mg alginate per mL of PBS was chosen for experiments because it has an apparent viscosity of 3.3 cP, which is similar to that of blood at typical physiological shear rates (10 s^{-1}–1000 s^{-1}).(Johnson 2008)

5.3.1 Alginate vs. PBS for Horizontal and Vertical Cell Injection

The number of HL-60 cells or MDA-MB-468 cells entering the MCID as a function of time was measured to quantify the effect of alginate on the settling of cells in feed tubing. The results of these experiments are plotted in figure 37. HL-60 (figure 37 a and b) and MDA-MB-468 (figure 37 c and d) are white blood cell and CTC models respectively. These cell types are often used in MCID validation studies.(Weigum 2007, King 2009, Myung 2010) Experiments were carried out in triplicates with syringes and tubing (figure 34) positioned horizontally (figure 37 a and c) or vertically (figure 37 b and d). Linear regression curves are also plotted (figure 37 a–d). The negative slopes of the curves are compared in figure 37e. The slopes of the regression curves are measurements of the rate of decrease in cells entering the device over time, which is strongly affected by cell settling.

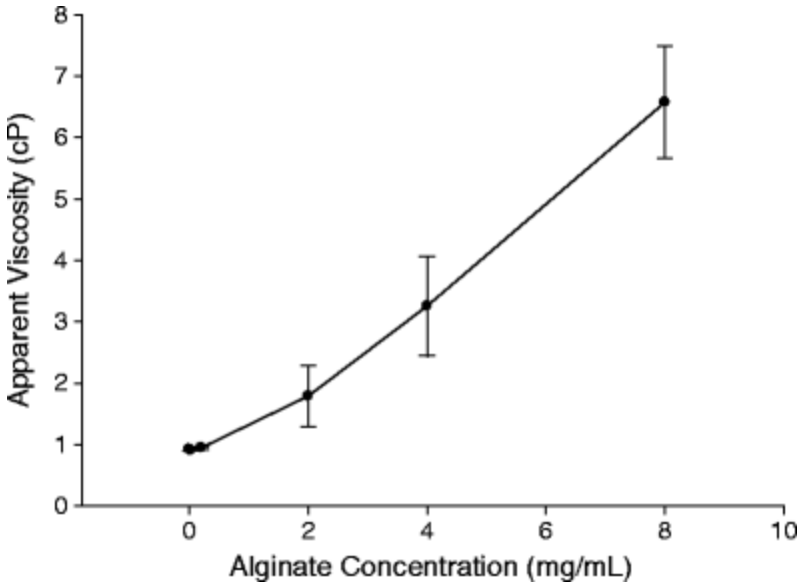

Figure 36. Apparent Viscosity of Alginate Solutions. The apparent viscosity of PBS solutions increases with increasing concentrations of alginate. A concentration of 4 mg ml^{-1} was used for the flow experiments in this work.

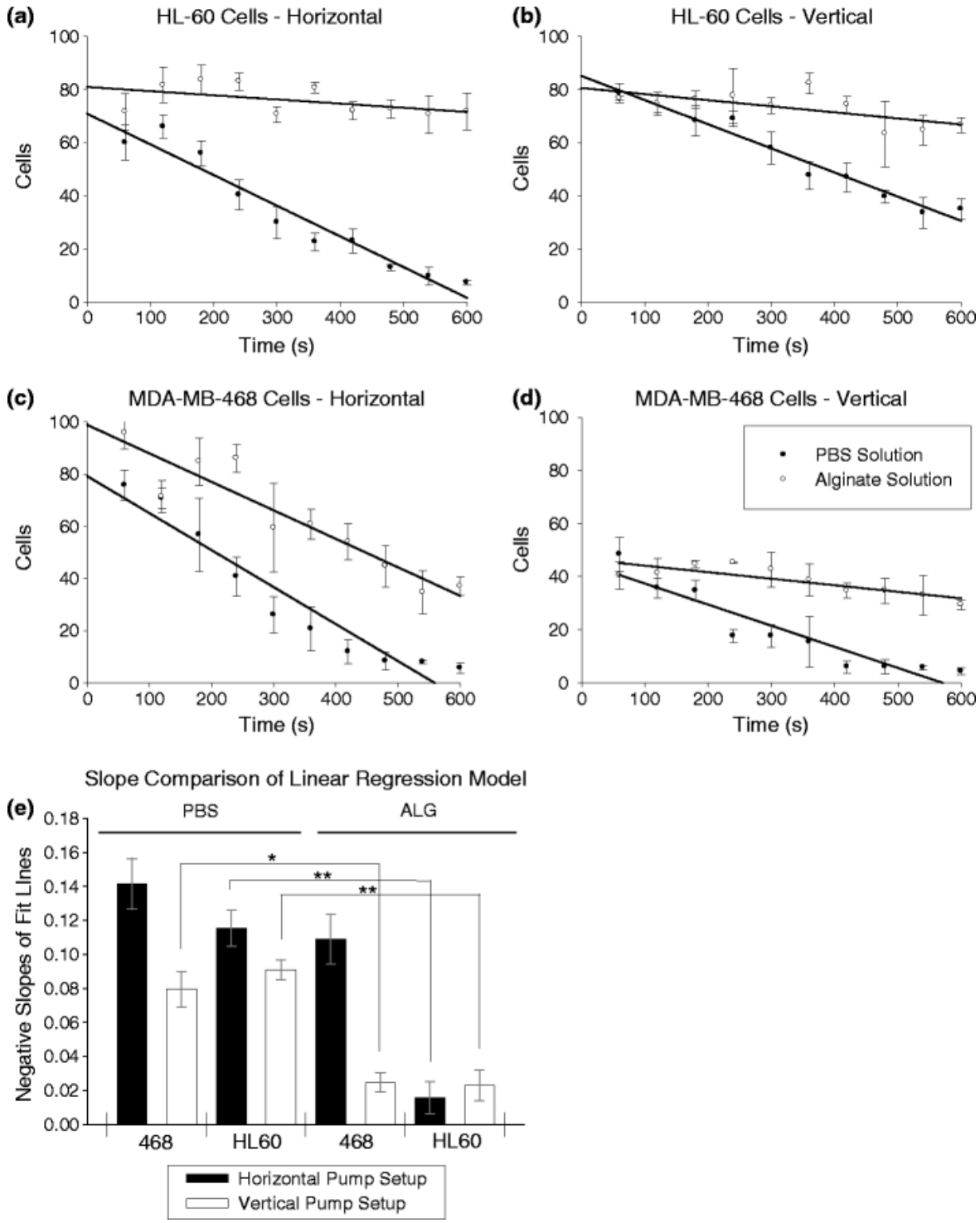

Figure 37. Alginate Effects on Cell Suspensions in Microchannel Feeds. HL-60 (a and b) and MDA-MB-468 (c and d) cells entering the device from horizontal (a and c) and vertical (b and d) configurations. The number of cells entering an MCID as a function of time is plotted for cells suspended in PBS (black points) or in PBS with alginate (white points). Data is represented as mean (n=3) +/− standard error. (e) Plot of the negative slopes of the regression curves in a - d.

As expected, alginate solutions had lower rates of decrease compared to equivalent PBS solutions due to decreased cell settling in the higher viscosity fluid (figure 37). Three of the four alginate groups had significantly lower rates of decrease: horizontal HL-60 ($p < 0.0005$), vertical HL-60 ($p < 0.0001$), and vertical MDA-MB-468 ($p < 0.0005$). The effect of the vertical versus horizontal set-up was not significant for the HL-60 cells in alginate or PBS for the time interval of this experiment. This is likely due to the fact that the HL-60 cells (radius ~6 μm) are smaller than the MDA-MB-468 cells (radius ~10 μm) and thus settle at a slower rate (because settling velocity is roughly proportional to the square of the particle radius). However, the effect of the vertical versus horizontal set-up was significant for the MDA-MB-468 cells in PBS and alginate solutions ($p < 0.0005$ and $p < 0.0001$ respectively). This is expected because gravitational settling of these cells occurs parallel to the direction of flow in the vertical set-ups, resulting in less cell interactions with the sides of the syringe and tubing.

The rate of decrease in the number of cells entering the device over time is represented in figure 37e. This plot shows the negative slopes of the linear regression models +/− standard error. With the exception of the MDA-MD-468 cells in the horizontal set-up, the alginate solutions had significantly lower rates of decrease compared to equivalent PBS solutions (*$p < 0.0005$, ** $p < 0.0001$). Also, the MDA-MB-468 cells in the vertical configurations had significantly lower rates of decrease compared to equivalent horizontal configurations (PBS $p < 0.005$, ALG $p < 0.0001$)

The groups in figure 37 with the smallest slopes had the least cell settling. These include the HL-60 cells in the alginate solution and the MDA-MB-468 cells in the alginate solution with the vertical set-up. Therefore, for the larger MDA-MB-468 cells, (for which cell settling is a problem) the best experimental set-up should include alginate buffer solutions with a vertical configuration.

5.3.2 Effect of Alginate and PBS on Capture Efficiency

In addition to the cell settling studies, CTC capture studies were carried out to show that alginate does not interfere with the functionality of capture surfaces. Since most CTCs are of epithelial origin, methods for CTC isolation are most often based on immunoaffinity to anti-EpCAM.(Yu 2011) The effect of alginate on specific binding was analyzed by testing tumor cell capture efficiencies of anti-EpCAM functionalized devices using cells suspended in PBS or alginate solution. The results from this experiment are reported in figure 38. The capture efficiency of devices tested with MDA-MB-468 cells in alginate solutions was 13%. The capture efficiency of devices tested with MDA-MB-468 cells in PBS was 12%. These values were not significantly different ($p = 0.69$).

These results indicate that alginate does not interfere with the specific binding interaction that is the basis of MCID functionality. However, it is also possible that alginate could facilitate the non-specific binding to the surfaces. The loss of specificity in binding to the capture surface would mean that white blood cells and other non-target cells could bind to the capture surface, reducing the purity of the separation. To check for effects on nonspecific binding, suspensions of HL-60 cells in either PBS or PBS-alginate were pumped into devices functionalized with anti-EpCAM and the capture efficiencies were determined. These results are also plotted in figure 38. Since HL-60 cells are a leukemia cell line, they do not express EpCAM and should not bind to the capture surface. An increase in the capture of HL-60 cells with the alginate solution would indicate that alginate facilitates non-specific binding of cells. However, as shown in figure 38, there is no significant difference in the capture efficiency between the alginate (0.04%) and PBS (0.07%) groups ($p = 0.33$).

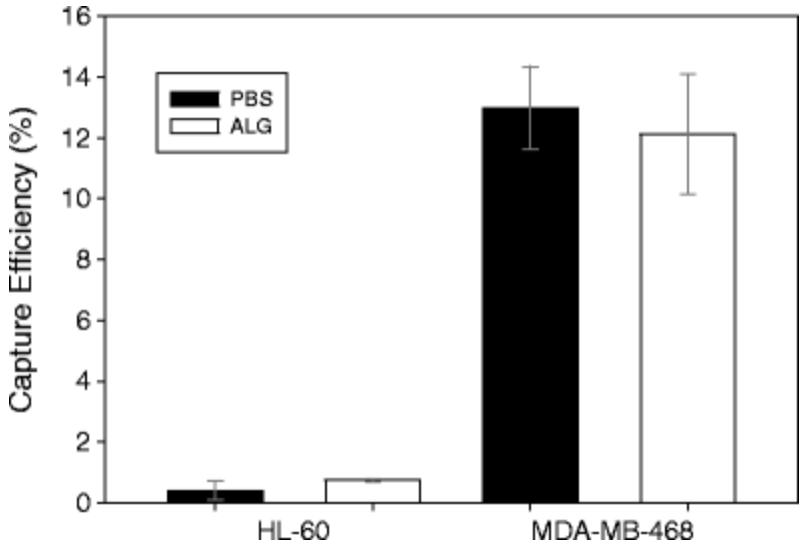

Figure 38. Cell Capture Efficiency in PBS or Alginate Suspensions. Cells suspended in PBS or alginate solutions were processed through MCIDs functionalized with anti-EpCAM. The capture efficiencies for the MDA-MB-468 and HL-60 cells were not significantly different between the PBS and alginate solutions.

5.4 Computational Analysis of Hydrophoresis in Microfluidic Mixers

5.4.1 COMSOL 3.5 Modeling Studies

Single channel slanted groove mixers were modeled in COMSOL Multiphysics modeling software. The particle tracing module was used to estimate cell paths through the device (figure 39 a and b). Pressure and velocity fields in the model device were solved for and used to predict cells' paths under drag forces in mixers with groove and channel heights ranging from 50 µm to 100 µm. Models were solved for two fluid viscosities; those of PBS and blood (figure 39c). In the particle tracing study the device models with blood needed to be 10 µm shorter than the devices with PBS for the model cell to come into contact with the capture surface. For the mixer feature dimensions in this study the cells in both PBS and blood contacted the surface in the 50 µm height devices.

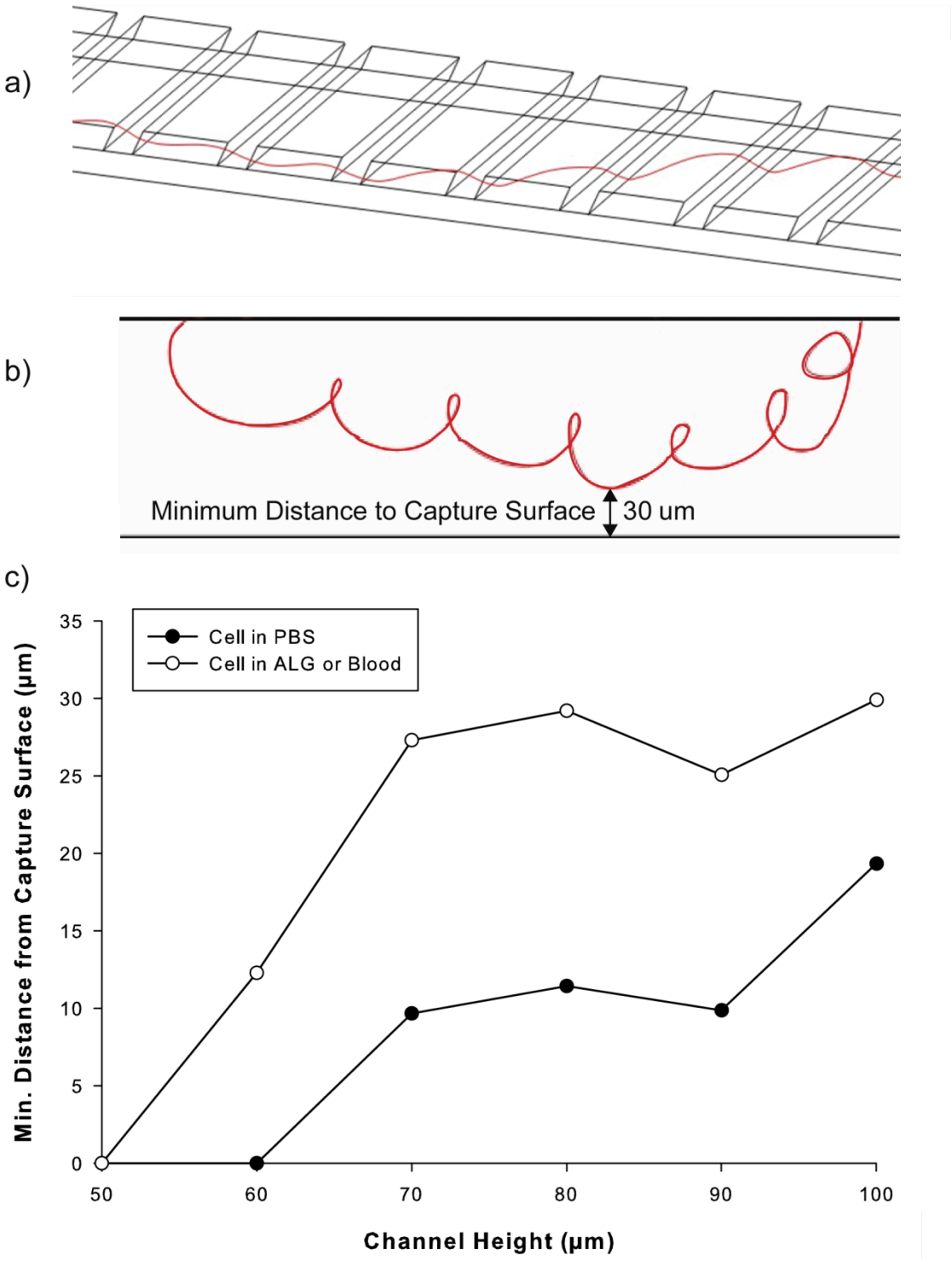

Figure 39. COMSOL 3.5 Modeling Particle Tracing Results. (a) Wireframe view of a slanted groove mixer computational fluid dynamics simulation with predicted cell path. (b) End view of predicted cell path showing the point in the cell path nearest the channel surface. (c) Plot of channel height vs. model cell's minimum distance from capture surface.

5.4.2 COMSOL 4.2a Modeling Studies

Cell transport in chevron and herringbone micromixer devices was modeled in COMSOL Multiphysics modeling software version 4.2 as described in the appendix. Preliminary results are reported in table V, which shows the estimated particle/cell transmission probabilities for mixers of different widths. One model (indicated in table V with an asterisk) was of the same dimensions as the herringbone-chip mixer described in the literature review (Stott 2010). In the models, the herringbone mixers had constant transmission probability with variable channel widths. Conversely, transmission probabilities in the chevron mixers were variable with width and generally decreased with decreasing channel width. The 330, 300, and 220 µm Chevron mixers had the lowest transmission efficiency (i.e. the highest capture efficiency).

An important observation regarding these model solutions is that the majority of cells were captured within the mixer features as illustrated in figure 40. This image shows a side view of a 400 µm width herringbone mixer with cells that have been immobilized upon contact with the surface. The color scheme demonstrates that the cells on the mixer features are exposed to lower shear than the cells adhered to the channel floor.

Table V. Transmission Probability for Mixers with Different Channel Widths.

Mixer Type	Width (µm)	Transmission Probability
Herringbone	200	0.16
Chevron	220	0
Chevron	300	0.05
Herringbone*	300	0.15
Chevron	330	0.04
Herringbone	400	0.15
Chevron	440	0.22
Chevron	550	0.17
Chevron	660	0.36

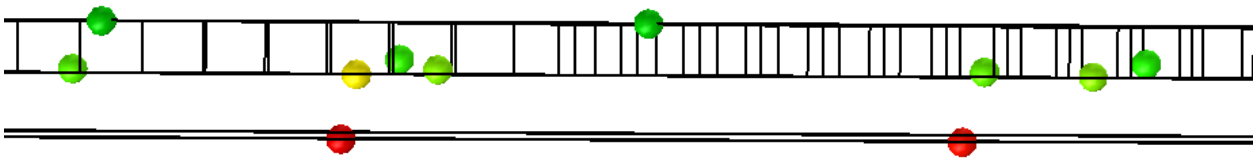

Figure 40. Side View of Herringbone Mixer with Captured Cells. The color scale represents the shear stress on the cells, with red corresponding to the greatest shear, yellow to moderate shear and green the lowest shear.

5.5 Flow Studies with Dendrimer Immobilized Proteins

Three sets of flow experiments were carried out to examine the utility of PAMAM dendrimer-facilitated multivalent binding in microfluidic immunoaffinity-based cell isolation devices. In the first set of flow experiments, dendrimer immobilized anti-EpCAM was compared to aE-ES protein mixture functionalized surfaces.

Anti-EpCAM was immobilized on dendrimer functionalized microchannel surfaces as described in section 4.3.1. Other capture surfaces were prepared for comparison by immobilizing methylated PEG (mPEG), or by immobilizing anti-EpCAM or protein mixture directly onto GMBS (section 4.3.1). MCF-7 and HL-60 cells were stained and prepared as described in section 4.1 and flow studies were carried out as described in section 4.3.2.

The results of these flow studies are shown in figure 41. The protein mixture and dendrimer functionalized surfaces had significantly higher tumor cell capture efficiency than the anti-EpCAM surfaces ($p < 0.05$ and $p < 0.01$, respectively). While the mixture and dendrimer functionalized surfaces did not have significantly different MCF-7 cell capture efficiencies ($p > 0.05$), the dendrimer functionalized surface did have significantly less HL-60 cell capture than the mixer functionalized surfaces ($p < 0.01$).

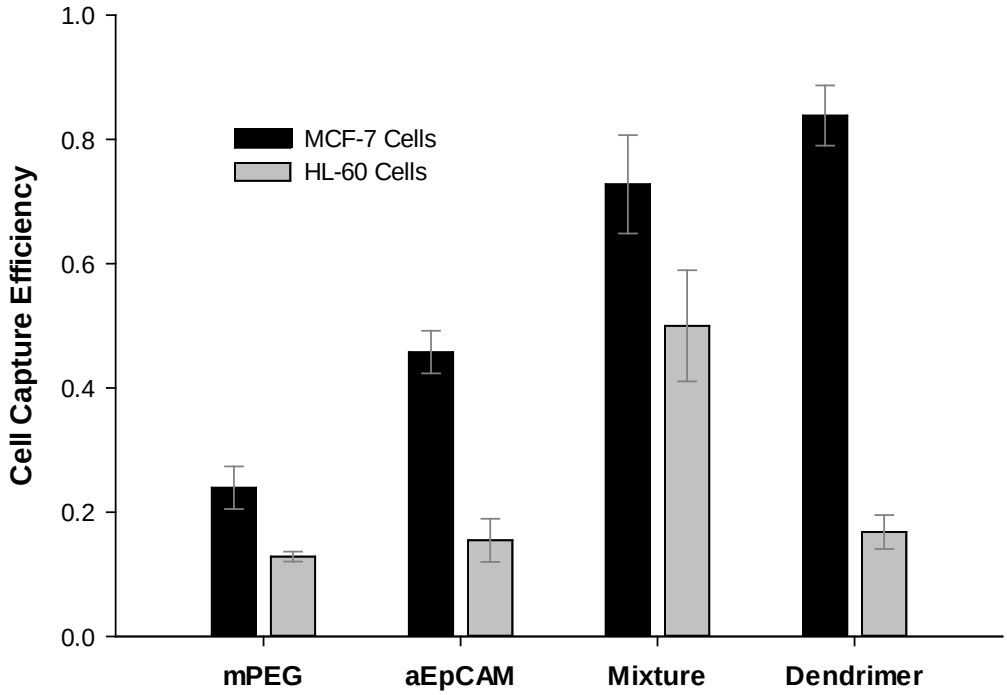

Figure 41. MCF-7 and HL-60 Cell Capture Efficiencies on Protein Mixture and Dendrimer Functionalized Surfaces.

In the second set of flow studies, PEG immobilized anti-EpCAM surfaces were compared to dendrimer immobilized anti-EpCAM surfaces in mixer and flat channel devices. Chevron mixers and flat walled devices were fabricated as described in section 4.5.3. These devices were functionalized with anti-EpCAM via PEG or dendrimer as described in section 4.3.1. Flow studies were carried out as described in section 4.3.2. The results from this study are plotted in figure 42.

As expected, the dendrimer immobilized ant-EpCAM mixer device had the highest capture efficiency, which was significantly greater ($p < 0.001$) than the PEG and PEG with mixer

devices. Both the PEG and dendrimer mixer devices had higher tumor cell capture efficiencies than their corresponding flat walled devices, although the differences were not statistically significant ($p > 0.05$).

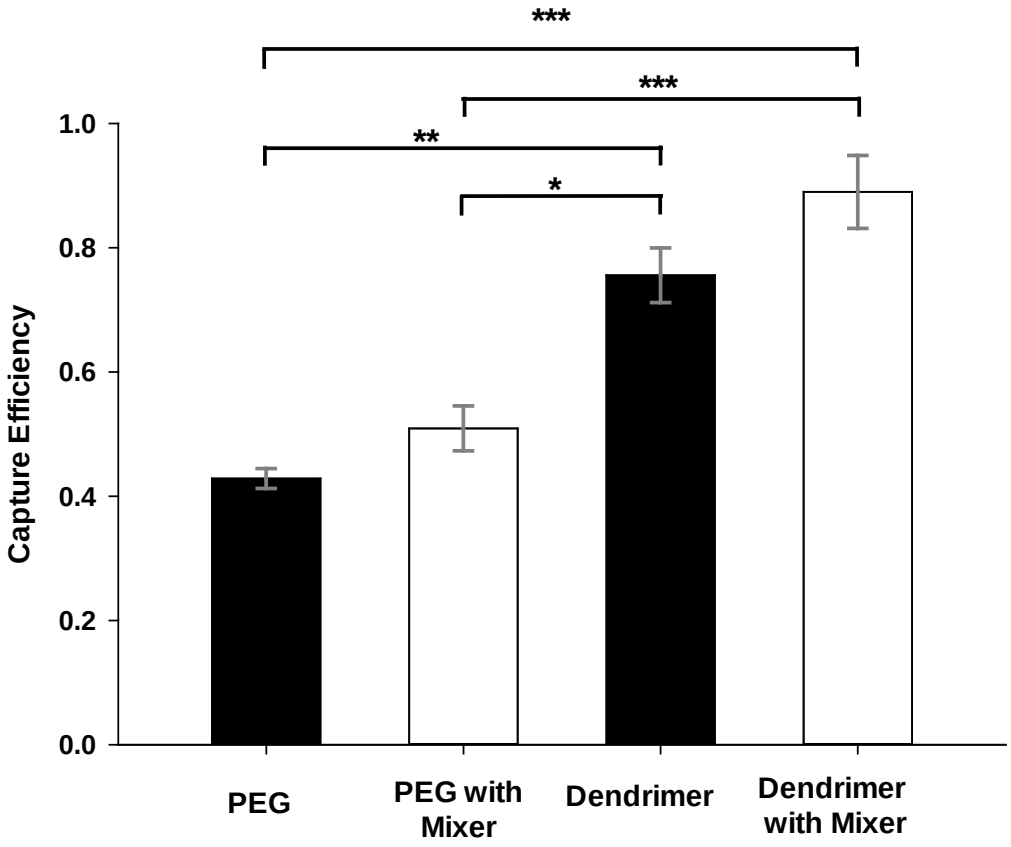

Figure 42. MCF-7 Cell Capture in Mixer Devices. Mean ± Standard Error. One way ANOVA: * $p < 0.05$, ** $p < 0.01$, *** $p < 0.001$

In the final round of dendrimer flow studies, PEG-immobilized anti-EpCAM and dendrimer-immobilized anti-EpCAM surfaces were compared in terms of their ability to capture tumor cells and maintain binding at different flow rates. Flat walled devices were fabricated as described in section 4.5.3 and these devices were functionalized with anti-EpCAM via PEG or dendrimer as described in section 4.3.1. Cell capture efficiency and post rinsing retention efficiency were determined as described in section 4.3.2. The results from this study are plotted in figures 43 and 44.

For the PEG and dendrimer surfaces, both the capture and retention efficiencies showed a strong flow rate dependency, each decreasing with increasing flow rates. The MCF-7 cell capture efficiency was significantly higher for the dendrimer surfaces compared to the PEG surfaces only at the 8 μL min^{-1} flow rate ($p < 0.01$). The PEG and dendrimer capture efficiencies were nearly identical at the 64 μL min^{-1} flow rate ($p = 0.497$). Interestingly the PEG and dendrimer surfaces did not have statistically significant differences in retention efficiency for any of the flow rates tested. Unlike the capture efficiency results, the retention efficiencies for the PEG and dendrimer surfaces were nearly identical ($p = .936$) at the lowest flow rate, with the dendrimer performing better than the PEG surface only at the higher flow rates.

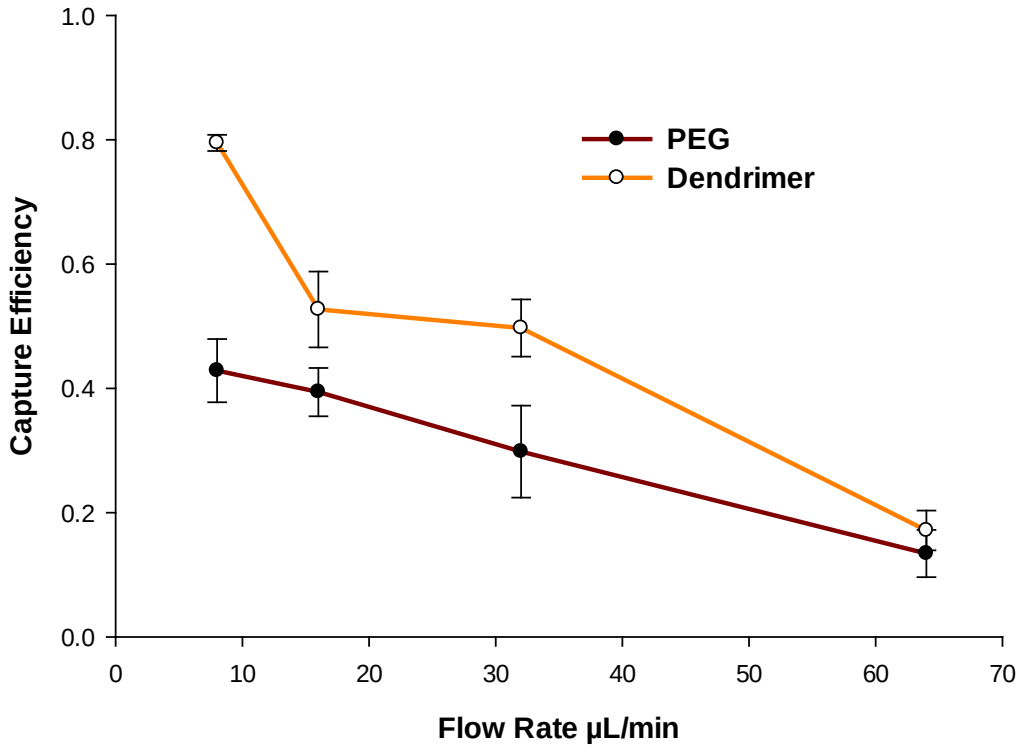

Figure 43. MCF-7 Cell Capture Efficiency at Different Flow Rates.

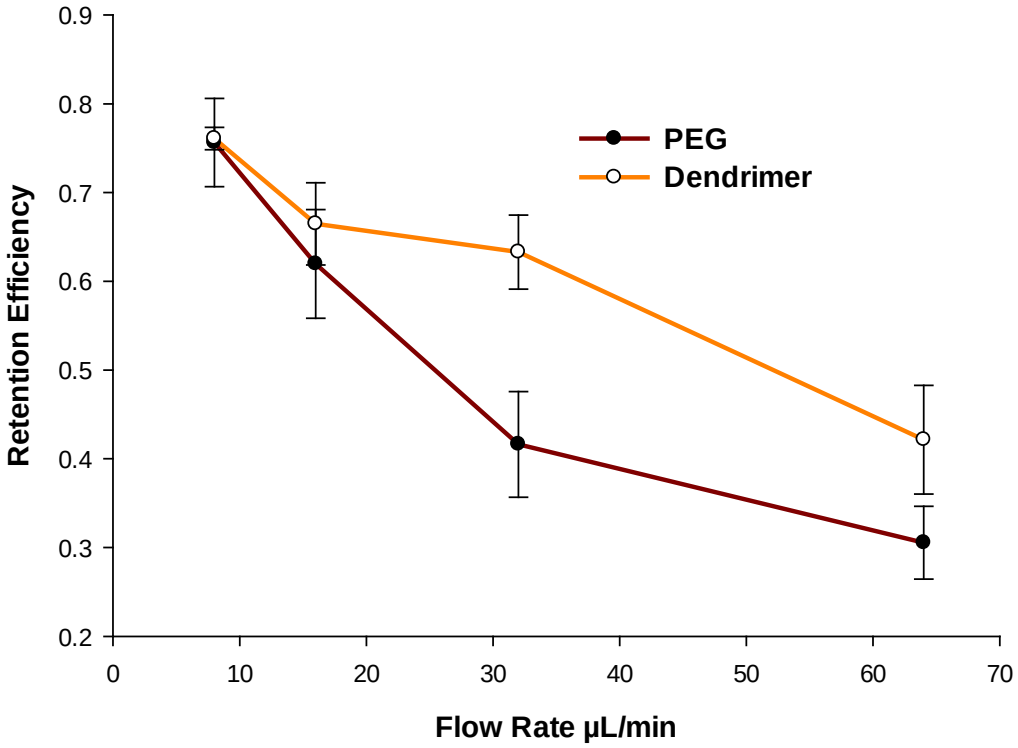

Figure 44. MCF-7 Cell Retention Efficiency at Different Flow Rates.

Chapter VI. Discussion

6.1 Biomimetic Protein Combination

The flow studies reported in section 5.2.2 show that adding E-selectin to an anti-EpCAM capture surface can increase microfluidic tumor cell capture efficiency up to 1.9 fold. This is an important achievement for improving the sensitivity of immunoaffinity based capture of rare CTCs. However, these studies also show that the addition of E-selectin increases leukocyte capture up to 4.8 fold. In order for this biomimetic protein combination to be practical for CTC isolation in terms of capture purity, this unwanted increase in leukocyte capture needs to be negated. We have done this here using protein patterning and a special leukocyte elution buffer.

6.2 Leukocyte Elution Buffer for Increased Capture Purity

In this work we demonstrated a reduction in the number of leukocytes retained on E-selectin-augmented capture surfaces by deactivating E-selectin binding in two ways. First the molecular displacement of Ca^{2+} from the E-selectin ligand binding site was achieved by adding Mg^{2+} to the rinsing buffer. Second, Ca^{2+} removal from the system was achieved by chelation with a Ca^{2+} specific cheating agent (EGTA). This combination blocked E-selectin binding and allowed leukocytes to migrate over the surface faster and be flushed out of the device. The Mg^{2+}/EGTA rinse buffer removed 87% of leukocytes captured on an aE-ES surface. This will translate to improved capture purity for tumor cell isolation from cell mixtures, such as blood or mononucleated cell preparations.

There are two likely reasons why the rinse buffer was not 100% effective. The first reason why some leukocytes remain on the capture surface is non-specific binding. Leukocytes may bind to a capture surface through electrostatic, hydrophobic, or other interactions that are

not affected by E-selectin deactivation. The second reason involves the calcium displacement from E-selectin's ligand binding site (the suspected cause of E-selectin deactivation). It has been hypothesized that calcium cannot be displaced from the analogous L-selectin receptor if a ligand is already present in the binding site.(Koenig 1998) This could also be the case with E-selectin. Recall that the E-selectin bond has a short lifetime under flow conditions. This is what allows cell rolling, and is the reason that the rinse buffer can be effective even if Ca^{2+} cannot be displaced when a ligand is bound. However, as the surface density of E-selectin increases, the rolling velocity of cells decreases.(Myung 2010) If the surface density of E-selectin is high enough, then cells can become arrested on E-selectin functionalized surfaces. It is possible that locally high E-selectin densities cause the immobilization of leukocytes in these regions. In this case, the E-selectin bond lifetimes may be much longer, thereby reducing the ability of the rinse buffer to displace Ca^{2+} and release cells from the capture surface.

6.3 Two Component Protein Micropatterning

Since leukocyte elution buffer is not 100% effective at leukocyte removal, a second method was employed to reduce leukocyte capture and increase tumor cell capture purity. This method consisted of surface micropatterning regions with and without E-selectin so that captured leukocytes can roll a short distance and detach (figure 16).

6.3.1 Tumor Cell Capture on Patterned Surfaces

It was found that the patterned surfaces were able to increase anti-EpCAM based capture as effectively as the aE-ES surface, (100% E-selectin coverage) despite having only 50% or 77% of their surface areas functionalized with E-selectin. This indicates a strong effect of E-selectin and possibly a maximum capture rate due to transport limitations in this flat-walled device. Some have reported the use of herringbone mixer structures to improve transport and CTC capture.(Stott , Wang 2011) If the patterned surfaces described here are incorporated into

a complete CTC isolation system, mixing structures or other features should be considered to overcome transport limitations to allow maximum CTC capture efficiency. Since the surface modification technique described here is based on photopatterning (as opposed to contact based patterning), the technology is expected to translate well to corrugated surfaces (e.g. mixer features) as other photopatterning technologies have.(Kim 2010, Martin 2011)

Anti-EpCAM was co-immobilized with E-selectin in this study as an example of an immunospecific adhesion molecule. Other such molecules could be co-immobilized with E-selectin for efficient capture of tumor cells that have low EpCAM expression. It should be noted, however, that some CTC specific capture molecules (such as cadherins) are calcium-dependent and the leukocyte elution step is not compatible with surfaces functionalized with those molecules. Alternately, the elution buffer from these studies could be used to recover CTCs captured with those molecules.

6.3.2 Leukocyte Cell Capture on Patterned Surfaces

We demonstrated in section 5.2.2 that HL-60 cell capture on patterned surfaces was not significantly different than HL-60 cell capture on negative control surfaces. Since HL-60 cell binding on negative control surfaces is facilitated by non-specific interactions, it is likely that much of the remaining HL-60 binding on the patterned surfaces was also due to non specific interactions. This supports the hypothesis that the protein patterning/elution buffer combination effectively negates the specific interactions between leukocytes and capture surface E-selectin. This is necessary for E-selectin augmented capture to be a practical alternative to existing CTC isolation platforms.

While leukocyte capture on patterned surfaces was not higher than non-specific capture on negative control surfaces, non-specific capture on all surfaces was higher than is ideal for CTC isolation from real biological samples. To improve capture purity, Zheng et al. (Zheng 2011) demonstrated a technique where they increasingly ramp the shear during the rinsing step

to preferentially remove non-target cells. This technique could be used to augment the methods of leukocyte removal discussed herein to further reduce non-specific capture. A second potential method for reducing non-specific capture would be to modify the capture surface itself. The monomer composition for the photopolymerization reaction could be adjusted, for example, to contain more neutral monomers to reduce electrostatic interactions with cells. Also, some of the many commercially available spacer/linker molecules could be investigated for their ability to prevent non-specific binding.

Although HL-60 cell capture was not significantly different for the different width patterns (table IV j), there was a correlation between pattern width and HL-60 cell capture. This trend indicates that the density of surface boundaries may be a factor in leukocyte release efficiency. Surfaces with higher boundary densities may have improved leukocyte removal for two reasons. A shorter rolling distance between the site of HL-60 cell capture and the adjoining anti-EpCAM region could reduce the probability that the cell will reach a localized region of higher E-selectin density and become arrested, before it can be released at the anti-EpCAM boundary. Additionally, increasing the number of boundaries increases the space where leukocyte binding is being destabilized and detachment is occurring, leading to more total leukocyte detachment.

6.4 Rheologically Biomimetic Cell Suspensions

In this work we reported that a vertical feed tube configuration helps mitigate carcinoma cell settling problems in microfluidic feeds. We also reported that adding alginate to a cell suspension further reduces the effects of cell settling - without disrupting the specific binding interactions that are the basis of carcinoma cell capture in MCIDs. These results indicate that vertical equipment configurations and the addition of alginates can be used to reduce cell settling in buffer based MCID testing and other applications involving large cells suspended in buffer solution.

When using alginate solutions as a blood analog, it should be noted that while both alginate suspensions and blood exhibit shear thinning behavior, the elastic and viscous behavior of the two differ slightly and are highly shear and concentration dependent.(Cho 1991, Brandenberger 1998) The optimum alginate concentrations for mimicking blood rheology will be dependent on the shear operating range of a device.

Many elastic effects are negligible at higher shear rates for both blood and alginate solutions. However, these effects may be considerable at low shear rates, such as those present in syringes.(Tanguy 1985, Thurston 2006) Due to the aggregation of red blood cells in low shear environments, blood is able to store elastic energy.(Anand 2004) Elastic energy results in the formation of cell settling columns, which can have a 10 fold greater sedimentation velocity than non-aggregated cells.(Yu 2006) While alginate solutions are only weakly elastic (Tanguy 1985) they should not be used with very high cell concentrations. This will avoid unwanted aggregation-based cell settling at low shear. The cell concentrations commonly used in MCID testing, 10^2–10^7 mL^{-1}, are sufficiently low concentrations.

Also important to note are the differences between dilute polymer solutions like PBS-alginate, and dense particle suspensions like blood. Despite maintaining similar viscoelastic properties in regular bulk flow, viscoelastic fluids based on long linear polymer chains can behave differently than suspensions, particularly at channel expansions and bifurcations.(Cho 1991) Furthermore, the mechanism and magnitude of shear-induced particle migration will differ between blood and a polymer based blood analog. Since shear-induced migration scales with shear rate, this discrepancy between blood and the blood analog is unlikely to be a problem in low shear microdevices. However, this phenomenon should be taken into account if an alginate blood analog is to be used in a high shear environment.

6.5 Computational Analysis of Hydrophoresis in Microfluidic Mixers

The preliminary modeling studies of particle transport reported in section 5.4.2 showed that chevron mixers of certain dimensions had more cell contact with channel walls than herringbone mixers of similar dimensions. This indicates that chevron micromixers may be a viable alternative to herringbone mixers for enhancing tumor cell capture in immunoaffinity isolation devices. These types of devices may be more effective than chaotic herringbone mixers, because, as discussed in section 3.3, chevron mixers hydrophoretically process cells in a symmetric manner, while fluid is chaotically folded in herringbone mixers. However, extensive simulations and physical studies are still necessary to determine the most effective configuration for optimum cell transport to microfluidic capture surfaces.

An important observation in the modeling studies was that the majority of cells were captured (i.e. made wall contact) in the mixer features rather than the main channel. This is likely a result of the lower shear environment in the mixers. Figure 45 shows an end view frame of cells traversing a herringbone mixer. The color scale on the cells reflects the shear stress on these cells, with green indicating low shear and red indicating high shear. In this image it is apparent that the cells near the bottom and side walls of the channel experience the highest shear stress while the cells in the center and near the mixer regions experience lower shear.

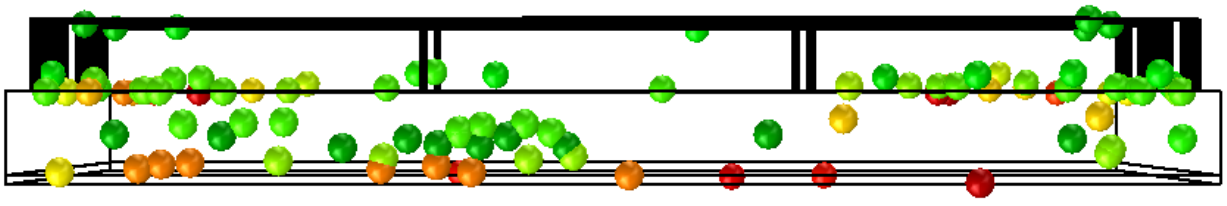

Figure 45. End View of Herringbone Mixer with Captured Cells. Color scale represents shear stress on the cells, with red corresponding to the greatest shear and green corresponding to the least shear.

Interestingly, the only group to have published work on the simulation of particle surface interactions in a herringbone mixer reported an opposite cell capture pattern. Forbes and Kralj (Forbes 2012) stated that the majority of particle capture in their herringbone mixer models occurred on the bottom of the channel. The discrepancy between those models and the ones described here is likely due to the differences in mixer dimensions, since the location of cell capture is likely to be highly dependent on the relative fluidic resistance between the main channel and the mixer grooves. These discrepancies further support the need for additional studies.

6.6 Multivalent Binding with Dendrimer Immobilized anti-EpCAM

Three sets of flow experiments were carried out to examine the utility of PAMAM-dendrimer facilitated multivalent binding in microfluidic immunoaffinity-based cell isolation devices (section 5.5). In the first set of flow experiments, dendrimer immobilized anti-EpCAM was compared to anti-EpCAM and aE-ES immobilized directly onto GMBS crosslinker. These results agreed with those of our coworkers (Myung 2011), which showed that dendrimer immobilized anti-EpCAM has more tumor cell capture than anti-EpCAM immobilized on a monovalent PEG platform.

In the second set of flow studies, PEG immobilized anti-EpCAM was compared to dendrimer immobilized anti-EpCAM in mixer and flat channel devices. Mixer devices had higher, but not significantly higher, tumor cell capture efficiencies than the flat walled devices. The reason for the insignificance is likely a result of the PBS suspension model used in place of whole blood. It has been reported that the effects of the herringbone chip mixer were not significant when tested with cells suspended in buffer solution. This notion is further supported by the results of the COMSOL 3.5 modeling studies reported in section 5.4.1. These COMSOL results showed that a mixer channel had to be shorter (relative to the PBS models) in a

suspension having the viscosity of blood for the cells to reach the capture surface. This indicates that cells are more easily transported to a capture surface in the lower viscosity solutions, which would make the mixer less relevant with PBS cell suspensions. These results support the use of alginate (if blood is not available) in early validation studies, particularly those involving fluid manipulation such as passive mixing.

In the third round of dendrimer flow studies, PEG immobilized anti-EpCAM and dendrimer immobilized anti-EpCAM surfaces were compared in terms of their ability to capture tumor cells and maintain binding at different flow rates. Interestingly, the dendrimer surfaces did not perform better than the PEG surfaces, in terms of capture efficiency, at the higher flow rates. This could indicate that, once shear increases beyond the range in which anti-EpCAM can effectively bind its antigen, the multivalent effect becomes of little utility. This limitation supports the use of E-selectin, either adjacent to the capture surface (Myung 2011), or integrated into the capture surface, to improve capture under shear in dendrimer devices. It may be possible to reduce this shear limitation with further engineering of the multivalent platform. For example, the G7 dendrimers used in this study are relatively stiff and can only support 3 to 5 anti-EpCAM molecules. A different platform, such as a lower generation dendrimer with PEG spacers on its tips, may support more anti-EpCAM molecules or retain more conformational freedom. This could improve multivalent binding under shear.

Chapter VII. Conclusions

7.1 Two Component Protein Micropatterning

E-selectin has previously been indicated for in-vitro cell binding under flow.(Rana 2009) The work described in this thesis expanded that idea by co-immobilizing E-selectin with a capture molecule that provides immuno-specificity for tumor cell isolation (Myung 2010). The resulting increase in tumor cell capture under flow conditions is an important step towards reducing the shear dependency of immunospecific CTC capture (Hughes 2012) and increasing the throughput of CTC isolation independently of parallelization. This will reduce the amount of parallelization required for a desired throughput and reduce total costs of device production.

In this thesis a new multi-protein patterning technique was described that generates a surface pattern, after a channel has been sealed, but before proteins are immobilized on the substrate, thereby avoiding many common complications associated with the immobilization of sensitive biomolecules. Patterning alternating regions of anti-EpCAM and biomimetic protein mixture provides a way to leverage the increased tumor cell capture efficiency of the protein combination while reducing leukocyte impurity buildup. Also, a leukocyte elution buffer consisting of Ca^{2+} chelating EGTA and Ca^{2+} displacing Mg^{2+} effectively deactivates E-selectin to increase the efficiency of leukocyte release during device rinsing. After further validation with physiological samples, these patterned surfaces may be integrated into CTC isolation systems for applications in research, cancer diagnosis, and disease monitoring.

7.2 Rheologically Biomimetic Cell Suspensions

In this thesis, problematic settling of large cells in microfluidic systems was addressed. To reduce cell settling, the viscosities of cell suspension solutions were increased via the addition of alginate polymer. Reduced cell settling was demonstrated as a slower decrease in

the rate of cells entering the microfluidic devices over time. Tubing and syringe orientations were also investigated for their ability to mitigate the effects of cell settling on feed stream cell concentrations. Vertical orientations were shown to have a stabilizing effect on carcinoma cells' feed rate into a microfluidic device. The feasibility of using alginate solutions in immunoaffinity capture devices was supported by demonstrating that adding alginate to PBS cell suspension does not significantly alter specific or non-specific cell-surface interactions. Currently, most MCID validation studies using carcinoma cell lines suspended in PBS ignore cell settling or address this issue with agitation. Using an alginate based blood analog to prevent cell settling is simple and cost effective and has the additional benefit of creating a biomimetic fluid rheology for device testing.

Alginate solutions are particularly effective at reducing cell settling in syringes because they are highly viscous in this low shear environment. However, due to their shear thinning behavior, they can have a much lower viscosity in the higher shear environment of a microfluidic device. For these reasons alginate could be used to reduce problematic cell settling in other microfluidic applications that involve the processing of large cell types.

7.3 Micromixers and Multivalent Binding

The preliminary modeling studies reported herein indicate that symmetric chevron mixers may be a viable alternative to the staggered herringbone mixers currently in use in MCIDs. However, due to the lack of computational and physical studies on microfluidic hydrophoresis in dense suspensions, there is still much to be done before an optimum mixer configuration can be defined. In this work, chevron mixers and flat walled devices (with PEG or dendrimer immobilized anti-EpCAM) were compared. The mixers had higher tumor cell capture efficiencies. However, these differences in capture were not significant, therefore the

experiments should be repeated with cells suspended in blood or blood analog to observe the full effect of the mixer.

On the contrary, the benefits of PAMAM dendrimer facilitated multivalent binding in MCIDs were shown to be significant in this work. Dendrimer immobilized anti-EpCAM out performed PEG immobilized anti-EpCAM in terms of capture efficiency (although the effect decreased with increasing flow rates). Interestingly, the dendrimer surface did not have significantly higher tumor cell retention rates under shear. Overall, multivalent binding shows promise and could be a powerful tool in MCIDs with further engineering of the multi-ligand construct.

References

Abbitt, K. B., Rainger, G. E. and Nash, G. B. (2000). "Effects of fluorescent dyes on selectin and integrin-mediated stages of adhesion and migration of flowing leukocytes." Journal of immunological methods 239(1-2): 109-119.

Adams, A. A., Okagbare, P. I., Feng, J., et al. (2008). "Highly efficient circulating tumor cell isolation from whole blood and label-free enumeration using polymer-based microfluidics with an integrated conductivity sensor." J Am Chem Soc 130(27): 8633-8641.

Alix-Panabieres, C., Vendrell, J. P., Pelle, O., et al. (2007). "Detection and characterization of putative metastatic precursor cells in cancer patients." Clinical chemistry 53(3): 537-539.

Alix-Panabieres, C., Vendrell, J. P., Slijper, M., et al. (2009). "Full-length cytokeratin-19 is released by human tumor cells: a potential role in metastatic progression of breast cancer." Breast cancer research : BCR 11(3): R39.

Allan, A. L., Vantyghem, S. A., Tuck, A. B., et al. (2005). "Detection and quantification of circulating tumor cells in mouse models of human breast cancer using immunomagnetic enrichment and multiparameter flow cytometry." Cytom Part A 65A(1): 4-14.

Anand, M. and Rajagopal, K. R. (2004). "A shear thinning viscoelastic fluid model for describing the flow of blood." International Journal of Cardiovascular Medicine and Science 4(2): 59-68.

Astruc, D., Boisselier, E. and Ornelas, C. t. (2010). "Dendrimers Designed for Functions: From Physical, Photophysical, and Supramolecular Properties to Applications in Sensing, Catalysis, Molecular Electronics, Photonics, and Nanomedicine." Chemical Reviews 110(4): 1857-1959.

Balasubramanian, P., Yang, L., Lang, J. C., et al. (2009). "Confocal images of circulating tumor cells obtained using a methodology and technology that removes normal cells." Molecular pharmaceutics 6(5): 1402-1408.

Barthel, S. R., Gavino, J. D., Descheny, L., et al. (2007). "Targeting selectins and selectin ligands in inflammation and cancer." Expert Opin Ther Targets 11(11): 1473-1491.

Belisle, J. M., Correia, J. P., Wiseman, P. W., et al. (2008). "Patterning protein concentration using laser-assisted adsorption by photobleaching, LAPAP." Lab on a Chip 8(12): 2164-2167.

Belisle, J. M., Kunik, D. and Costantino, S. (2009). "Rapid multicomponent optical protein patterning." Lab on a Chip 9(24): 3580-3585.

Bernard, A., Delamarche, E., Schmid, H., et al. (1998). "Printing Patterns of Proteins." Langmuir 14(9): 2225-2229.

Bernard, A., Fitzli, D., Sonderegger, P., et al. (2001). "Affinity capture of proteins from solution and their dissociation by contact printing." Nat Biotech 19(9): 866-869.

Bernard, A., Renault, J. P., Michel, B., et al. (2000). "Microcontact Printing of Proteins." Advanced Materials 12(14): 1067-1070.

Bhatnagar, P., Malliaras, G. G., Kim, I., et al. (2010). "Multiplexed Protein Patterns on a Photosensitive Hydrophilic Polymer Matrix." Advanced Materials 22(11): 1242-1246.

Bieri, C., Ernst, O. P., Heyse, S., et al. (1999). "Micropatterned immobilization of a G protein-coupled receptor and direct detection of G protein activation." Nat Biotech 17(11): 1105-1108.

Blawas, A. S., Oliver, T. F., Pirrung, M. C., et al. (1998). "Step-and-Repeat Photopatterning of Protein Features Using Caged-Biotin−BSA: Characterization and Resolution." Langmuir 14(15): 4243-4250.

Brandenberger, H. and Widmer, F. (1998). "A new multinozzle encapsulation/immobilisation system to produce uniform beads of alginate." Journal of Biotechnology 63(1): 73-80.

Brizzolara, R. A. (2000). "Patterning multiple antibodies on polystyrene." Biosensors and Bioelectronics 15(1–2): 63-68.

Brookshier, K. A. and Tarbell, J. M. (1993). "Evaluation of a transparent blood analog fluid: aqueous xanthan gum/glycerin." Biorheology 30(2): 107-116.

Cabrales, P., Tsai, A. G. and Intaglietta, M. (2004). "Hyperosmotic-Hyperoncotic Versus Hyperosmotic-Hyperviscous: Small Volume Resuscitation in Hemorrhagic Shock." Shock 22(5): 431-437.

Cabrales, P., Tsai, A. G. and Intaglietta, M. (2005). "Alginate plasma expander maintains perfusion and plasma viscosity during extreme hemodilution." American journal of physiology. Heart and circulatory physiology 288(4): H1708-1716.

Capretto, L., Cheng, W., Hill, M., et al. (2011). "Micromixing within microfluidic devices." Topics in current chemistry 304: 27-68.

Chan, E. W. L. and Yousaf, M. N. (2008). "A photo-electroactive surface strategy for immobilizing ligands in patterns and gradients for studies of cell polarization." Molecular BioSystems 4(7): 746-753.

Chang, Y., Ahn, Y. S., Hahn, H. T., et al. (2007). "Sub-micrometer Patterning of Proteins by Electric Lithography." Langmuir 23(8): 4112-4114.

Chen, H. and Meiners, J. C. (2004). "Topologic mixing on a microfluidic chip." Biophys J 86(1): 482a-482a.

Chen, H. H., Sun, B. B., Tran, K. K., et al. (2009). "A Microfluidic Manipulator for Enrichment and Alignment of Moving Cells and Particles." J Biomech Eng-T Asme 131(7).

Chen, S. and Smith, L. M. (2009). "Photopatterned Thiol Surfaces for Biomolecule Immobilization." Langmuir 25(20): 12275-12282.

Cho, Y. I. and Kensey, K. R. (1991). "Effects of the non-Newtonian viscosity of blood on flows in a diseased arterial vessel. Part 1: Steady flows." Biorheology 28(3-4): 241-262.

Choi, S. and Park, J. K. (2007). "Continuous hydrophoretic separation and sizing of microparticles using slanted obstacles in a microchannel." Lab on a Chip 7(7): 890-897.

Choi, S., Song, S., Choi, C., et al. (2007). "Continuous blood cell separation by hydrophoretic filtration." Lab on a Chip 7(11): 1532-1538.

Christman, K. L., Schopf, E., Broyer, R. M., et al. (2008). "Positioning Multiple Proteins at the Nanoscale with Electron Beam Cross-Linked Functional Polymers." Journal of the American Chemical Society 131(2): 521-527.

Cruz, I., Ciudad, J., Cruz, J. J., et al. (2005). "Evaluation of multiparameter flow cytometry for the detection of breast cancer tumor cells in blood samples." Am J Clin Pathol 123(1): 66-74.

Danila, D. C., Heller, G., Gignac, G. A., et al. (2007). "Circulating tumor cell number and prognosis in progressive castration-resistant prostate cancer." Clin Cancer Res 13(23): 7053-7058.

Danila, D. C., Pantel, K., Fleisher, M., et al. (2011). "Circulating Tumors Cells as Biomarkers: Progress Toward Biomarker Qualification." The Cancer Journal 17(6): 438-450 410.1097/PPO.1090b1013e31823e31869ac.

De Giorgi, V., Pinzani, P., Salvianti, F., et al. (2010). "Application of a Filtration- and Isolation-by-Size Technique for the Detection of Circulating Tumor Cells in Cutaneous Melanoma." J Invest Dermatol 130(10): 2440-2447.

del Campo, A. and Bruce, I. (2005). "Substrate Patterning and Activation Strategies for DNA Chip Fabrication Immobilisation of DNA on Chips I." 260: 77-111.

Delamarche, E., Bernard, A., Schmid, H., et al. (1997). "Patterned Delivery of Immunoglobulins to Surfaces Using Microfluidic Networks." Science 276(5313): 779-781.

Devriese, L. A., Bosma, A. J., van de Heuvel, M. M., et al. (2012). "Circulating tumor cell detection in advanced non-small cell lung cancer patients by multi-marker QPCR analysis." Lung Cancer 75(2): 242-247.

Dharmasiri, U., Balamurugan, S., Adams, A. A., et al. (2009). "Highly efficient capture and enumeration of low abundance prostate cancer cells using prostate-specific membrane antigen aptamers immobilized to a polymeric microfluidic device." Electrophoresis 30(18): 3289-3300.

Dillmore, W. S., Yousaf, M. N. and Mrksich, M. (2004). "A Photochemical Method for Patterning the Immobilization of Ligands and Cells to Self-Assembled Monolayers." Langmuir 20(17): 7223-7231.

Doh, J. and Irvine, D. J. (2004). "Photogenerated Polyelectrolyte Bilayers from an Aqueous-Processible Photoresist for Multicomponent Protein Patterning." Journal of the American Chemical Society 126(30): 9170-9171.

Douvas, A., Argitis, P., Misiakos, K., et al. (2002). "Biocompatible photolithographic process for the patterning of biomolecules." Biosensors and Bioelectronics 17(4): 269-278.

Duffy, D. C., McDonald, J. C., Schueller, O. J. A., et al. (1998). "Rapid prototyping of microfluidic systems in poly(dimethylsiloxane)." Analytical Chemistry 70(23): 4974-4984.

Falconnet, D., Koenig, A., Assi, F., et al. (2004). "A Combined Photolithographic and Molecular-Assembly Approach to Produce Functional Micropatterns for Applications in the Biosciences." Advanced Functional Materials 14(8): 749-756.

Fehm, T., Muller, V., Alix-Panabieres, C., et al. (2008). "Micrometastatic spread in breast cancer: detection, molecular characterization and clinical relevance." Breast cancer research : BCR 10 Suppl 1: S1.

Fiddes, L. K., Chan, H. K., Lau, B., et al. (2010). "Durable, region-specific protein patterning in microfluidic channels." Biomaterials 31(2): 315-320.

Fizazi, K., Morat, L., Chauveinc, L., et al. (2007). "High detection rate of circulating tumor cells in blood of patients with prostate cancer using telomerase activity." Annals of Oncology 18(3): 518-521.

Forbes, T. P. and Kralj, J. G. (2012). "Engineering and Analysis of Surface Interactions in a Microfluidic Herringbone Micromixer." Lab on a Chip.

Galanzha, E. I., Shashkov, E. V., Kelly, T., et al. (2009). "In vivo magnetic enrichment and multiplex photoacoustic detection of circulating tumour cells." Nat Nano 4(12): 855-860.

Ganesan, R., Kratz, K. and Lendlein, A. (2010). "Multicomponent protein patterning of material surfaces." Journal of Materials Chemistry 20(35): 7322-7331.

Ganesan, R., Lee, H. J. and Kim, J. B. (2009). "Photoactive diazoketo-functionalized self-assembled monolayer for biomolecular patterning." Langmuir 25(16): 8888-8893.

Ganesan, R., Yoo, S. Y., Choi, J.-H., et al. (2008). "Simple micropatterning of biomolecules on a diazoketo-functionalized photoresist." Journal of Materials Chemistry 18(6): 703-709.

Gascoyne, P. R. C., Noshari, J., Anderson, T. J., et al. (2009). "Isolation of rare cells from cell mixtures by dielectrophoresis." Electrophoresis 30(8): 1388-1398.

Gaver, D. P. and Kute, S. M. (1998). "A theoretical model study of the influence of fluid stresses on a cell adhering to a microchannel wall." Biophys J 75(2): 721-733.

Gerlinger, M., Rowan, A. J., Horswell, S., et al. (2012). "Intratumor heterogeneity and branched evolution revealed by multiregion sequencing." The New England journal of medicine 366(10): 883-892.

Gestwicki, J. E., Cairo, C. W., Mann, D. A., et al. (2002). "Selective Immobilization of Multivalent Ligands for Surface Plasmon Resonance and Fluorescence Microscopy." Analytical Biochemistry 305(2): 149-155.

Gleghorn, J. P., Pratt, E. D., Denning, D., et al. (2010). "Capture of circulating tumor cells from whole blood of prostate cancer patients using geometrically enhanced differential immunocapture (GEDI) and a prostate-specific antibody." Lab on a Chip 10(1): 27-29.

Gormally, E., Caboux, E., Vineis, P., et al. (2007). "Circulating free DNA in plasma or serum as biomarker of carcinogenesis: Practical aspects and biological significance." Mutat Res-Rev Mutat 635(2-3): 105-117.

Gupta, G. P. and Massague, J. (2006). "Cancer metastasis: building a framework." Cell 127(4): 679-695.

Han, M., Chen, P. and Yang, X. (2005). "Molecular dynamics simulation of PAMAM dendrimer in aqueous solution." Polymer 46(10): 3481-3488.

Hardingham, J. E., Kotasek, D., Farmer, B., et al. (1993). "Immunobead-PCR: a technique for the detection of circulating tumor cells using immunomagnetic beads and the polymerase chain reaction." Cancer research 53(15): 3455-3458.

He, W., Halberstadt, C. R. and Gonsalves, K. E. (2004). "Lithography application of a novel photoresist for patterning of cells." Biomaterials 25(11): 2055-2063.

Hermanson, G. (2008). Bioconjugate Techniques, Elsevier.

Hiraiwa, K., Takeuchi, H., Hasegawa, H., et al. (2008). "Clinical Significance of Circulating Tumor Cells in Blood from Patients with Gastrointestinal Cancers." Ann Surg Oncol 15(11): 3092-3100.

Hlady, V. and Buijs, J. (1996). "Protein adsorption on solid surfaces." Current Opinion in Biotechnology 7(1): 72-77.

Holden, M. A. and Cremer, P. S. (2003). "Light Activated Patterning of Dye-Labeled Molecules on Surfaces." Journal of the American Chemical Society 125(27): 8074-8075.

Holden, M. A., Jung, S.-Y. and Cremer, P. S. (2004). "Patterning Enzymes Inside Microfluidic Channels via Photoattachment Chemistry." Analytical Chemistry 76(7): 1838-1843.

Hong, S., Lee, D., Zhang, H., et al. (2007). "Covalent immobilization of p-selectin enhances cell rolling." Langmuir 23(24): 12261-12268.

Hong, S., Leroueil, P. R., Majoros, I. J., et al. (2007). "The binding avidity of a nanoparticle-based multivalent targeted drug delivery platform." Chem Biol 14(1): 107-115.

Hsu, C. H., Di Carlo, D., Chen, C. C., et al. (2008). "Microvortex for focusing, guiding and sorting of particles." Lab on a Chip 8(12): 2128-2134.

Hughes, A. D., Mattison, J., Western, L. T., et al. (2012). "Microtube Device for Selectin-Mediated Capture of Viable Circulating Tumor Cells from Blood." Clinical chemistry.

Hur, S. C., Henderson-MacLennan, N. K., McCabe, E. R. B., et al. (2011). "Deformability-based cell classification and enrichment using inertial microfluidics." Lab on a Chip 11(5): 912-920.

Jackson, B. L. and Groves, J. T. (2006). "Hybrid Protein−Lipid Patterns from Aluminum Templates." Langmuir 23(4): 2052-2057.

Jiang, F., Drese, K. S., Hardt, S., et al. (2004). "Helical flows and chaotic mixing in curved micro channels." AIChE Journal 50(9): 2297-2305.

Johnson, M. A. and Ross, J. M. (2008). "Staphylococcal presence alters thrombus formation under physiological shear conditions in whole blood studies." Annals of biomedical engineering 36(3): 349-355.

Johnson, T. J., Ross, D. and Locascio, L. E. (2001). "Rapid Microfluidic Mixing." Analytical Chemistry 74(1): 45-51.

Johnsson, B., Löfås, S. and Lindquist, G. (1991). "Immobilization of proteins to a carboxymethyldextran-modified gold surface for biospecific interaction analysis in surface plasmon resonance sensors." Analytical Biochemistry 198(2): 268-277.

Jonkheijm, P., Weinrich, D., Schröder, H., et al. (2008). "Chemical Strategies for Generating Protein Biochips." Angewandte Chemie International Edition 47(50): 9618-9647.

Karnik, R., Hong, S., Zhang, H., et al. (2008). "Nanomechanical control of cell rolling in two dimensions through surface Patterning of receptors." Nano Lett 8(4): 1153-1158.

Katz, J. S., Doh, J. and Irvine, D. J. (2006). "Composition-tunable properties of amphiphilic comb copolymers containing protected methacrylic acid groups for multicomponent protein patterning." Langmuir 22(1): 353-359.

Kiessling, L. L. and Pohl, N. L. (1996). "Strength in numbers: non-natural polyvalent carbohydrate derivatives." Chemistry & Biology 3(2): 71-77.

Kim, J.-B., Ganesan, R., Yoo, S. Y., et al. (2006). "Simple Patterning of Cells on a Biocompatible Nonchemically Amplified Resist." Macromolecular Rapid Communications 27(17): 1442-1445.

Kim, K., Yang, H., Jon, S., et al. (2004). "Protein Patterning Based on Electrochemical Activation of Bioinactive Surfaces with Hydroquinone-Caged Biotin." Journal of the American Chemical Society 126(47): 15368-15369.

Kim, M., Choi, J. C., Jung, H. R., et al. (2010). "Addressable micropatterning of multiple proteins and cells by microscope projection photolithography based on a protein friendly photoresist." Langmuir 26(14): 12112-12118.

King, M. R., Western, L. T., Rana, K., et al. (2009). "Biomolecular Surfaces for the Capture and Reprogramming of Circulating Tumor Cells." Journal of Bionic Engineering 6(4): 311-317.

Ko, Y., Klinz, M., Totzke, G., et al. (1998). "Limitations of the reverse transcription polymerase chain reaction method for the detection of carcinoembryonic antigen-positive tumor cells in peripheral blood." Clin Cancer Res 4(9): 2141-2146.

Koenig, A., Norgard-Sumnicht, K., Linhardt, R., et al. (1998). "Differential interactions of heparin and heparan sulfate glycosaminoglycans with the selectins. Implications for the use of unfractionated and low molecular weight heparins as therapeutic agents." The Journal of clinical investigation 101(4): 877-889.

Köhn, M. (2009). "Immobilization strategies for small molecule, peptide and protein microarrays." Journal of Peptide Science 15(6): 393-397.

Krivacic, R. T., Ladanyi, A., Curry, D. N., et al. (2004). "A rare-cell detector for cancer." Proceedings of the National Academy of Sciences of the United States of America 101(29): 10501-10504.

Kumar, A. and Whitesides, G. M. (1993). "Features of gold having micrometer to centimeter dimensions can be formed through a combination of stamping with an elastomeric stamp and an alkanethiol ‘‘ink’’ followed by chemical etching." Applied Physics Letters 63(14): 2002-2004.

Kwon, K. W., Choi, J. C., Suh, K. Y., et al. (2011). "Multiscale fabrication of multiple proteins and topographical structures by combining capillary force lithography and microscope projection photolithography." Langmuir 27(7): 3238-3243.

Lamb, S. A. (1994). Hydrodynamics. Cambridge, Cambridge University Press.

Latza, U., Niedobitek, G., Schwarting, R., et al. (1990). "Ber-EP4: new monoclonal antibody which distinguishes epithelia from mesothelial." Journal of clinical pathology 43(3): 213-219.

Launiere, C., Gaskill, M., Czaplewski, G., et al. (2012). "Channel Surface Patterning of Alternating Biomimetic Protein Combinations for Enhanced Microfluidic Tumor Cell Isolation." Analytical Chemistry 84(9): 4022-4028.

Launiere, C. A., Czaplewski, G. J., Myung, J. H., et al. (2011). "Rheologically biomimetic cell suspensions for decreased cell settling in microfluidic devices." Biomedical microdevices 13(3): 549-557.

Lee, C. H., Bose, S., Van Vliet, K. J., et al. (2011). "Examining the lateral displacement of HL60 cells rolling on asymmetric P-selectin patterns." Langmuir 27(1): 240-249.

Lee, H. J., Yan, Y., Marriott, G., et al. (2005). "Quantitative functional analysis of protein complexes on surfaces." The Journal of Physiology 563(1): 61-71.

Lee, K.-B., Lim, J.-H. and Mirkin, C. A. (2003). "Protein Nanostructures Formed via Direct-Write Dip-Pen Nanolithography." Journal of the American Chemical Society 125(19): 5588-5589.

Lee, R. T. and Lee, Y. C. (2000). "Affinity enhancement by multivalent lectin–carbohydrate interaction." Glycoconjugate Journal 17(7): 543-551.

Leshansky, A. M., Bransky, A., Korin, N., et al. (2007). "Tunable Nonlinear Viscoelastic "Focusing" in a Microfluidic Device." Phys Rev Lett 98(23): 234501.

Li, N. and Ho, C.-M. (2008). "Photolithographic patterning of organosilane monolayer for generating large area two-dimensional B lymphocyte arrays." Lab on a Chip 8(12): 2105-2112.

Liu, R. H., Stremler, M. A., Sharp, K. V., et al. (2000). "Passive mixing in a three-dimensional serpentine microchannel." Microelectromechanical Systems, Journal of 9(2): 190-197.

Long, M., Zhao, H., Huang, K. S., et al. (2001). "Kinetic measurements of cell surface E-selectin/carbohydrate ligand interactions." Annals of biomedical engineering 29(11): 935-946.

Lopez, M. and Graham, M. D. (2008). "Enhancement of mixing and adsorption in microfluidic devices by shear-induced diffusion and topography-induced secondary flow." Phys Fluids 20(5).

Love, J. C., Estroff, L. A., Kriebel, J. K., et al. (2005). "Self-Assembled Monolayers of Thiolates on Metals as a Form of Nanotechnology." Chemical Reviews 105(4): 1103-1170.

Lu, H., Koo, L. Y., Wang, W. C. M., et al. (2004). "Microfluidic shear devices for quantitative analysis of cell adhesion." Analytical Chemistry 76(18): 5257-5264.

Lu, J., Fan, T., Zhao, Q., et al. (2010). "Isolation of circulating epithelial and tumor progenitor cells with an invasive phenotype from breast cancer patients." Int J Cancer 126(3): 669-683.

Lynn, N. S. and Dandy, D. S. (2007). "Geometrical optimization of helical flow in grooved micromixers." Lab on a Chip 7(5): 580-587.

Maheswaran, S., Sequist, L. V., Nagrath, S., et al. (2008). "Detection of mutations in EGFR in circulating lung-cancer cells." The New England journal of medicine 359(4): 366-377.

Mammen, M., Choi, S. K. and Whitesides, G. M. (1998). "Polyvalent interactions in biological systems: Implications for design and use of multivalent ligands and inhibitors." Angew Chem Int Edit 37(20): 2755-2794.

Marrinucci, D., Bethel, K., Bruce, R. H., et al. (2007). "Case study of the morphologic variation of circulating tumor cells." Human pathology 38(3): 514-519.

Martin, T. A., Herman, C. T., Limpoco, F. T., et al. (2011). "Quantitative photochemical immobilization of biomolecules on planar and corrugated substrates: a versatile strategy for creating functional biointerfaces." ACS applied materials & interfaces 3(9): 3762-3771.

Mengeaud, V., Josserand, J. and Girault, H. H. (2002). "Mixing Processes in a Zigzag Microchannel: Finite Element Simulations and Optical Study." Analytical Chemistry 74(16): 4279-4286.

Mohamed, H., Murray, M., Turner, J. N., et al. (2009). "Isolation of tumor cells using size and deformation." J Chromatogr A 1216(47): 8289-8295.

Moreno, J. G., Miller, M. C., Gross, S., et al. (2005). "Circulating tumor cells predict survival in patients with metastatic prostate cancer." Urology 65(4): 713-718.

Moreno, J. G., O'Hara, S. M., Gross, S., et al. (2001). "Changes in circulating carcinoma cells in patients with metastatic prostate cancer correlate with disease status." Urology 58(3): 386-392.

Mourez, M., Kane, R. S., Mogridge, J., et al. (2001). "Designing a polyvalent inhibitor of anthrax toxin." Nat Biotech 19(10): 958-961.

Myung, J. H., Gajjar, K. A., Saric, J., et al. (2011). "Dendrimer-mediated multivalent binding for the enhanced capture of tumor cells." Angew Chem Int Ed Engl 50(49): 11769-11772.

Myung, J. H., Launiere, C. A., Eddington, D. T., et al. (2010). "Enhanced Tumor Cell Isolation by a Biomimetic Combination of E-selectin and anti-EpCAM: Implications for the Effective Separation of Circulating Tumor Cells (CTCs)." Langmuir 26(11): 8589-8596.

Nagrath, S., Sequist, L. V., Maheswaran, S., et al. (2007). "Isolation of rare circulating tumour cells in cancer patients by microchip technology." Nature 450(7173): 1235-1239.

Naume, B., Borgen, E., Beiske, K., et al. (1997). "Immunomagnetic techniques for the enrichment and detection of isolated breast carcinoma cells in bone marrow and peripheral blood." Journal of hematotherapy 6(2): 103-114.

Niemeyer, C. M., Adler, M. and Wacker, R. (2007). "Detecting antigens by quantitative immuno-PCR." Nat. Protocols 2(8): 1918-1930.

Ottino, J. M. (1989). The kinematics of mixing: stretching, chaos, and transport, Cambridge University Press.

Papadopoulou, E., Davilas, E., Sotiriou, V., et al. (2006). "Cell-free DNA and RNA in plasma as a new molecular marker for prostate and breast cancer." Ann Ny Acad Sci 1075: 235-243.

Papadopoulou, E., Davilas, E., Sotiriou, V., et al. (2006). "Cell-free DNA and RNA in plasma as a new molecular marker for prostate cancer." Tumor Biol 27: 44-44.

Paris, P. L., Kobayashi, Y., Zhao, Q., et al. (2009). "Functional phenotyping and genotyping of circulating tumor cells from patients with castration resistant prostate cancer." Cancer letters 277(2): 164-173.

Patel, N., Bhandari, R., Shakesheff, K. M., et al. (2000). "Printing patterns of biospecifically-adsorbed protein." J Biomat Sci-Polym E 11(3): 319-331.

Paterlini-Brechot, P., Vona, G. and Brechot, C. (2000). "Circulating tumorous cells in patients with hepatocellular carcinoma. Clinical impact and future directions." Semin Cancer Biol 10(3): 241-249.

Phillips, J. A., Xu, Y., Xia, Z., et al. (2009). "Enrichment of Cancer Cells Using Aptamers Immobilized on a Microfluidic Channel." Analytical Chemistry 81(3): 1033-1039.

Predki, P. F. (2004). "Functional protein microarrays: ripe for discovery." Curr Opin Chem Biol 8(1): 8-13.

Pritchard, D. J., Morgan, H. and Cooper, J. M. (1995). "Micron-Scale Patterning of Biological Molecules." Angewandte Chemie International Edition in English 34(1): 91-93.

Quintana, A., Raczka, E., Piehler, L., et al. (2002). "Design and Function of a Dendrimer-Based Therapeutic Nanodevice Targeted to Tumor Cells Through the Folate Receptor." Pharmaceutical Research 19(9): 1310-1316.

Quist, A. P., Pavlovic, E. and Oscarsson, S. (2005). "Recent advances in microcontact printing." Analytical and Bioanalytical Chemistry 381(3): 591-600.

Rana, K., Liesveld, J. L. and King, M. R. (2009). "Delivery of apoptotic signal to rolling cancer cells: a novel biomimetic technique using immobilized TRAIL and E-selectin." Biotechnology and bioengineering 102(6): 1692-1702.

Reynolds, N. P., Tucker, J. D., Davison, P. A., et al. (2009). "Site-Specific Immobilization and Micrometer and Nanometer Scale Photopatterning of Yellow Fluorescent Protein on Glass Surfaces." Journal of the American Chemical Society 131(3): 896-897.

Riethdorf, S., Fritsche, H., Muller, V., et al. (2007). "Detection of circulating tumor cells in peripheral blood of patients with metastatic breast cancer: a validation study of the CellSearch system." Clin Cancer Res 13(3): 920-928.

Rusmini, F., Zhong, Z. and Feijen, J. (2007). "Protein Immobilization Strategies for Protein Biochips." Biomacromolecules 8(6): 1775-1789.

Ryan, D., Parviz, B. A., Linder, V., et al. (2004). "Patterning Multiple Aligned Self-Assembled Monolayers Using Light." Langmuir 20(21): 9080-9088.

Sagiv, J. (1980). "Organized monolayers by adsorption. 1. Formation and structure of oleophobic mixed monolayers on solid surfaces." Journal of the American Chemical Society 102(1): 92-98.

Schmalenberg, K. E., Buettner, H. M. and Uhrich, K. E. (2004). "Microcontact printing of proteins on oxygen plasma-activated poly(methyl methacrylate)." Biomaterials 25(10): 1851-1857.

Schneider, M. H., Willaime, H., Tran, Y., et al. (2010). "Wettability Patterning by UV-Initiated Graft Polymerization of Poly(acrylic acid) in Closed Microfluidic Systems of Complex Geometry." Anal Chem.

Sequist, L. V., Nagrath, S., Toner, M., et al. (2009). "The CTC-chip: an exciting new tool to detect circulating tumor cells in lung cancer patients." J Thorac Oncol 4(3): 281-283.

Simpson, S. J., Vachula, M., Kennedy, M. J., et al. (1995). "Detection of Tumor-Cells in the Bone-Marrow, Peripheral-Blood, and Apheresis Products of Breast-Cancer Patients Using Flow-Cytometry." Exp Hematol 23(10): 1062-1068.

Somers, W. S., Tang, J., Shaw, G. D., et al. (2000). "Insights into the molecular basis of leukocyte tethering and rolling revealed by structures of P- and E-selectin bound to SLe(X) and PSGL-1." Cell 103(3): 467-479.

Sorribas, H., Padeste, C. and Tiefenauer, L. (2002). "Photolithographic generation of protein micropatterns for neuron culture applications." Biomaterials 23(3): 893-900.

Stott, S. L., Hsu, C. H., Tsukrov, D. I., et al. (2010). "Isolation of circulating tumor cells using a microvortex-generating herringbone-chip." Proceedings of the National Academy of Sciences of the United States of America 107(43): 18392-18397.

Stroock, A. D., Dertinger, S. K., Whitesides, G. M., et al. (2002). "Patterning Flows Using Grooved Surfaces." Analytical Chemistry 74(20): 5306-5312.

Stroock, A. D., Dertinger, S. K. W., Ajdari, A., et al. (2002). "Chaotic mixer for microchannels." Science 295(5555): 647-651.

Strother, T., Cai, W., Zhao, X., et al. (2000). "Synthesis and Characterization of DNA-Modified Silicon (111) Surfaces." Journal of the American Chemical Society 122(6): 1205-1209.

Talasaz, A. H., Powell, A. A., Huber, D. E., et al. (2009). "Isolating highly enriched populations of circulating epithelial cells and other rare cells from blood using a magnetic sweeper device." Proceedings of the National Academy of Sciences 106(10): 3970-3975.

Tan, S. J., Yobas, L., Lee, G. Y. H., et al. (2009). "Microdevice for the isolation and enumeration of cancer cells from blood." Biomedical microdevices 11(4): 883-892.

Tanguy, P., Choplin, L. and Fortin, M. (1985). "Shear-Thinning effects on dip coating." The Canadian Journal of Chemical Engineering 63(4): 533-538.

Tedder, T. F., Steeber, D. A., Chen, A., et al. (1995). "The selectins: vascular adhesion molecules." The FASEB journal : official publication of the Federation of American Societies for Experimental Biology 9(10): 866-873.

Thurston, G. B. and Henderson, N. M. (2006). "Effects of flow geometry on blood viscoelasticity." Biorheology 43(6): 729-746.

Tkaczuk, K. H., Goloubeva, O., Tait, N. S., et al. (2008). "The significance of circulating epithelial cells in Breast Cancer patients by a novel negative selection method." Breast cancer research and treatment 111(2): 355-364.

Tomalia, D. A., Baker, H., Dewald, J., et al. (1985). "A New Class of Polymers: Starburst-Dendritic Macromolecules." Polymer Journal 17(1): 117-132.

Tong, X., Yang, L., Lang, J. C., et al. (2007). "Application of immunomagnetic cell enrichment in combination with RT-PCR for the detection of rare circulating head and neck tumor cells in human peripheral blood." Cytometry. Part B, Clinical cytometry 72(5): 310-323.

Turchanin, A., Tinazli, A., El-Desawy, M., et al. (2008). "Molecular Self-Assembly, Chemical Lithography, and Biochemical Tweezers: A Path for the Fabrication of Functional Nanometer-Scale Protein Arrays." Advanced Materials 20(3): 471-477.

Van der Auwera, I., Peeters, D., Benoy, I. H., et al. (2009). "Circulating tumour cell detection: a direct comparison between the CellSearch System, the AdnaTest and CK-19/mammaglobin RT-PCR in patients with metastatic breast cancer." Br J Cancer 102(2): 276-284.

Vauchel, P., Arhaliass, A., Legrand, J., et al. (2008). "Decrease in dynamic viscosity and average molecular weight of alginate from Laminaria digitata during alkaline extraction." Journal of Phycology 44(2): 515-517.

Vona, G., Sabile, A., Louha, M., et al. (2000). "Isolation by size of epithelial tumor cells - A new method for the immunomorphological and molecular characterization of circulating tumor cells." Am J Pathol 156(1): 57-63.

Waichman, S., Bhagawati, M., Podoplelova, Y., et al. (2010). "Functional Immobilization and Patterning of Proteins by an Enzymatic Transfer Reaction." Analytical Chemistry 82(4): 1478-1485.

Wan, Y., Tan, J., Asghar, W., et al. (2011). "Velocity Effect on Aptamer-Based Circulating Tumor Cell Isolation in Microfluidic Devices." The Journal of Physical Chemistry B 115(47): 13891-13896.

Wang, S., Liu, K., Liu, J., et al. (2011). "Highly Efficient Capture of Circulating Tumor Cells by Using Nanostructured Silicon Substrates with Integrated Chaotic Micromixers." Angewandte Chemie International Edition 50(13): 3084-3088.

Wang, Z. P., Eisenberger, M. A., Carducci, M. A., et al. (2000). "Identification and characterization of circulating prostate carcinoma cells." Cancer 88(12): 2787-2795.

Weigum, S. E., Floriano, P. N., Christodoulides, N., et al. (2007). "Cell-based sensor for analysis of EGFR biomarker expression in oral cancer." Lab on a Chip 7(8): 995-1003.

Weissleder, R., Kelly, K., Sun, E. Y., et al. (2005). "Cell-specific targeting of nanoparticles by multivalent attachment of small molecules." Nat Biotech 23(11): 1418-1423.

Wolfenden, M. L. and Cloninger, M. J. (2006). "Carbohydrate-Functionalized Dendrimers To Investigate the Predictable Tunability of Multivalent Interactions." Bioconjugate Chemistry 17(4): 958-966.

Woller, E. K., Walter, E. D., Morgan, J. R., et al. (2003). "Altering the Strength of Lectin Binding Interactions and Controlling the Amount of Lectin Clustering Using Mannose/Hydroxyl-Functionalized Dendrimers." Journal of the American Chemical Society 125(29): 8820-8826.

Wu, Z., Hjort, K., Wicher, G., et al. (2008). "Microfluidic high viability neural cell separation using viscoelastically tuned hydrodynamic spreading." Biomedical microdevices 10(5): 631-638.

Wulfing, P., Borchard, J., Buerger, H., et al. (2006). "HER2-positive circulating tumor cells indicate poor clinical outcome in stage I to III breast cancer patients." Clin Cancer Res 12(6): 1715-1720.

Xu, Y., Phillips, J. A., Yan, J. L., et al. (2009). "Aptamer-Based Microfluidic Device for Enrichment, Sorting, and Detection of Multiple Cancer Cells." Analytical Chemistry 81(17): 7436-7442.

Yang, L., Lang, J. C., Balasubramanian, P., et al. (2009). "Optimization of an enrichment process for circulating tumor cells from the blood of head and neck cancer patients through depletion of normal cells." Biotechnology and bioengineering 102(2): 521-534.

Yen, G. S., Fujimoto, B. S., Schneider, T., et al. (2011). "A rapid and economical method for profiling feature heights during microfabrication." Lab Chip 11(5): 974-977.

Yoon, K. A., Park, S., Lee, S. H., et al. (2009). "Comparison of circulating plasma DNA levels between lung cancer patients and healthy controls." The Journal of molecular diagnostics : JMD 11(3): 182-185.

Yu, M., Stott, S., Toner, M., et al. (2011). "Circulating tumor cells: approaches to isolation and characterization." The Journal of cell biology 192(3): 373-382.

Yu, Z., Wachs, A. and Peysson, Y. (2006). "Numerical simulation of particle sedimentation in shear-thinning fluids with a fictitious domain method." Journal of Non-Newtonian Fluid Mechanics 136(2-3): 126-139.

Zanetti-Dallenbach, R., Wight, E., Fan, A. X., et al. (2008). "Positive correlation of cell-free DNA in plasma/serum in patients with malignant and benign breast disease." Anticancer research 28(2A): 921-925.

Zheng, S., Lin, H., Liu, J. Q., et al. (2007). "Membrane microfilter device for selective capture, electrolysis and genomic analysis of human circulating tumor cells." J Chromatogr A 1162(2): 154-161.

Zheng, X., Cheung, L. S., Schroeder, J. A., et al. (2011). "Cell receptor and surface ligand density effects on dynamic states of adhering circulating tumor cells." Lab Chip 11(20): 3431-3439.

Zheng, X., Cheung, L. S., Schroeder, J. A., et al. (2011). "A high-performance microsystem for isolating circulating tumor cells." Lab Chip 11(19): 3269-3276.

Copyright Permissions are available as a supplementary file.

Appendix COMSOL Modeling Parameters

In order to study their effect on tumor cell transport in microfluidic channels, two different passive mixer types were modeled in COMSOL Multiphysics modeling software version 4.2a. These were the staggered herringbone mixer and the chevron groove mixer (figure 29 b and c).

A.1 Theory

Fluid momentum transport was modeled by the stationary Navier-Stokes equations in three dimensions:

$$\rho(\boldsymbol{v} \bullet \nabla)\boldsymbol{v} = \nabla \bullet [-P\boldsymbol{I} + \mu(\nabla\boldsymbol{v} + (\nabla\boldsymbol{v})^T)]$$

where ρ is fluid density, P is pressure, μ is the dynamic viscosity, $\boldsymbol{v}$ is fluid velocity and T is temperature. Particle trajectories within the modeled flows were estimated with the following Newtonian formulation:

$$\frac{d}{dt}(m_p\boldsymbol{u}) = m_p F_d(\boldsymbol{v} - \boldsymbol{u})$$

where m_p is the particle mass and u is a particle velocity. F_d is the drag force on the particle and per unit mass, and was calculated according to stokes law with the equation:

$$F_d = \frac{18\eta}{\rho_p d_p^2}$$

where ρ_p is the particle density and d_p is the particle diameter.

A.2 Geometric Parameters

The COMSOL models were constructed with parameterized geometries. The parameters are listed in table VI.

Table VI. Mixer Geometric Parameters.

Name	Description	Values Herringbone Mixer (μm)	Values Chevron Mixer (μm)
L	Channel Length	6000	6000
W	Channel Width	variable	variable
H	Channel Height	50	50
D	Groove Depth	45	45
r	Ridge Width	50	50
g	Groove Width	50	50
a	Length of Arm 1	.33*W	.55*W
vel	Inlet Velocity	91.52 [um/s]	91.52 [um/s]
b	Length of Arm 2	.67*W	.55*W

The chevron mixer model geometry was constructed with a block to define the channel space (figure 46) and two arrayed hexahedrons to define the mixer features (figures 47 and 48). The chaotic (asymmetric) mixer features were defined in a similar way except the mixer features, in sets of 10, were transformed to achieve the alternating grooves described in section 2.5.1. The symmetric mixer was defined as follows.

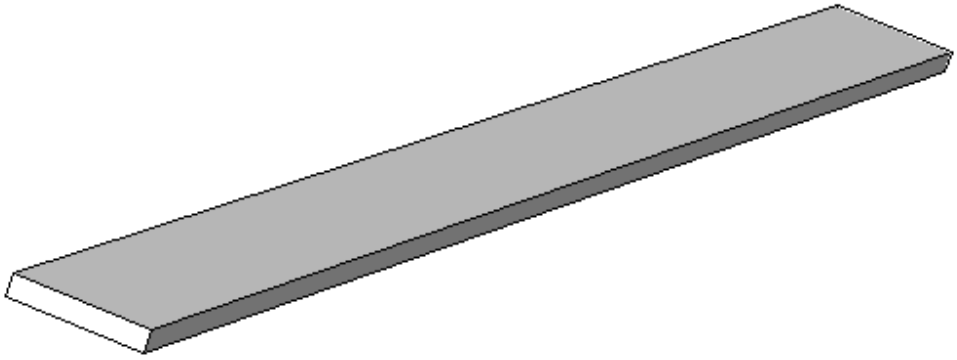

Figure 46. Mixer Block. Corner (W, -H, L), Axis (0,0,-1), Size (width W, depth H, height L)

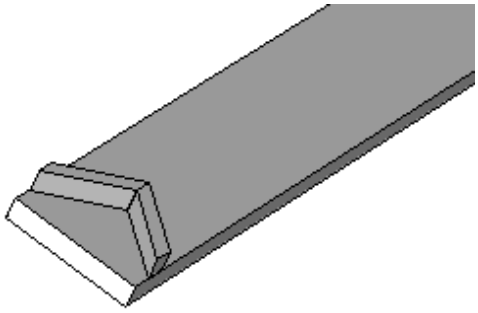

Figure 47. Mixer Hexahedrons. Parameters are defined in table VII.

Table VII. Hexahedron 1 vertices with X Y and Z Coordinates.

Hexahedron 1			
Vertex	X	Y	Z
1	a	D	r+(W-a)+g
2	a	0	r+(W-a)+g
3	a	0	r+(W-a)
4	a	D	r+(W-a)
5	W	D	r+g
6	W	0	r + g
7	W	0	r
8	W	D	r

Hexahedron 2			
Vertex	X	Y	Z
1	0	D	r +a
2	0	0	r+ a
3	0	0	r + a + g
4	0	D	r + a + g
5	a	D	r+(W-a)
6	a	0	r+(W-a)
7	a	0	r+(W-a)+g
8	a	D	r+(W-a)+g

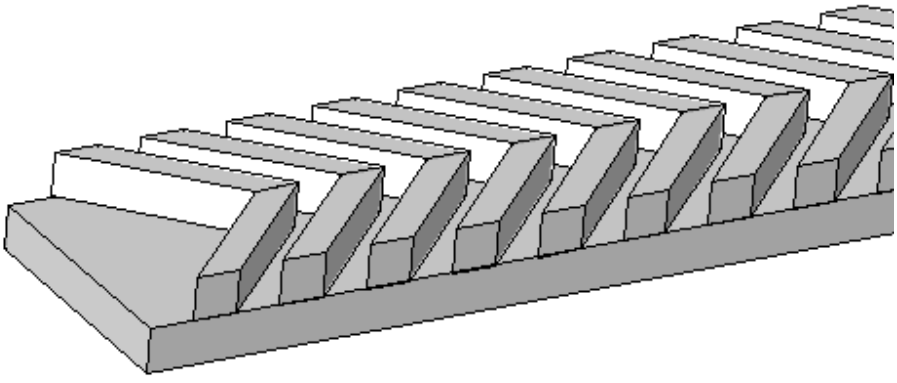

Figure 48. Hexahedron Arrays. Number of elements in the Z direction = (L/(r+g))-4

Displacement of hexahedrons in the Z direction = r + g

A.3 Model Meshing

Element meshing for the models was extra fine and calibrated for fluid dynamics. The meshing was initiated as a free triangular mesh at the base of a mixer feature (figure 49a). It was then copied to the other mixer feature bases (figure 49b). From there the mesh was swept to include the 3-D volume of the mixer features (figure 49c). After splitting any rectangular elements by inserting diagonal edges, the top of the rectangular channel (not including the mixer features) was meshed with a free triangular mesh (figure 49d). The top of the channel including the bottom of the mixer features was swept to mesh the remaining channel (figure 49d). Finally, any rectangular elements were split by the insertion of diagonal edges.

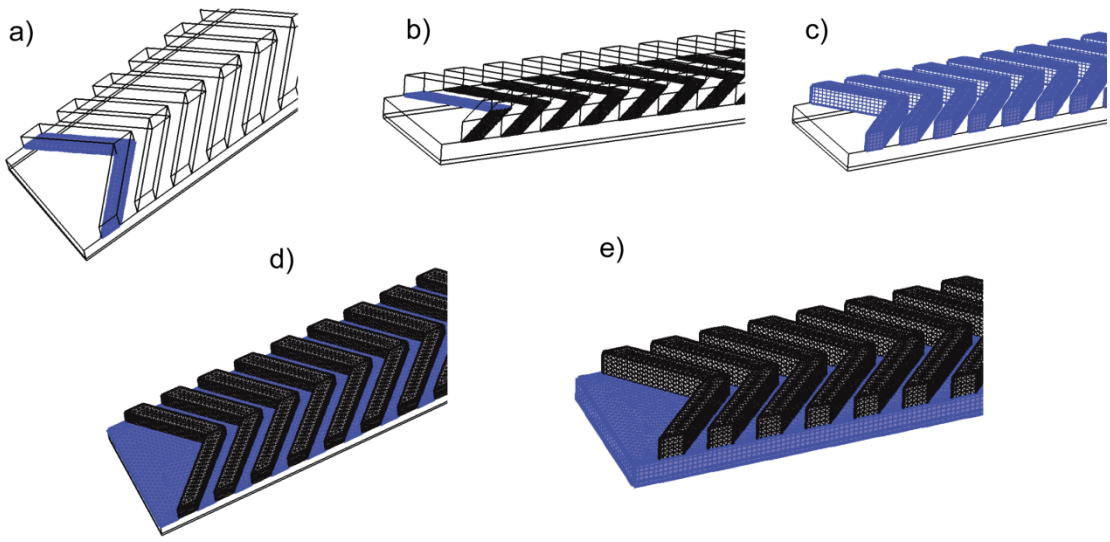

Figure 49. Meshing Sequence for Chevron Micromixers.

A.4 Steady State Flow Study

In the steady state and time-dependent models, the material properties were set to represent blood. This included a fluid density of 1.05 x 10^3 kg/m^3 and a dynamic viscosity of 2.7 x 10^{-3} Pa*s. The laminar flow fluid pressure and velocity fields were solved using COMSOL's built in pardiso solver.

Velocity profiles from the steady state solution were analyzed to ensure that the models accurately represent the physical phenomena . This included analysis of flow velocity in each of the 3 dimensions. Flows in the downstream direction (figure 50) appeared accurate based on the expected parabolic profile, with the higher velocity flows (red) in the center of the channel and the lowest velocity flows near the walls (blue). Flows in the transverse direction appeared accurate because the transverse flows follow the direction of the chevron grooves and return the other direction underneath the groove in an expected circular pattern (figure 51). The vertical flow profile also appeared accurate. This profile shows downward flows in the center where transverse flows collide are forced downward and the accompanying upward flows near the grooves' outside edges (figure 52).

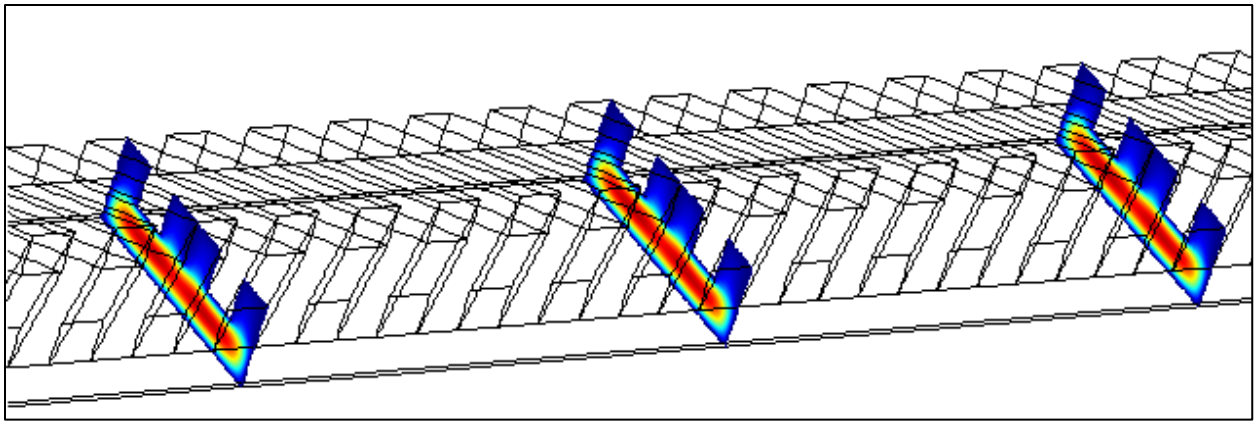

Figure 50. Downstream Velocity Flow Profile. Blue represents the lowest velocities, while red represents the highest velocities.

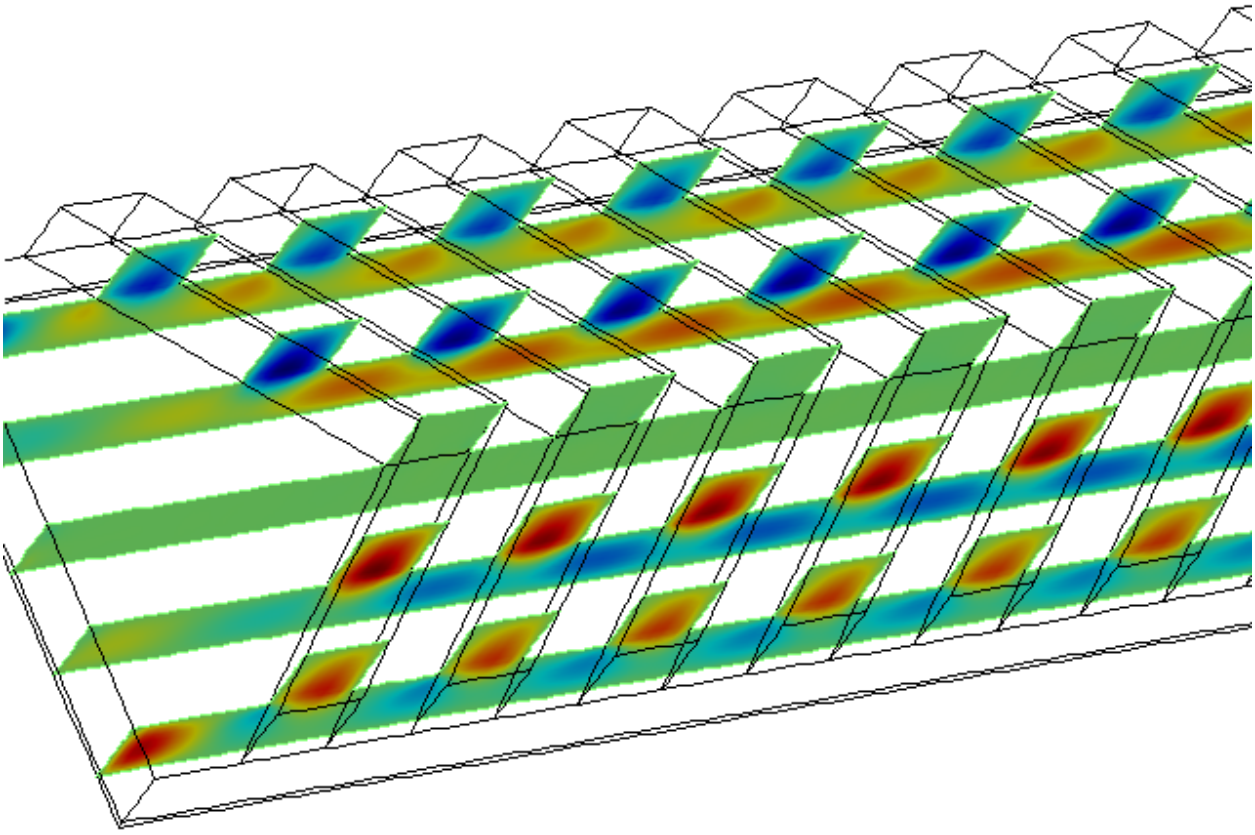

Figure 51. Transverse Velocity Flow Profile. Blue represents flow in one direction, red represents flow in the opposite direction, and green represents regions with no net fluid velocity in the transverse direction.

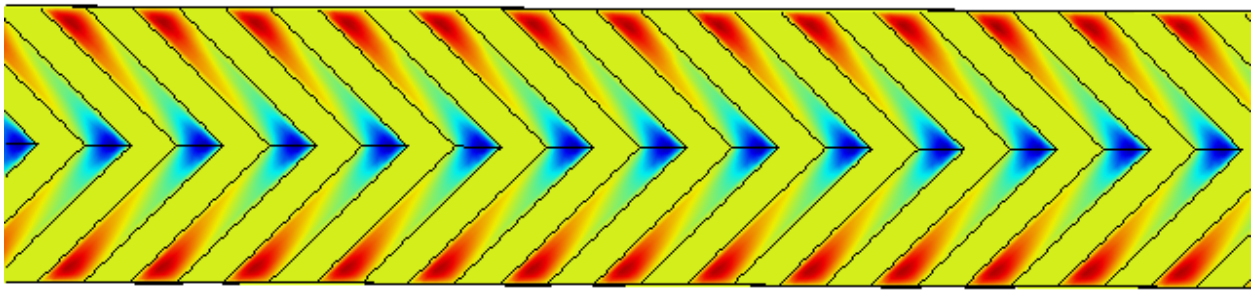

Figure 52. Vertical Velocity Flow Profile. Blue represents flows in the downward direction, while red represents flows in the upward direction.

A4. Time-Dependent Particle Tracing Studies

After solving the stationary flow studies, a time dependent analysis using COMSOL's "particle tracing for fluid flow" function was executed to estimate the path of cells through the device. The particle properties were set to approximate those of circulating tumor cells. The user defined properties were particle mass (4.44×10^{-12} kg) and particle density (1060 kg/m^3), and cell behavior upon wall contact (adhere). 100 cells were released at time zero and cell migration through the microdevices was monitored for 240 seconds. This time period proved long enough for each of the released cells to either contact a surface and be immobilized or to reach the end of the 6 mm section of channel.

Transmission probability, defined as the number of particles that reach the outlet of the mixer region divided by the number of cells released, was calculated using a built-in transmission probability function of COMSOL. Cells that do not reach the mixer outlet have contacted a channel surface and become immobilized. Therefore, devices with the lower transmission probabilities are likely to have the highest capture efficiencies in physical flow studies.

VITA

Cari Launiere

Education

University of Illinois at Chicago –*Doctor of Philosophy in Bioengineering* **2012**

Tulane University – *Bachelor of Science in Engineering* **2008**
Chemical and Biomolecular Engineering - Cell and Molecular Biology - Neuroscience
Triple Major and Minor in Biomedical Engineering
Graduated magna cum laude with Departmental Honors in Chemical and Biomolecular Engineering

Research Experience

Biological Microsystems Laboratory – *Graduate Research Assistant* **2008 - Present**
David Eddington, Ph.D., University of Illinois at Chicago, Department of Bioengineering

- Designed and validated microfluidic devices for affinity based isolation of rare cells
- Established and automated device validation protocols and data analysis
- Analyzed fluid and particle transport in devices using physical studies and computational fluid dynamics modeling
- Developed surface modification techniques for protein patterning
- Supervised 5 undergraduate researchers

Plant Cellular Stress Laboratory – *Graduate Research Assistant* **2009 - 2011**
Lon Kaufman, Ph.D., University of Illinois at Chicago, Department of Biological Sciences

- Engineered polymeric seed coatings for the delivery of phenylpropanoid products
- Developed assays that indicate extracts from transgenic plants as anti-cancer agents

Nanostructured Materials Laboratory – *Undergraduate Research Assistant* **2006 - 2008**
Vijay John, Ph.D., Chairman, Tulane University, Department of Chemical and Biomolecular Engineering

- Proposed and conducted independent research to improve epidermal penetration of drug bearing liposomes by mimicking skin-invading bacteria
- Demonstrated increased epidermal penetration in porcine models upon application of a biomimetic peptide using Boyden chamber assays, cryo-SEM, and confocal microscopy

Pathology Research Laboratory – *Undergraduate Research Assistant* **2005 - 2006**
Wai-Choi Leung, Ph.D., Tulane University School of Medicine, Department of Pathology

- Documented phase behavior of thermo-sensitive self-assembling polymer nanospheres

Publications

C. Launiere, M. Gaskill, G. Czaplewski, J.H. Myung, S. Hong, and D. Eddington (2012) "*Channel Surface Patterning of Alternating Biomimetic Protein Combinations for Enhanced Microfluidic Tumor Cell Isolation*", Analytical Chemistry, 84(9): 4022–4028.

C. Launiere, G. Czaplewski, J.H. Myung, S. Hong, and D. Eddington (2011) "*Rheologically biomimetic cell suspensions for decreased cell settling in microfluidic devices*", Biomedical Microdevices,13(3): 549-557.

J.H. Myung, K. Gajjar, R. Pearson, **C. Launiere**, D. Eddington, and S. Hong (2011) "*Direct Measurements on CD24-Mediated Rolling of Human Breast Cancer MCF-7 Cells on E-selectin*" Analytical Chemistry, 83(3): 1078-1083.

J.H. Myung, **C. Launiere**, D. Eddington, and S. Hong (2010) "*Enhanced Tumor Cell Isolation by a Biomimetic Combination of E-selectin and anti-EpCAM: Implications for the Effective Separation of Circulating Tumor Cells*", Langmuir, 26(11): 8589-8596.

Patents

Methods and Devices for Capturing Circulating Tumor Cells, S. Hong, D. Eddington, J.H. Myung, **C. Launiere**, US Patent App. 13/265,916, WO Patent WO/2010/124,227

Conference Proceedings

C. Launiere, M. Gaskill, J.H. Myung, S. Hong and D. Eddington (2011) "Patterning of Alternating Proteins Inside a Microfluidic Channel for Enhanced Tumor Cell Isolation", *Proceedings of the 15th International Conference on Miniaturized Systems for Chemistry and Life Sciences*, 1227-1229, Seattle, WA.

C. Launiere, G. Czaplewski, J.H. Myung, S. Hong and D. Eddington (2011) Academic Travel Award Winner Poster Presentation: "Biomimetic System for Circulating Tumor Cell Isolation", *Society for Laboratory Automation Annual Conference*, p57, Palm Springs, CA.

C. Launiere, G. Czaplewski, J.H. Myung, S. Hong and D. Eddington (2010) "Increased Viscosity for Decreased Settling in Microfluidic Circulating Tumor Cell Diagnostics", *Biomedical Engineering Society Annual Meeting*, Austin, TX.

C. Launiere, V. John (2008) Podium Presentation: "Mimicking Microbes to Enhance Flexible Liposome Skin Penetration", *American Institute of Chemical Engineers Southern Regional Conference*, p12, Auburn, AL.